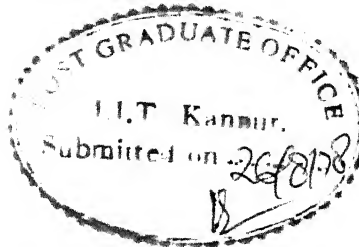# STUDY OF PHOTOVOLTAIC DEVICES BASED ON METAL - SEMICONDUCTOR STRUCTURES

A Thesis Submitted
In Partial Fulfilment of the Requirements
for the Degree of
DOCTOR OF PHILOSOPHY

By
BASABI BHAUMIK

to the

DEPARTMENT OF ELECTRICAL ENGINEERING

INDIAN INSTITUTE OF TECHNOLOGY KANPUR
AUGUST, 1978

POST GRADUATE OFFICE
I.I.T Kanpur.
Submitted on 26/8/78

CERTIFICATE

Certified that this work "STUDY OF PHOTOVOLTAIC DEVICES BASED ON METAL SEMICONDUCTOR STRUCTURES" by Miss Basabi Bhaumik has been carried out under my supervision and that it has not been submitted elsewhere for a degree.

(R. SHARAN)
Professor
Department of Electrical Engineering
Indian Institute of Technology
Kanpur

ACKNOWLEDGEMENT

I am greatly indebted to Dr. R. Sharan for sparking off my interest in the field of Solid State Devices. It is far beyond the scope of a formal acknowledgement to express my gratitude for his patient guidance, help and cooperation during the course of this work.

I would like to thank Mrs. Raka Sharan for many a pleasant evenings we have had during my stay in I.I.T. Kanpur. I would also like to thank many other friends of mine, who not only made my sojourn pleasant but also aided me in getting a clearer perspective of life.

Finally, I would like to thank Shri K.N. Tewari for his efficient and neat typing.

TABLE OF CONTENTS

LIST OF FIGURES

LIST OF TABLES

SYNOPSIS

STUDY OF PHOTOVOLTAIC DEVICES BASED ON METAL-SEMICONDUCTOR STRUCTURES

By

BASABI BHAUMIK
Department of Electrical Engineering
Indian Institute of Technology, Kanpur, India

August 1978

Recently there has been an intense interest in utilising photovoltaic conversion of solar energy for terrestrial applications. This has led to the exploration of novel structures which would provide an alternative to the conventional P-N junction solar cells. Our interest in this thesis has been in studying some of these novel structures which are based on metal-semiconductor junctions and act as Schottky barriers or analogously related devices. Particular attention has been paid to the understanding of the following aspects of these novel structures.

1. The characteristics of the Schottky barrier solar cells (SBSC) are rather well known [1]. In the published literature, there are also some reports on the effect of temperature on the characteristics of these cells. For example, it has been reported that the short circuit current I_{SC} of silicon SBSC increases with increasing operating temperature. Following the concepts prevalent at that time (1975), the increase in I_{SC} has been attributed to the availability of extra photons, belonging to the long-wavelength range of the solar spectrum, due to the lowering

of the forbidden energy gap of silicon with increasing
temperature. Our study [2], presented in Chapter 1 of the
thesis, however, shows that the contribution to the increase
of I_{SC} due to the mechanism mentioned above is negligible
and cannot explain the experimental results. Instead, it
has been found that good agreement with experimental results
is obtained when the increase in I_{SC} with increasing
temperature is calculated by taking the change of the
absorption coefficient of the semiconductor with temperature
at all wavelengths. This conclusion is not limited only to
SBSCs but would be valid for P-N junctions or other type of
cells made on indirect bandgap semiconductors like silicon.

2. The major disadvantage of SBSCs is due to their low
open circuit voltage. There are two ways in which this can
be obviated. One of these is by using Schottky (MIS) cells
[1]and the other is by using Schottky (oppositely doped
semiconducting interface) cells [3]. In the case of former
cells, the performance critically depends on the thickness
of the interfacial insulating layer. When this thickness
is large, both the short circuit current and the open circuit
voltage decrease leading to a decrease of the conversion
efficiency. The mechanisms responsible for this behaviours
have been found to be the variation of the 'illuminated
barrier height' and that of the density-of-surface states
with the variation of the thickness of the interfacial layer.
The details of this analysis are given in the second chapter.

The other type of cells where an oppositely doped semiconducing interface layer is sandwitched between the metal and the bulk semiconductor have so far not received the attention they deserve. Keeping in view that the increase of effective barrier height, which is obtained due to the presence of a thin oppositely doped semiconducting interface, would be of interest not only from the point of view of solar cells but of many other devices where Schottky barriers are employed, we have developed a rather general method of analysis including the effect of mobile carriers for these devices [3]. This is given in the third chapter.

3. All the devices mentioned above require a very thin film of metal to form the Schottky barrier because these films have to be transparent to light. This places stringent demand on the choice of the metal because it is required to simultaneously meet the optical, electrical and mechanical criteria. A way out would be to use a lateral (gridded) structure where the metal film is not thin and continuous, but thick and very finely gridded. Since the carriers are photogenerated in the area where there is no metal and are laterally collected by the thick film of metal forming the Schottky barrier, we call this a lateral SBSC. Its analysis entails the solution of a two-dimensional continuity equation. A further complication arises because all the boundary conditions are not known. A method of analysis which assumes the functional form of the

boundary condition has been developed [4]and is given

in the fourth chapter. It allows the determination of

the boundary condition by proper matching and leads to the

solution of the continuity equation. A brief summary of the

properties of different types of cells considered in this

thesis is given in the concluding fifth chapter.

References

1. H.J. Hovel, "Solar Cells", Semiconductor and Semimetals, Vol.11, Eds. R.K.Willardson and A.C. Beer, Academic Press, New York, 1975.

2. B. Bhaumik and R.Sharan, "Temperature effects in Schottky-barrier solar cells", Appl.Phys.Lett., Vol.29, p.257,1976.

3. B. Bhaumik and R. Sharan, "Potential-Profile of Doped Interface Schottky Barrier Diodes", IEEE Trans. ED, Submitted in Nov.1977, revised manuscript to be submitted.

4. B. Bhaumik and R. Sharan, "Two dimensional analysis of lateral Schottky barrier solar cells", IEEE Trans. ED, submitted in April 1977, revised in Nov.1977.

CHAPTER 1

SCHOTTKY BARRIER SOLAR CELLS

Introduction

The photovoltaic effect in semiconductor P-N junctions
is well known and has been extensively utilized for power
generation using solar energy in space. Lately there have
been attempts to use this phenomenon for terrestrial generation
of electrical power. The main impediment towards this, which
again is well known, is the cost. To overcome this impediment
two major approaches have been taken; first approach is towards
cutting down the cost of P-N junction photovoltaic cells and
the other approach is to search for novel structures which may
prove viable. The work in this thesis is concerned with the
latter approach [1-5].

The structures that have been investigated are based
on the photovoltaic properties of Schottky barrier (metal-
semiconductor) diodes and related devices like metal-(thin)
insulator-semiconductor, metal-(thin)P-N, metal-(thin)N-P,
metal-(thin) insulator-(thin)P-N and metal-(thin) insulator-
(thin)N-P diodes and are given in Chapters 1, 2 and 3. A
common disadvantage of all these devices is that they require
a very thin metallic film which is almost transparent to light.
This thin metal film has different lattice constant and
different temperature coefficient of expansion from the

substrate and has to undergo temperature cycling during actual operation. Thus, there are chances that the metallic film would peel off, affecting the durability of these types of cells. This can be obviated by evaporating a very closely spaced metallic grid structure which can be thick, rather than evaporating the conventional continuous metallic layer which has to be thin [3,6,7]. In the case of gridded structure, the carriers are photogenerated in the exposed region of the semiconductor and are laterally collected by the metallic strip forming a contact based on any of the structures mentioned above. Such a cell has been called a lateral cell and, as is obvious, it entails a two-dimensional analysis [3]. This is the subject matter of Chapter 4. We start the considerations of this chapter with a study of Schottky barrier solar cell.

1.1 Schottky Barrier Solar Cell (SBSC)

A good review of Schottky barrier solar cell (SBSC) is available in the book by Hovel [8]. Here we mention those aspects which are either required later or are necessary for the sake of completeness. A particular aspect needed later concerns the temperature variation of the characteristics of solar cells. Though the development given in this chapter is in the context of SBSC, the arguments are general enough to hold in the case of other photovoltaic structures also. The consideration of dependence of performance on temperature

has been necessitated by the fact that in actual operation
the operating temperature of a solar cell keeps on changing.
A perusal of the literature showed that there were some
ambiguities regarding the physical mechanisms responsible
for the dependence of the characteristics of SBSC on
temperature. A clarification of these [1] is given in
Section 1.3, and is preceeded by a brief historical comment
and the derivation of the current voltage characteristics
of SBSC.

The photovoltaic properties of those metal semi-
conductor contacts which form a Schottky barrier have been
known for a fairly long time [9]. At an earlier stage of
development these were mostly used as photodiodes. The
basic operative mechanism of this system as photovoltaic
device for energy conversion has been discussed by Lehovec
[10] in 1948. However, barring these sporadic efforts, till
recently no systematic attempt had been made to correlate the
output characteristics of these devices with the process of
fabrication. The recent resurgence of interest in the
photovoltaic conversion of solar energy and ensuing search
for photovoltaic structures which would provide alternatives
to conventional P-N junction solar cells have, however, changed
this picture. An important step in this direction was the
theoretical analysis of Pulfrey and McQuat [11] which showed
that under ideal conditions the efficiency of a Schottky

barrier solar cell (SBSC) would be comparable to that of a
P-N junction solar cell. Added to this is the advantage
that the fabrication of SBSC would be simpler and processing
could be done at lower temperature. In actual practice,
however, the conventional SBSC has not lived upto the promise
due to its low open circuit voltage and the ensuing lower
efficiency. The structure that seem to be viable are based
on the analogous metal-(thin) insulator-semiconductor and structures
are called tunnelling MIS (or MOS) diodes. These have higher
open circuit voltage and efficiency as compared to SBSC. We
would take up their study in the next chapter after studying
the behaviour of SBSC, which is simpler, in this chapter.

A convenient, but round-about, way of coming to the
operative mechanisms of SBSC is through those of a P-N
junction solar cell which are more widely known. The energy
band diagram of a P-N junction with light incident on it from
the left is shown in Fig. 1.1(a). Here, the photons which
have energy larger than the bandgap of the semiconductor create
electron-hole pairs. The electric field in the region of the
metallurgical junction acts to separate the pairs which are
generated in the depletion region, and provide drift field for
the minority carriers which manage to diffuse to the edges of
the depletion regions on both P and N sides. Finally the
separated carriers are collected by the two ohmic contacts,
one on the back side (N side) being continuous and the other
on the front (P side) being gridded to let the light in. In
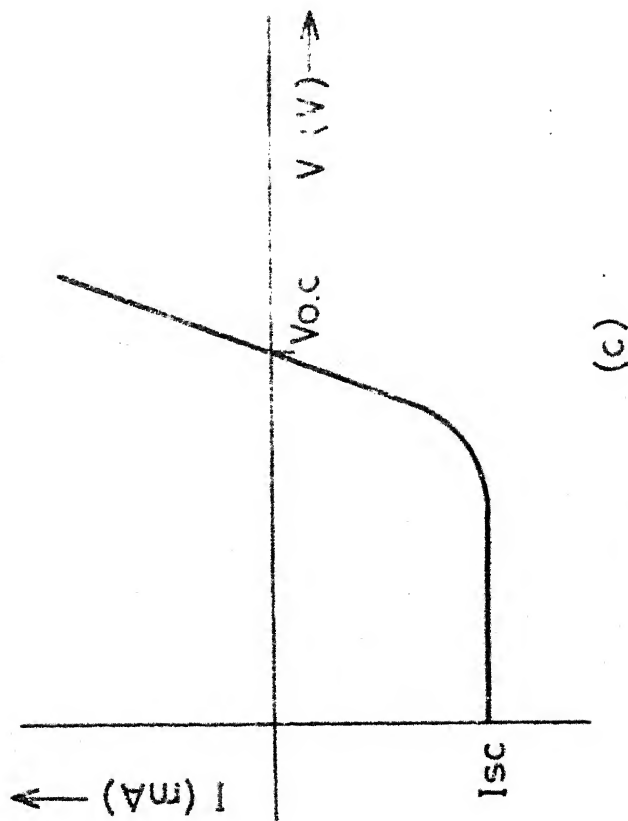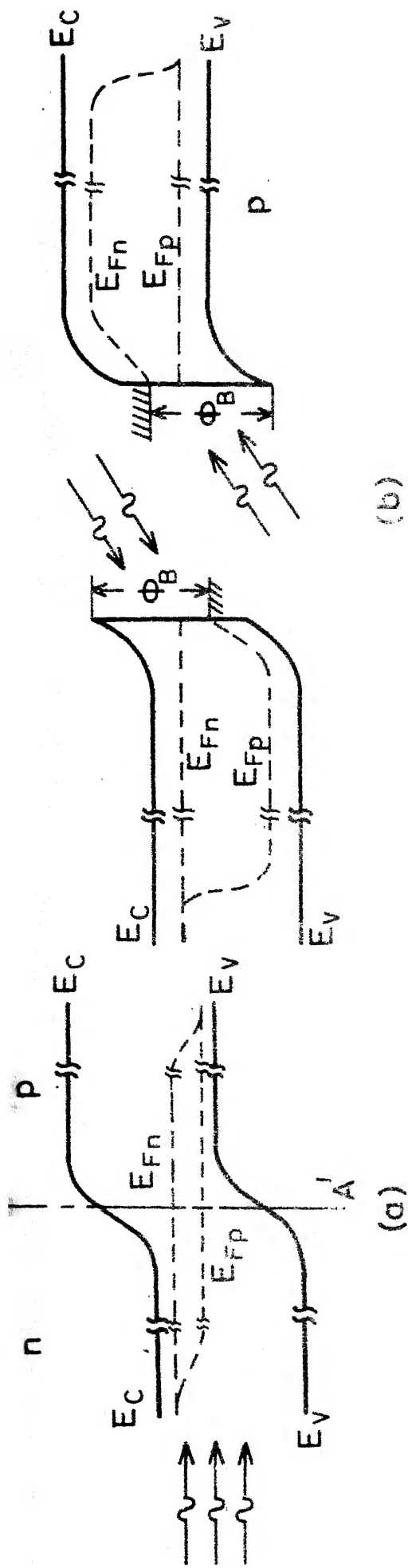
Fig.1.1 Energy band diagram of (a) a p-n junction solar cell,(b) a metal-n semiconductor and a metal-p semiconductor schottky barrier solar cell,(c) Typical I-V characteristics of solar cell

summary, the operation of a photovoltaic cell requires the photo-generation of electron-hole pairs, their separation by an electric field and the collection of these separated carriers by the metallic contacts so that they can flow through the external circuit. In addition one of the metallic contacts should be in position to let the light in, i.e. either it has to be very thin or of gridded structure.

For a moment let us now imagine that the P-N junction is sectioned at plane AA' and light is incident from the left of plane AA'. When one considers the possibility of using this structure for photovoltaic conversion one finds that it meets the necessary conditions of generation of electron-hole pairs and their separation by an electric field, but does not meet the requirement of proper collection of the photogenerated carriers. Of course, there is the question that in the absence of P semiconductor how has the band bending to the right of AA' been obtained. Both this and the requirement of collection can be simultaneously met if one puts metallic contact at AA' so that it forms a Schottky barrier as shown in Fig. 1.1(b). It is needless to say that this metallic contact should be almost transparent to the incident radiation. This is the basic principle of operation of a Schottky barrier solar cell (SBSC) based on metal-N type structure. If we repeat our argument by looking to the left of AA' and by considering light incident from right, a metal-P type SBSC can be observed.

The considerations given above clearly show the analogy between SBSC and P-N junction solar cells. Thus they allow us to carry through, but with caution, many of the concepts developed for the latter in the case of SBSC also.

1.2 I-V Characteristics of SBSC

Here there are two cases of interest. (i) The diode is forward   biased by an applied voltage V and an I-V relation ensues . There is no illumination hence we would call this as the characteristics of the 'dark'diode. (ii) The diode gets forward biased at a voltage V by the connection of a load R_L in the presence of illumination. Part of the I-V characteristic is in the fourth quadrant and would be denoted as the characteristics of the 'illuminated' diode. We take up the case of dark diode first.

1.2.1 Dark current of Schottky barrier

Current voltage characteristics of dark Schottky barriers have been well studied in the published literature [12]. Most of these studies are limited to small area diodes so that the fluctuations of any parameter on the diode do not complicate the properties. By necessity, solar cells have to be of comparatively larger area and due to this some new considerations come in. These considerations have been briefly pointed out after first giving a method to determine the mechanism of current transport in diodes which have homogeneous properties.

It is by now well established that depending upon the barrier height, doping, temperature and applied bias the mechanism of current transport through a Schottky barrier diode can either be thermionic emission (TE), thermionic field emission (TFE) or field emission (FE). It would be of interest to find a method so that by making measurements on a finished Schottky barrier one could determine as to which one of the three mechanisms mentioned above is operative in the diode.Such a method has been suggested by Saxena [13]. The method consists of experimentally plotting a graph of nT versus T where n is the ideality factor of the diode. A typical plot of this is shown in Fig. 1.2. The graph I corresponds to the case of an ideal thermionic emission with n=1, whereas graph II also corresponds to thermionic emission but with n > 1 . There is one more case shown by graph III where thermionic emission is the mechanism,but this graph does not pass through origin, rather it is parallel to n=1 line. This is the case of $'T_o'$ anamoly and has been discussed by several workers [14 a, 14b].

In the case that the thermionic field emission is the mechanism of current transport through the diode under consideration one obtains graph IV as the plot, whereas in the case of the field emission graph V results. Thus, one sees that the plot of nT versus T provides a simple method for knowing the mechanism of current transport. However, the perusal of recent literature shows that there have been some
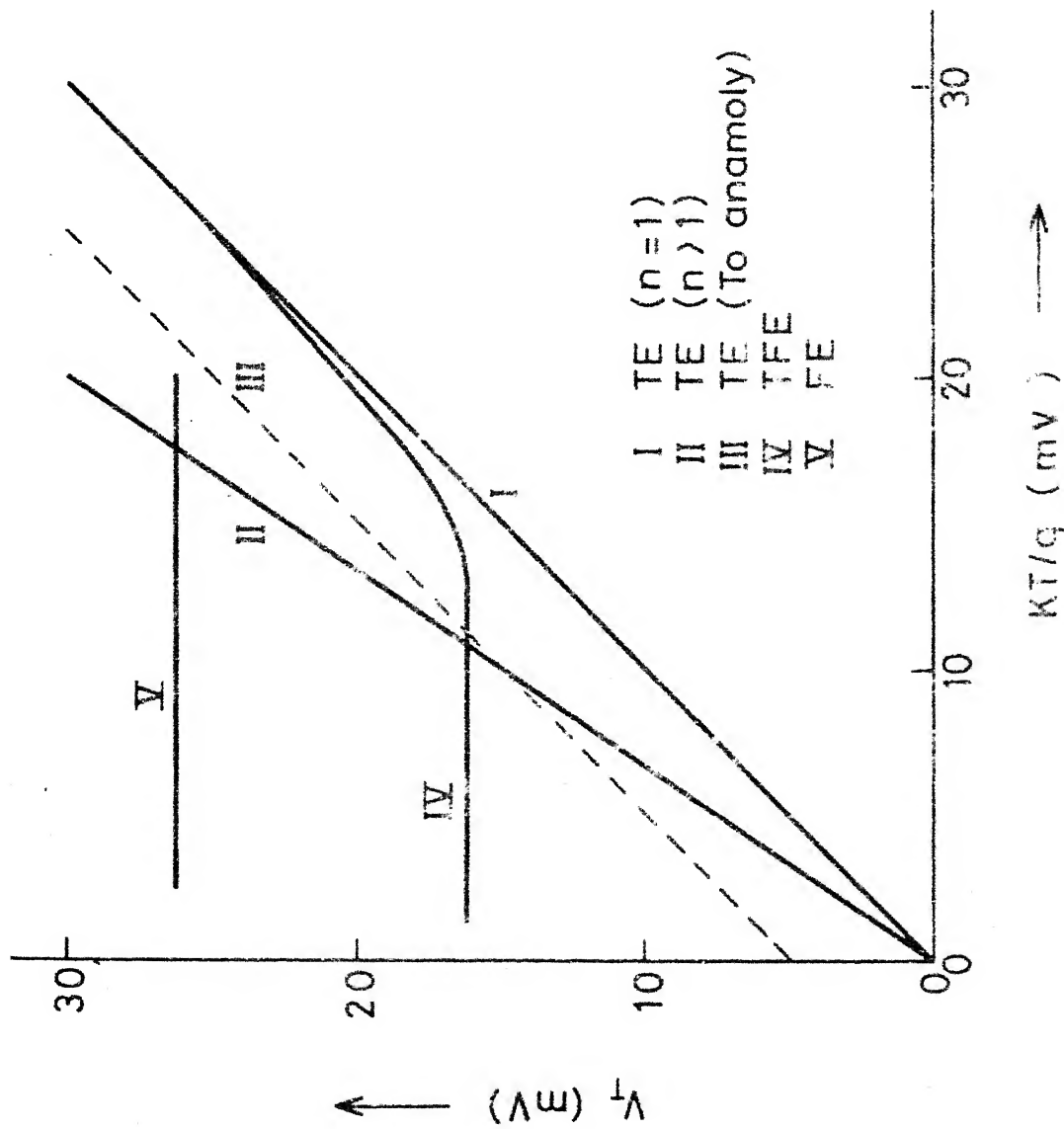
Fig. 1.2 Plot of V versus (KT/q) to determine the mechanism of current transport in Schottky Barriers (See Text)

ambiguities in this regard. A case in point is the experi-
mental results of Vernon and Anderson [15]. They have fabri-
cated large area Schottky barrier solar cells and in order to
determine the mechanism of current transport in their samples,
they have plotted nT versus T from the I-V characteristics of
SBSC. They have found this plot to be independent of tempera-
ture and have concluded therefrom that field emission is the
dominant mechanism of current transport. This conclusion,
however, seems to be suspect because neither is the semicon-
ductor degenerately doped nor is the temperature low enough
for field emission to dominate in current transport. It is
true that if one only considers the conventional mechanisms
(thermionic emission, thermionic field emission, and field
emission) of current transport in a Schottky barrier diode,
one is left with no choice but to conclude that the mechanism
in this case is field emission. It should be noted, however,
that the SBSC's are large area devices with no guard rings.
In a large area device it is quite possible that the barrier
height is not uniform over the whole sample. Johnson etal.[16],
in a different context, have investigated the effect of the
variation of barrier height on the I-V characteristic of a
metal-semiconductor junction. In some cases they have observed
that the plot of the product of the temperature and the inverse of slope
of the log I-V characteristic versus temperature is   independent
of temperature and have ascribed this to the variation of
barrier height. Although the argument is not conclusive, it

may be that this rather than field emission is the controlling
mechanism of current transport in large area SBSC's.

Thus it is evident that in the case of large area
Schottky barrier diodes great care must be exercised in using
the method of Saxena to determine the mechanism of current
transport. This has been followed through by another worker
of our group [17]. In this thesis, however, unless otherwise
specified, we would take the mechanism of current transport
to be thermionic emission and use the equation:

$$I = I_o [\exp(qV/nkT) -1] \qquad (1.1)$$

where $I_o = aJ_o$, a being the area of the diode and

$$J_o = A^{**}T^2 [\exp(-q\phi_B/kT)] \qquad (1.1a)$$

for the dark current of SBSC. Here A^{**} is the Richardson
constant, ϕ_B is the barrier height, T is temperature, q is
the charge of electron and k is the Boltzmann constant.
The value of n would be taken to be unity unless otherwise
specified.

1.2.2 I-V characteristics of SBSC

The typical nature of current voltage characteristic
in the presence of illumination is shown in Fig. 1.1(c). At
a given load R_L, a voltage V is developed across the cell.
For the present let us assume that the effect of the series
and shunt resistances and the recombination of photo-generated

carriers in the depletion region and at the interface are
negligible. Under these conditions, the following analysis
holds. At the voltage V, let the current be I and the
current density be J for a given area a. Let us consider a
metal-P semiconductor Schottky barrier cell. At any cross-
section of the cell, we have

$$J = J_p(x) + J_n(x) \qquad\qquad (1.2)$$

where $J_p(x)$ is due to the flow of majority carriers and
under the assumptions given above, can be obtained from
eqn.(1.1). $J_n(x)$ is due to the flow of minority carriers
and is determined below. In general, it is given as:

$$J_n(x) = J_{nD}(x) + J_{nQ}(x) + J_{R1}(x) + J_{R2}(x) \qquad\qquad (1.2a)$$

where $J_{nD}(x)$ is the current due to the photo-generated
carriers in the depletion region, $J_{nQ}(x)$ is due to diffusion
of photo-generated carriers in the quasi-neutral region just
beyond the depletion region, $J_{R1}(x)$ and J_{R2} are due to the
recombination of carriers in the depletion region and at the
interface, respectively. As mentioned earlier, here we would
neglect the contribution of $J_{R1}(x)$ and J_{R2}. The expressions
for $J_{nQ}(x)$ and $J_{nD}(x)$ are developed below. Under ecommonly
employed assumptions [18] $J_{nQ}(x)$ can be obtained by using
the continuity equation for the excess minority carriers
n_p which is given as [1]

$$D_n \frac{d^2 n_p}{dx^2} - \frac{n_p}{\tau_n} + Q(\lambda) \ \{1-R(\lambda)\}\alpha(\lambda)\exp\{ -\alpha(\lambda)(x+b)\}= 0 \qquad (1.3)$$

Here b is the width of the depletion region (Fig.1.3a) and other symbols are explained in ḍ....... First of all, let us consider eqn.(1.3) when the cell is short circuited.

The boundary conditions are

at $x = b$; $n_p = N$ $\qquad\qquad$ (1.4)

at $x = W$; $D_n \left.\frac{dn_p}{dx}\right|_{x=W} = -s \ n_p(W)$ $\qquad\qquad$ (1.5)

Here s is the surface recombination velocity at $x=W$ and W is the total width of the semiconductor. A comment on the choice of the boundary conditions at $x = b$ is given later. For the present we note that the solution of eqn.(1.3) with constraints of eqns. (1.4) and (1.5) is given as

$$n_p = c_1 \exp(x/L_n)+ c_2 \exp(-x/L_n)+ \frac{Q(1-R)\ \alpha\ \exp(- x)}{D_n(\frac{1}{L_n^2} - \alpha^2)} \qquad (1.6)$$

where

$$c_1 = \chi\{ [(\alpha D_n-s)\exp\{ -(\frac{b}{L_n} + W)\} + (s + \frac{D_n}{L_n})\ \exp(-\alpha b)$$

$$\exp(\frac{W-2b}{L_n})] \ /2A - \exp(-\{ \frac{b}{L_n} +\alpha b\})\} + N \exp(- \frac{b}{L_n})$$

$$\{ 1- [(s + \frac{D_n}{L_n})/2A] \exp(\frac{W-b}{L_n}) \} \qquad\qquad (1.6a)$$

$$c_2 = -\chi [(\alpha D_n - s)\exp(- \alpha W + \frac{b}{L_n}) + (s+ \frac{D_n}{L_n})\exp(- \alpha b+ \frac{W}{L_n})] \ /2A$$

$$+ N(s+ \frac{D_n}{L_n})\exp(W/L_n)/2A \qquad\qquad (1.6b)$$

where

$$\chi = Q(1-R)\ \alpha\ / \ D_n(L_n^{-2} - \alpha^2) \qquad\qquad (1.6c)$$
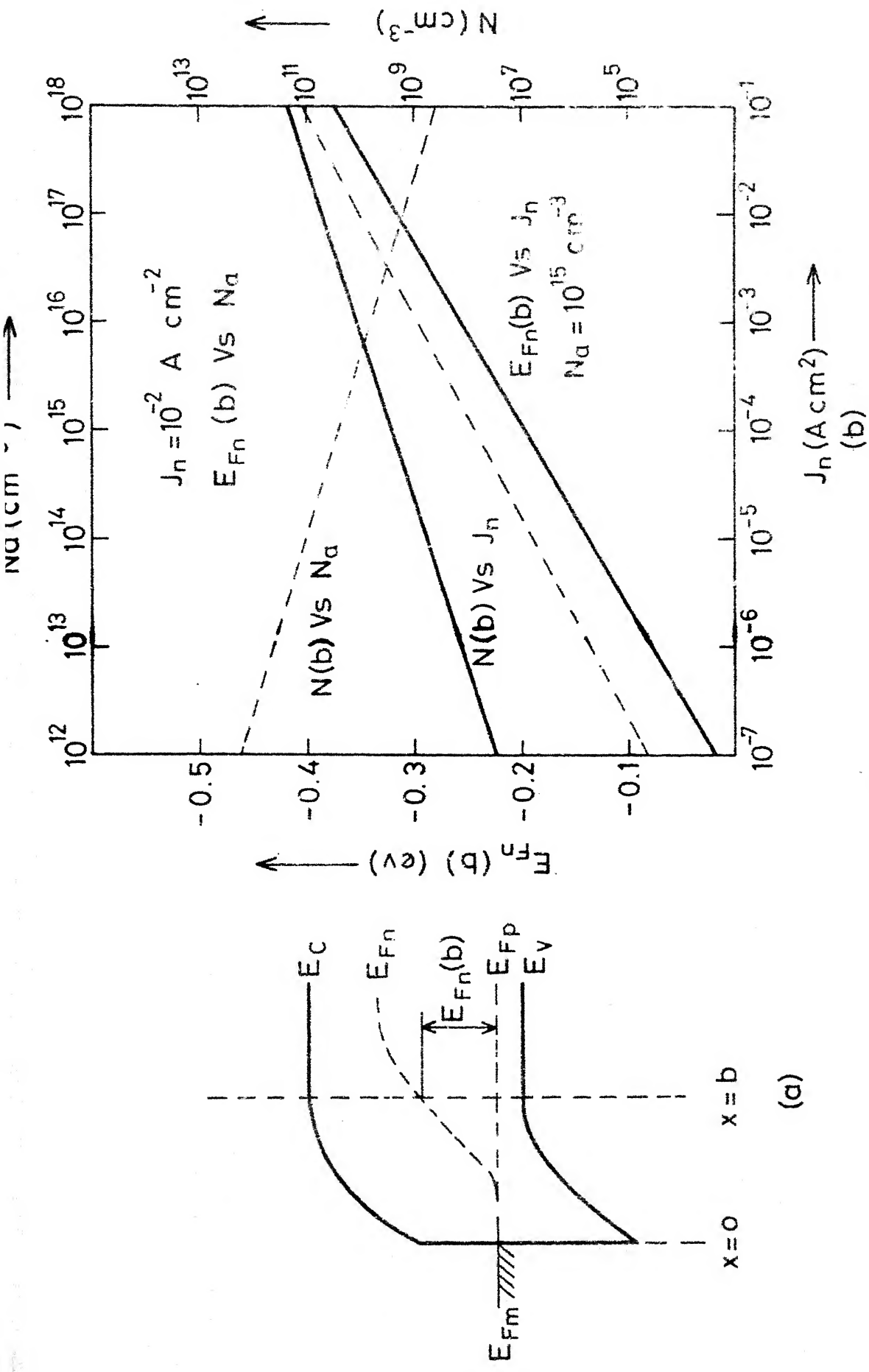
Fig.1.3(a) Energy band diagram of a P-semiconductor diode showing the quasi fermi levels. (b) Plot of $E_{Fn}(b)$ and N versus J_n (or N_a). (See text).

$$A = s \sinh [(W-b)/L_n] + \frac{D_n}{L_n} \cosh [(W-b)/L_n] \qquad (1.6d)$$

From eqn. (1.6) one obtains the short circuit current $I_{SCQ}(\lambda)$ as:

$$I_{SCQ}(\lambda) = qaD_n \frac{dn_p}{dx} \Big|_{x=b}$$

$$= qaQ(1-R) \frac{\alpha L_n \exp(-\alpha b)}{(1- \alpha^2 L_n^2)} [\frac{(\alpha D_n - s)}{A \exp(\alpha W)} + \frac{\frac{B}{A} - \alpha L_n}{\exp (\alpha b)}] + C$$

$$(1.7)$$

where $L_n^2 = D_n \tau_n$, a is the area of the cell and

$$B = s \cosh[(W-b)/L_n] + (D_n/L_n) \sinh[(W-b)/L_n] \qquad (1.7a)$$

$$C = \frac{qaD_n N}{L_n} [1 - \frac{D_n}{A}(\frac{s}{D_n} + \frac{1}{L_n}) \exp(\frac{W-b}{L_n})] \qquad (1.7b)$$

Note that inadvertently a printing error in eqn.(1.7b) has appeared in Ref. [1] . The corrected equation is given here.

Before proceeding further we would like to comment on the component C of short circuit current. It is customary in the case of short circuited cell to take N = 0 in the boundary condition at x=b (eqn. 1.4),in which case C becomes zero. The fact that N is non-zero even in the case of a short circuited cell can be seen as follows [19-21]. Let us consider the energy band diagram of a metal P semiconductor Schottky barrier solar cell shown in Fig. 1.3(a). The considerations for the metal N-semiconductor SBSC are very similar. At the metal-semiconductor interface the minority carrier imref E_{Fn}

is shown to merge with the metal Fermi level E_{Fm}, indicating an infinite recombination velocity. Following an analysis similar to that of Card [19], it can be shown that the minority carrier imref E_{Fn} does not remain constant in the depletion region as is commonly assumed. Let us take the reference of energy at the metal Fermi level and denote the value of E_{Fn} at the edge of the depletion region at $x = b$ by $E_{Fn}(b)$. The minority carrier current density in the absence of recombination is given by

$$J_n = q\, n\, \mu_n \frac{d\,E_{Fn}}{dx} \qquad (1.8a)$$

where

$$n = N_C \exp\left(-\frac{E_C - E_{Fn}}{kT}\right) \qquad (1.8b)$$

The symbols are defined in Appendix A.

Using eqn. (1.8), rearranging, and integrating for $0 < x < b$ one gets

$$\int_o^b \frac{J_n}{N_C\, \mu_n} \exp(E_C/kT)\, dx = \int_{E_{Fn}(o)}^{E_{Fn}(b)} \exp(E_{Fn}/kT)\, dE_{Fn} \qquad (1.9a)$$

Evaluating this, and making some simplifying assumptions, one obtains:

$$\exp\left(\frac{E_{Fn}(b) - E_{Fn}(o)}{kT}\right) - 1 = J_n\, N_a^{\frac{1}{2}} (1/\, n_i^2 \mu_n)(\pi \varepsilon_s / 2q^2 kT)^{\frac{1}{2}} \exp\left[\frac{-E_{Fn}(o)}{kT}\right]$$
$$(1.9b)$$

In metal P semiconductor Schottky barrier diodes, $E_{Fn}(o) = 0$. Using this, one obtains the equivalent expression of Card [19].

In the case of metal N-type contacts, eqn. (1.9b) still holds with E_{Fn}, N_a and μ_n replaced by $-E_{Fp}$, N_d and μ_p respectively.

A plot of $E_{Fn}(b)$ as a function of photo-generated current density J_n using eqn.(1.9b) is given in Fig.1.3. Also shown on this graph is the value of N given as

$$N = N_C \exp [-(E_G - E_{Fn}(b) - qV_p)/kT] \qquad (1.10a)$$

$$= n_{po} \exp [E_{Fn}(b)/kT] \qquad (1.10b)$$

where qV_p is the difference between Fermi level and the valence band. The existence of non-zero value of N in the case of short circuited photodiode was first noted by Berry [20] in the case of P-N junctions, and the numerical value of N was deduced from the short-circuited photo-capacitance of commercial solar cells. The value obtained in this case was $N = 10^{14}$ cm^{-3}. Moore [21] suggested that the analytical model of Berry based on depletion region photo-capacitance was not correct, rather a diffusion model of photocapacitance should be used. This correction gave a value of $N \simeq 10^{11}$ cm^{-3}. The point to note is that if one evaluates the current component C using $N \simeq 10^{11}$ cm^{-3} then the contribution of the term is negligible compared to the other terms. Hence the presence of N in the case of Schottky barrier solar cells is only of academic interest. However, this term becomes of considerable significance in the case of MIS solar cells as would be shown in the next chapter.

There we would use an expression for the current density J_{diff} which is equal to $(-C/a)$ where C is given by eqn.(1.7b). If we evaluate the current C by assuming that $W \gg L_n$ such that the recombination velocity s at the contact $x = W$ does not come into picture, one obtains a modified form of eqn.(1.7b) as

$$C = \frac{q \, a \, D_n}{L_n} (N - n_{po})$$

Use of eqn.(1.10b) in this expression gives an expression for J_{diff}, which has been defined above, as:

$$J_{diff} = -C/a = \frac{q \, D_n}{L_n} n_{po} \{ \exp(\frac{E_{Fn}(b)}{kT}) -1 \} \qquad (1.11a)$$

In the case of a metal N semiconductor Schottky barrier diode eqn.(1.11a) gets modified as:

$$J_{diff} = -C/a = q \frac{D_p}{L_p} p_{no} \{ \exp (- \frac{E_{Fp}(b)}{kT}) -1 \} \qquad (1.11b)$$

where $E_{Fp}(b) < 0$, if metal Fermi level is taken to be the reference energy. As already mentioned, these equations would be used in the next chapter while analysing Schottky (MIS) solar cells.

The current generated in the space charge region $(0 < x < b)$ when recombination is neglected is given by

$$I_{SCD}(\lambda) = q \, a \{ 1-R(\lambda) \} \int_0^b Q(\lambda) \alpha(\lambda) \exp\{ - \alpha(\lambda)x \} dx \qquad (1.12)$$

The total current $I_{SC}(\lambda)$ for a monochromatic light of

wavelength λ is given by the sum of eqns. (1.7) and (1.12) as

$$I_{SC}(\lambda) = I_{SCQ}(\lambda) + I_{SCD}(\lambda) = a\, J_L(\lambda) + C \qquad (1.13)$$

This current has been evaluated for a metal I-silicon Schottky barrier solar cell and the values are given when we calculate the efficiency of the cell.

Having obtained the short circuit current let us obtain the open circuit voltage. This can be obtained by equating the sum of the majority and minority carrier currents to zero and solving for the voltage. The majority carrier component can be obtained either by using the thermionic emission model or by diffusion model of current transport. If thermionic emission model is used then the use of eqn.(1.1) and (1.3) gives the total current as

$$I = I_o [\exp(qV/kT) - 1] - I_{SC} \qquad (1.14)$$

By equating $I = 0$ and solving for V one gets the well known expression for V_{OC} as

$$V_{OC} = \frac{n\,kT}{q}\; \ln[1 + \frac{I_{SC}}{I_o}] \qquad (1.15)$$

An expression for V_{OC} using the diffusion model of the majority carrier transport has been obtained by Dubey and Paranjape [22]. They have used a method of boundary matching and obtained the expression of V_{OC} in terms of a recombination velocity at the metal semiconductor interface.

However, for the parameters that are commonly useful in solar cells, it is more likely that thermionic emission model rather than diffusion model would hold true, hence we would use eqn. (1.15) for V_{OC}.

To complete the analysis, we want to obtain an expression for the efficiency of the cell. This can be done in the conventional manner using eqn. (1.14). The power output is given by $P = IV$ and the voltage V_{mp}, at which the maximum power is available, is obtained by solving for $\partial P/\partial V = 0$. This leads to a transcendental equation

$$(1 + \frac{qV_{mp}}{kT}) \exp(\frac{qV_{mp}}{kT}) = (1 + \frac{I_{SC}}{I_0}) \tag{1.16}$$

where I_0 is the reverse saturation current of the diode and I_{SC} is obtained by integrating eqn. (1.13) over the range of wavelength of interest.

Using the value of V_{mp} obtained from eqn. (1.16) in eqn. (1.14) the value of the current I_{max} at the maximum power point can be obtained. The expression for the efficiency (η) is now obtained as

$$\eta = \frac{I_{max} V_{max}}{aP_{in}} = (F.F.) \frac{I_{SC} V_{OC}}{aP_{in}} \tag{1.17}$$

where P_{in} is the intensity per unit area of the incident light and F.F. is the fill factor, which is given by the ratio

$$F.F. = \frac{I_{max} V_{max}}{I_{SC} V_{OC}} \tag{1.18}$$

It is important to point out here that the theoretically calculated efficiency of the same system using eqn.(1.17) can vary between wide limits depending upon the assumptions made and the values of parameter assumed. For example, for cells made on N-type silicon the values of efficiency ranging from approximately 20% [11] (obtained for the equilibrium barrier height $\emptyset_B$ of the order of the energy gap E_G and assuming negligible recombination and unit quantum efficiency) to 5% [23] (in the case of gold silicon contact taking incomplete absorption and some recombination into account) has been reported. Thus, caution must be exercised in completly specifying the conditions under which a number for efficiency has been obtained from the theoretical calculations. It is also worthwhile to note here that during the earlier stages of the development of SBSC's, one very intriguing feature had appeared. It had been found that the experimentally obtained efficiencies where higher than theoretical efficiencies calculated taking realistic assumptions into account. It was soon realized that this situation had arisen because the experimental cells were not actually Schottky barrier cells for which the theoretical model was built. The presence of the thin oxide layer formed during processing, between the metal and silicon, had given rise to tunneling MIS solar cells which requires different modelling than SBSC's. A calculation of the efficiency for a SBSC made on P-type silicon and operating at 300°K has been done as follows:

(i) $I_{SC}(\lambda)$ has been evaluated from eqn.(1.13) using the following values of parameters. $D_n = 10$ cm^2/sec., $L_n = 100$ μm, $s = 10^4$ cm/sec., $W = 200$ μm, $a = 1$ cm, $b = 1$ μm. $Q(\lambda)$ corresponding to AMO sunlight [24] and the values of $\alpha(\lambda)$ from Dash and Newman [25] have been used. The total short circuit current has been obtained by integrating $I_{SC}(\lambda)$ from $\lambda = 0.4$ μm to $\lambda = 1.1$ μm. This calculation gives $I_{SC} = 25$ mA/cm^2 for R = 0.1 and 16.5 mA/cm^2 for R = 0.4

(ii) Before calculating V_{OC} from eqn. (1.15), we want to note some of its features. If $(I_{SC}/I_0) \gg 1$, and $I_0 = aJ_0$, where J_0 is given by eqn. (1.1a),

$$V_{OC} = n\emptyset_B + \frac{nkT}{q} \ln \left[\frac{I_{SC}}{aA^{**} T^2} \right] \qquad (1.19)$$

Taking $I_{SC} = 25$ mA/cm^2, $a = 1$ cm^2, $A^{**} = 32$ Amp/cm^2/°K^2, $n = 1$, and $T = 300$°K, one gets:

$$V_{OC} = \emptyset_B - 0.5 \text{ volts}$$

If one takes $\emptyset_B = E_G = 1.12$ eV, then $V_{OC} = 0.62$ V and if $\emptyset_B = 0.8$ eV then $V_{OC} = 0.3$ V. Thus it is apparant that for realistic values of barrier heights the open circuit voltage of SBSC would be very small as compared to that of P-N junction solar cells. This is a serious limitation of SBSC and has limited its usefulness.

(iii) The calculated values of the efficiency of SBSC would depend upon the choice of $\emptyset_B$. If we take $\emptyset_B = E_G$ we get $\eta = 6.5\%$ for R = 0.0 which is an upper limit on the efficiency in this case.

1.3 Variation of Parameters of SBSC with Temperature

The main reason for the interest in the study of temperature dependence of performance of a solar cell is due to the fact that in actual operation it has to undergo temperature cycling. Naturally this problem had attracted attention at an early stage of the development of solar cells [26]. Recently, Vernen and Anderson [15] have experimentally measured the temperature dependence of the short circuit current, open circuit voltage and some other parameters of silicon SBSC's. Let us consider first the variation of the short circuit current I_{SC}. It has been found that it increases with increasing temperature [15]. The explanation given for this increase is that as temperature increases the bandgap E_G decreases, thus making the absorption of some more photons of longer wavelengths, which were unutilized earlier, possible. Particularly for their data, Vernan and Anderson have suggested that "the increase in I_{SC} can be accounted for by 100°C temperature increase producing a 0.03 eV decreased energy gap and 0.03 μm increased useful wavelength range". That this is not the case can be physically seen from the following arguments.

Let $\lambda_1^{T_1}$ be the wavelength of the photons corresponding to E_G at temperature T_1 and $\lambda_2^{T_2}$ be the wavelength of the photons corresponding to E_G at temperature T_2.

For silocon: $\lambda_1^{T_1} = 1.1$ μm at 300°K

and $\lambda_2^{T_2} = 1.13$ μm at 400°K.

Here use has been made of the expression [27]

$$E_G(T) = E_G(0) - \frac{\alpha T^2}{(T + \beta)} \tag{1.20}$$

where for silicon $\alpha = 7.02 \times 10^{-4}$ (eV/°K); $\beta = 1108$°K

and $E_G(0) = 1.16$ eV. This expression for $E_G(T)$ is valid for 0°

to 900°K.

The value of the absorption coefficient at $\lambda \approx 1.1\ \mu m$

for silicon is around 10 cm^{-1} [25], which means that the

photons at these wavelengths would be absorbed at a depth

of 1000 μ m. For good silicon crystal the diffusion length is

of the order of 100 μ m. Hence it is evident that photo-

carriers generated at these wavelengths can not contribute to

the short circuit current and thus do not account for the

experimentally obtained value of dI_{SC}/dT. Instead, in the

present work, it has been found [1] that for the range of

wavelengths (λ) of solar radiation useful for photogeneration

in silicon, the increase in the absorption coefficient α with

increase in temperature is the dominant mechanism which gives

rise to the increase of I_{SC} with temperature. To show this

the expression for $I_{SC}(\lambda)$ as the sum of eqns. (1.7) and (1.11)

is used. At each temperature, $I_{SC}(\lambda)$ is integrated over the

whole useful wavelength range. By repeating the process at

different temperatures, the temperature dependence of I_{SC} is

obtained. The results of the computations are shown in Fig.1.4.

Fig. 1.4 I_{sc} versus T, with L_n as parameter.
Inset shows schematic of SBSC.

Schematic of SBSC
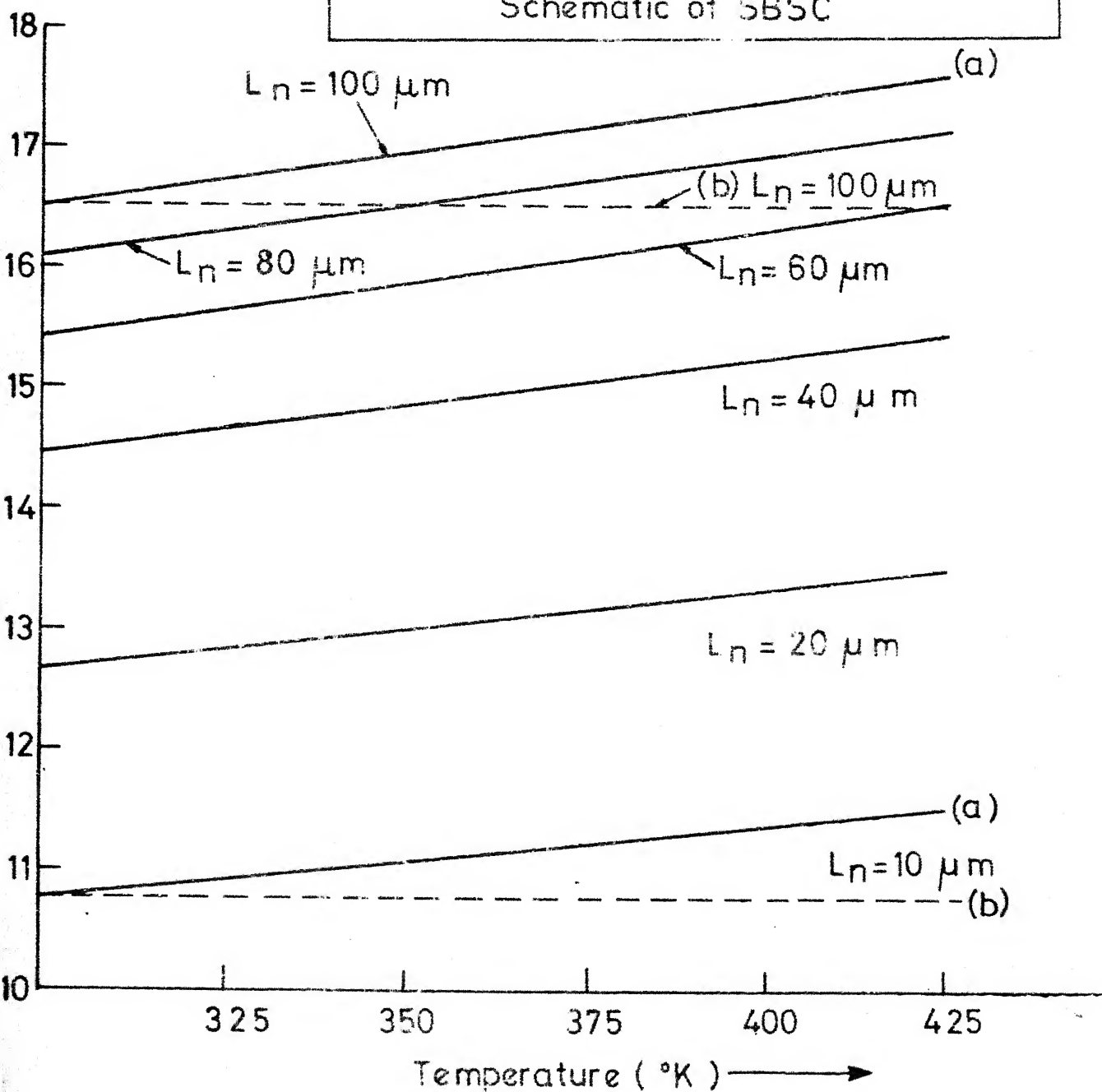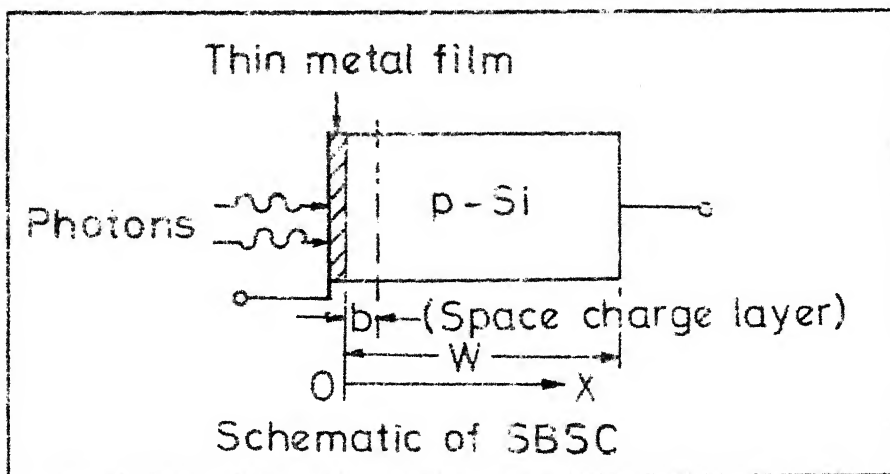
Temperature (°K)

The computations for $I_{SC}(\lambda)$ have been done for an area a of 1 cm^2 and between the temperatures 300° and 425°K. D_n and S_n have been taken [28] to be 10 cm^2 sec^{-1} and 10^4 cm sec^{-1}, respectively. L_n is treated as a parameter ranging from 10 to 100 μm. The width W = 200 μm and the width of the depletion region b = 1 μm. The temperature variation of E_G for silicon is already given by eqn.(1.20). $Q(\lambda)$ corresponding to AM0 sunlight has been used, and it has been assumed that the transmittance of the thin metal film is unity over the whole range and there is 40% reflection at the metal semiconductor interface. The value of the absorption coefficient $\alpha(\lambda)$ at different temperatures has been evaluated by using the equation [29,30]

$$\alpha = \sum_i \left[\frac{(h\nu - E_G + K\theta_i)^2}{\exp(\theta_i/T) - 1} + \frac{(h\nu - E_G - K\theta_i)^2}{1 - \exp(-\theta_i/T)} \right] C_i \quad (1.21)$$

Here $h\nu$ is the energy of photons, $K\theta_i$ is the energy of phonons, i is the index for different types of phonons participating in the process, and C_i is a constant. We have taken $C_i = 4.5 \times 10^3$ cm^{-1} eV^{-2} over the whole range of wavelengths and temperatures. This value of C_i has been obtained by comparing eqn.(1.21) with the data of Dash and Newmann [25] and by considering the proper threshold energies for different type of phonons as given by McLean [31]. The value of θ_i in the range 1.175-1.21 eV has been taken to be 212°K corresponding to transverse accoustical phonons, and

in the range 1.21 - 3.0 eV to be 670°K corresponding to transverse optical phonons. Thus the absorption coefficient α has been computed in the range 300-425°K, which are also the respective ranges in the calculation of I_{SC}.

The calculated plot of I_{SC} versus temperature is shown in Fig. 1.4. The following features should be noted.

(a) The dashed curves in Fig. 1.4 do not show any variation with temperature. They have been calculated by changing the integration limit to take care of the lowering of E_G with increase in temperature, but the value of $\alpha(\lambda)$ is kept fixed to the value at 300°K. Thus, it is not true that "the increase in I_{SC} can be accounted for by 100°C temperature increase producing 0.03 eV decreased energy gap and 0.03 μm increased useful wavelength range. This can be seen physically in the following way. The absorption coefficient in silicon for photons corresponding to E_G at 300°K is ~ 10 cm^{-1}. When E_G decreases with increasing temperature, the number of excess photons absorbed is negligible due to the extremely low value of α in this range.

(b) The solid lines in Fig. 1.4 show variation with temperature and dI_{SC}/dT ranges from 4 to 7 μA cm^{-2}/°K for values of L_n from 10 to 100 μm. In these calculations temperature variation of α, as described earlier, has been incorporated along with the proper change in the limits of integration to take care of the variation of E_G with temperature. The values of dI_{SC}/dT in Fig. 1.4 are comparable with

the experimental value [15] of 5 μA cm^{-2}/°K. An exact
agreement could only be sought if the parameters of the
experimental samples were known exactly. It is to be noted
that the considerations given here are not limited only to
SBSC. We consider this to be an important contribution of
the present work.

Having studied the temperature dependence of I_{SC}, it
would also be of interest to know the temperature dependence
of the open circuit voltage which is given by eqn.(1.19).
We observe that the evaluation of this equation at different
temperatures requires a knowledge of the variation of $\emptyset_B$ and
n with temperature. A survey of the published literature has
shown that $(d\emptyset_B/dT)$ and (dn/dT) are sensitive to the method
of fabrication and this has given rise to several conflicting
reports. This situation has been succinctly summarized
by Hackam and Haroop [32] and we reproduce some of their
comments in Table 1.1. A perusal of this shows that $d\emptyset_B/dT$
and dn/dT should be found for a particular device and using
these the value of (dV_{OC}/dT) should be calculated. The same
uncertainties that affect the calculation of dV_{OC}/dT also
affect the uncertainties in (dn/dT), hence in these cases
we have not carried out the computations any further.

To conclude, in this chapter, we have obtained the
expressions for the current voltage characteristics of
SBSCs' and have studied some aspects of their temperature

Table 1.1: Temperature dependence of $\emptyset_B$ and n in silicon.

Metal-Si systems	$d\emptyset_B/dT$ and dn/dT	References
Cr-nSi	Same values of $\emptyset_B$ and n at 77°K, 196°K and 289°K are obtained by $\frac{1}{C^2}$ -V method	Cowley etal, IEEE Trans., ED-15,761,1968
Titanium-Si (both P and N-type)	The barrier heights were determined from measurements of the reverse current density and activation of reverse current. $d\emptyset_B/dT$ varies from 0 to -1×10^{-5} ev/°K near 300°K	Cowley,Solid-St.-Electron., 12, 403, 1970.
Au,Ag and Cu on n-Si	$d\emptyset_B/dT = -(2.67 \pm 0.60) \times 10^{-4}$ eV °K and n varies from 1.01 to 1.02.	Arizumi etal., Jap.J.Appl. Phys,8,749,19?
Au-nSi	Equality of temperature dependence of $\emptyset_B$ and E_G	Crowell etal., App.Phys.Lett. 4,91,1964
Au-nSi	$d\emptyset_B/dT \sim 0$ from capacitively determined $\emptyset_B$; $d\emptyset_B/dT \sim$ large for $\emptyset_B$ determined by photoelectric technique	Kahng, Solid st.Electron., 6,281,1963
NiCr-nSi	n depends on forward bias voltage. At low voltage, n decreased with increasing temperature while at higher bias n was independent of temperature	Yu and Snow, J.Appl.Phys., 39,3008,1968
Cr-nSi	Both $\emptyset_B$ and n depend on bias voltage	Levine,J.Appl Phys.,42,3991, 1971
Ni-Si Au-Si	(i) $d\emptyset_B/dT > 0$; C-V method used, Temperature range used is 77°K-300°K. (ii) $d\emptyset_B/dT \sim 0$ from activation energy plots. But this plot yields higher value of Richardson constant. When $d\emptyset_B/dT = -2 \times 10^{-4}$/°K is invoked, accepted literature value of Richardson constant is obtained.	Padovani,J.Ap. Phys., 38,891, 1967.

dependence.   As has already been mentioned, the SBSCs'
have not lived upto their promise so far efficiency of
energy conversion is concerned.This is mainly because of
their low open circuit voltage.   Tunneling MIS solar cells
have shown better performance and are the subject matter of
the next chapter.

CHAPTER 2

SCHOTTKY (MIS) SOLAR CELLS

2.1 Introduction

It has been found both experimentally [1-5] and
theoretically [6-15] that interposition of a thin insulating
layer between the metal and the semiconductor of a Schottky
barrier solar cell increases the open circuit voltage, thereby
the efficiency. This increase, however, critically depends on
the thickness of the insulating layer, δ. A typical experi-
mental curve, obtained by Lillington and Townsend [1] exhibiting
the dependence of the open circuit voltage V_{OC} and short circuit
current I_{SC} on δ, in the case of a Au-SiO_2-nSi cell, is given
in Fig.2.1. The notable features of this plot are the following:

(i) I_{SC} remains constant with δ upto a critical thickness
        δ_{SC} and then decreases.

(ii) V_{OC} increases with δ, reaches a maximum and flattens
        out and then at a critical thickness δ_{OC} starts
        decreasing.

Although some heuristic arguments have been provided
in the published literature to explain the behaviour of Fig.2.1,
to the best of our knowledge no analytical attempt has been
made to quantitatively obtain the behaviour of V_{OC} for
$\delta > \delta_{OC}$ and I_{SC} for $\delta > \delta_{SC}$. In this chapter we attempt
to develop such an analytical theory. This has been possible
because of the inclusion of (a) The variation of the density
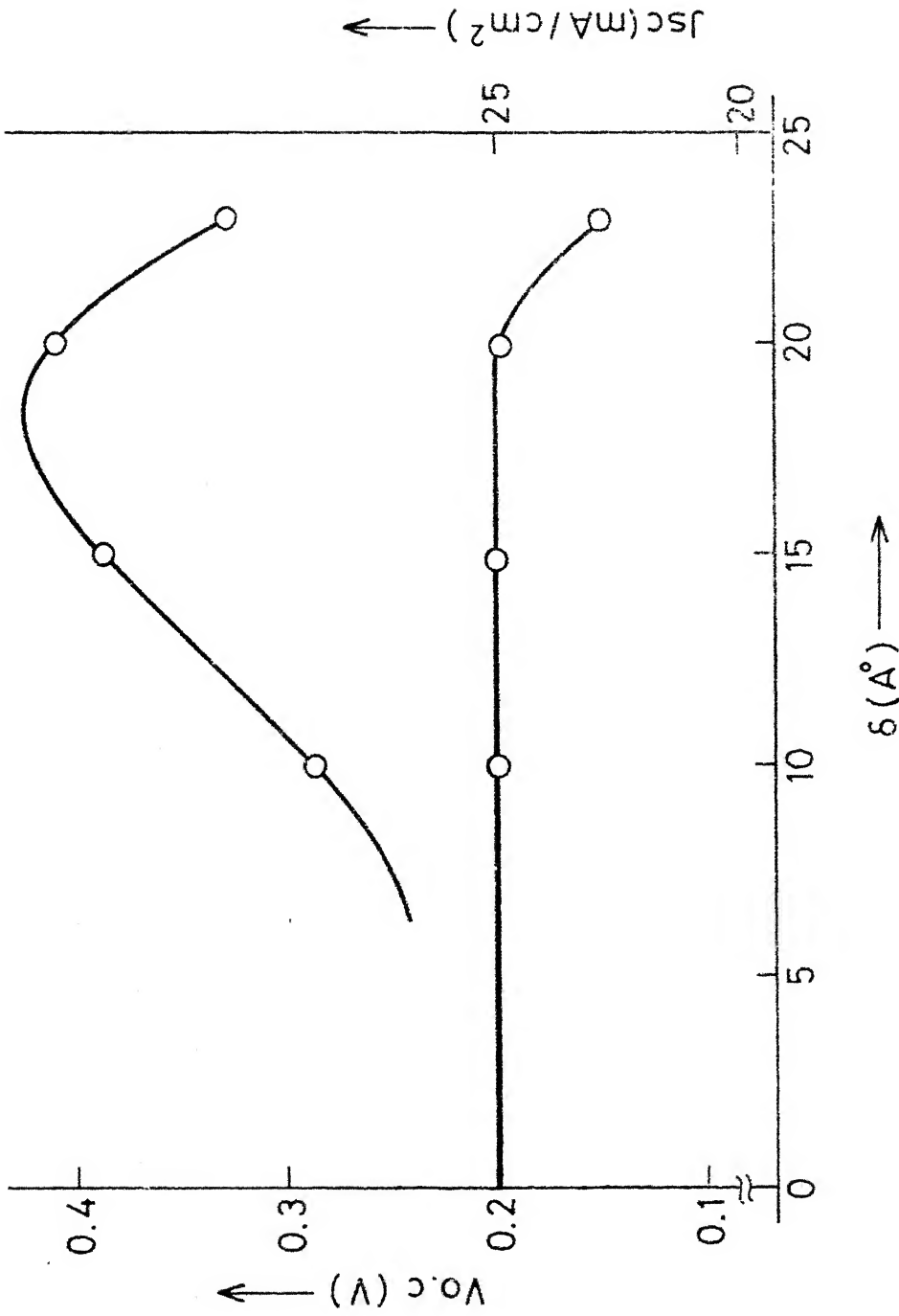
Fig.2.1 A plot of the **short** circuit current density Jsc and the open circuit voltage Voc versus the oxide thickness δ, taken from experiments {Lillington and Townsend [1]}

of surface states with δ, while calculating the interface
recombination current and the barrier height and (b) The
shift, under illumination, of the minority carrier quasi-
Fermi level from the metal Fermi level.

In the published literature there are several [15]
theoretical analysis of MIS solar cells. Each of these has
emphasized different aspects of the problem. In particular,
we would like to mention here the works of Landsberg and
Klimpke [12], Buxo etal.[13], Card and Yang[11] and Card [14].
Landsberg and Klimpke have considered the effect of recombina-
tion at the interface in detail and have investigated the effect
of the density of surface states on the efficiency of the cell,
but they have ignored the splitting of the minority carrier
quasi-Fermi level from the metal Fermi level. This latter
effect has been taken into account by Buxo etal.[13], but
these authors have ignored any recombination at the interface
or any other effect due to the density of surface states.Card
and Yang [11] were perhaps the first to point out the role
played by the splitting of the quasi Fermi level of the minority
carriers from the metal Fermi level, but they have restricted
themselves to a qualitative [11] or a semi-quantitative [14]
analysis. The work of some other workers in the area has
already been reviewed by Olsen in a recent paper [15] hence
is not being repeated here. In the present work attention has
been restricted mainly to the analysis of the variation of the

short circuit current and the open circuit voltage with the oxide thickness. To do this both the factors (a) and (b) mentioned above have been included. Though several workers have considered them separately, their joint effect, to the best of our knowledge has not been investigated earlier. It is also to be pointed out that the importance of variation of the density of surface states with the oxide thickness in explaining the behaviour of MIS cells has not been realized in any of the earlier published works.

The expressions for V_{OC} and I_{SC} with the inclusion of the factors (a) and (b) mentioned above have been developed in Sec.2.3, where it has also been shown that with suitable approximation in the expression given here, the familiar expressions for V_{OC} given in the literature by other workers fall out. In order to obtain numerical values from these expressions one would need the value of the barrier height under illumination and the values of some other parameters. The expressions for these have been developed in Sec. 2.2. The chapter has been concluded by developing an iterative scheme, which though complicated, allows the calculations of the illuminated current voltage characteristics of the Schottky (MIS) solar cell.

2.2 Energy Band Diagram

Our main interest is in developing the expressions for the open circuit voltage and the short circuit current

of an MIS cell. Before doing it, it is necessary to discuss
the features of the energy band diagram of an MIS solar cell.
These band diagrams (i) in thermal equilibrium,(ii) under
illumination (such that a forward voltage develops when a
load is connected) and (iii) under forward bias (but without
illumination), are given in Fig.2.2. The semiconductor is
taken to be N-type but similar considerations would also hold
for P-type semiconductor. In the following we consider the
diagrams of Fig.2.2 one by one.

2.2.1 Thermal Equilibrium

In thermal equilibrium, the interest is in knowing
the barrier height ϕ_B. This has been calculated by Cowley and
Sze [16] taking the occupation probability as a step function,
i.e. a 0°K approximation; and by Landsberg and Klimpke [12]
by taking the occupation probability as Fermi Dirac distribu-
tion function and is given below (see Appendix B, equation
(B.16))

$$\phi_B \approx (\phi_M - \chi) - \frac{\delta^2 \rho_o}{2\,\epsilon_i} + \frac{qD_s\,\delta}{\epsilon_i} \; [E_G - kT \; \ln \{\frac{1+\exp(q\phi_B/kT)}{1+\exp(\frac{q\phi_B - E_G}{kT})} \}]$$

$$- \frac{q^2\,\delta}{\epsilon_i} D_s\phi_o - \frac{\delta}{\epsilon_i} \; \{2\,\epsilon_s \; qN_D(\phi_B - V_n) \}^{\frac{1}{2}} \qquad (2.1a)$$

where the symbols ϕ_M, χ , ϕ_o, ϵ_i, ϵ_s, q, N_D, E_G, ϕ_B, V_n
and D_s are described in the list of symbols in Appendix A
and δ and ρ_o represent, respectively the thickness of the
oxide layer and the fixed charge esntity in the oxide layer
under thermal equilibrium.

(a) Thermal equilibrium.
(b) Illuminated diode with load connected.
(c) With a forward bias voltage.
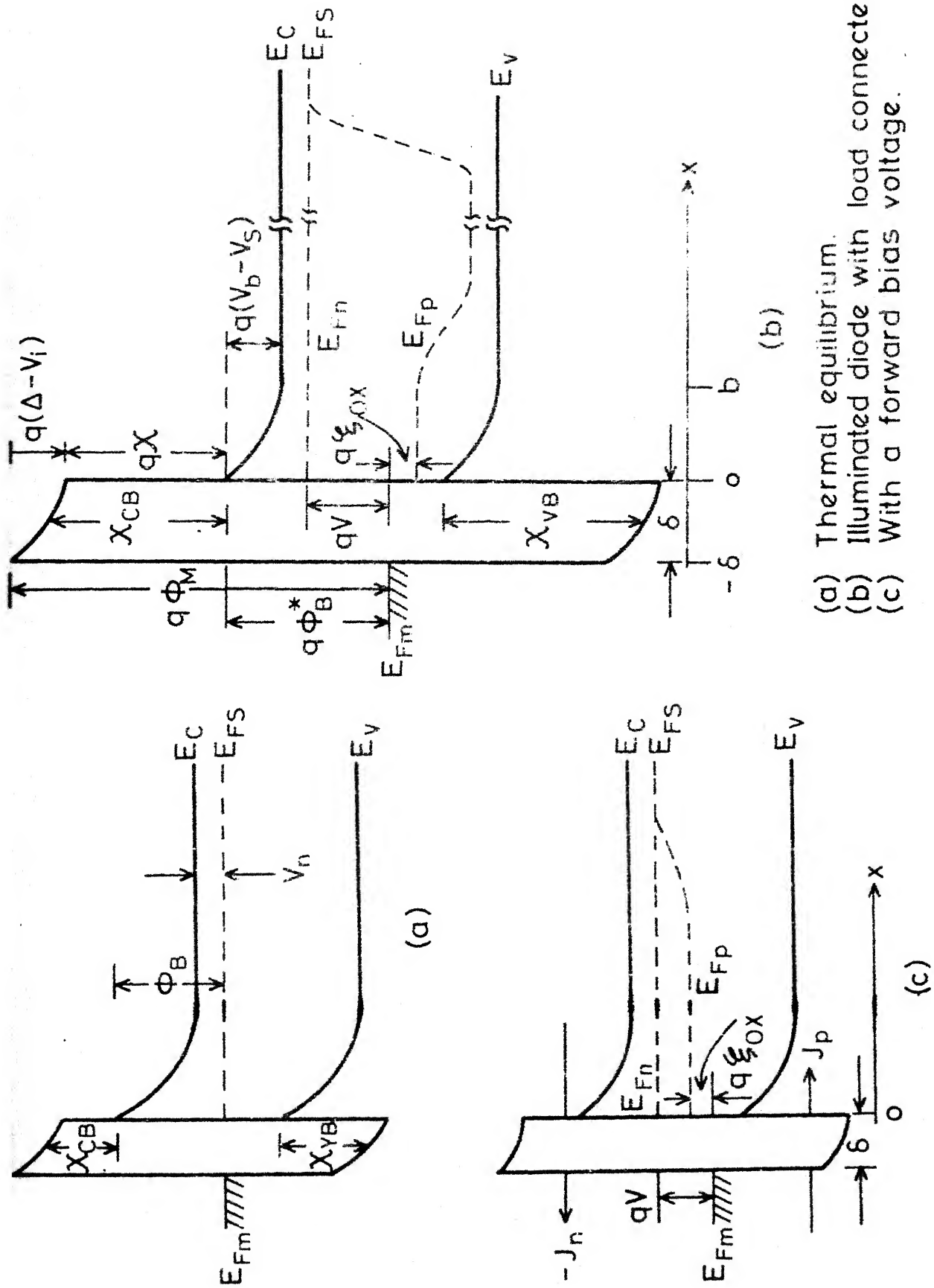
Fig.2.2 Energy band diagram of MIS diode.

Let us consider the role of ρ_0 in determining the barrier height $\emptyset_B$. There are four possibilities that can arise; these are positive and negative ρ_0 in the case of either N type or P type semiconductor. Let us consider the case of positive oxide charge first. For an M-I-N semiconductor cell a perusal of eqn. (2.1a) shows that with positive ρ_0, $\emptyset_B$ would decrease. Similar considerations show that with positive ρ_0, $\emptyset_B$ for the case of M-I-P semiconductor cell increases. Thus, since a large value of $\emptyset_B$ is desirable one would like to obtain if possible, positive oxide charge in a P type semiconductor and negative oxide charge in N type semiconductor. Technological difficulties in silicon, at the present perclude the presence of negative oxide charges, thus leaving the only case of interest as positive oxide charge in P type semiconductor. An analysis of this has been done by Pulfrey [9].

In the case that $\rho_0 = 0, \exp(q\emptyset_B/kT) \gg 1$ and $\exp\{(q\emptyset_B - E_G)/kT\} \ll 1$, eqn. (2.1a) reduce to the basic quadratic equation in $\emptyset_B$ of Cowley and Sze (see eqn. 21, p.374 of [17]). As is well known, Cowley and Sze have further obtained that in the case that a constant C_1 is given as

$$C_1 = \{ 2q \, \varepsilon_s \, N_D \, \delta^2 / \, \varepsilon_i^2 \}$$

is negligible, the barrier height is given by

$$\emptyset_{Bn} = C_2(\emptyset_M - \chi) + (1-C_2)(\frac{E_G}{q} - \emptyset_o) \qquad (2.1b)$$

where $C_2 = (1 + \frac{q^2 \delta}{\varepsilon} \cdot \frac{D_s}{i})^{-1}$.

It is interesting to note here that the neglect of the term containing C_1 is in effect equivalent to ignoring the space charge in the semiconductor, which means that a biased case such that a flat band occurs is being considered. If this consideration is introduced in the beginning itself, i.e. in the charge neutrality equation, then eqn.(2.1b) falls directly without requiring the solution of a quadratic [18]. Once $\emptyset_B$ is known, the equilibrium potential drop $V_b(=\emptyset_B-V_n)$ across the semiconductor, can be easily calculated by knowing V_n which depends on the doping and the temperature.

2.2.2 Illuminated Cells

When the cell is suitably illuminated from the metal side and a load is connected, the band diagram of Fig.2.2(b) ensues. The following points regarding this diagram should be noted.

(i) Under illumination and with a load connected, the MIS cell develops a potential difference V such that

$$V = V_s + V_i \qquad (2.2)$$

where (V_b-V_s) and $(\Delta - V_i)$ are respectively the potential drops across the semiconductor and the oxide layer. Here V_b is the diffusion potential. Expressions for Δ and V_i are developed in Sec. 2.2.3. Knowing V_i, a value of V_s

can be obtained from eqn. (2.2) for a given value of V.

(ii) The barrier height in this case gets modified and is denoted by $\emptyset_B^*$ where

$$\emptyset_B^* = (V_b - V_s) + V_n + V = (V_b + V_n) + (V - V_s)$$
$$= \emptyset_B + V_i \qquad (2.3)$$

(iii) Due to photogeneration of carriers in the semi-conductor two quasi-Fermi levels, one for electrons (E_{Fn}) and another for holes (E_{Fp}) have been shown in Fig.2.2(b). It has been assumed that the majority and minority carrier quasi-Fermi levels are constant in the depletion region. A justification of this is given later. Here we note that at a inter-face the minority carrier quasi-Fermi level E_{Fp} has been shown to be separated from the metal Fermi level E_{Fm} by an amount of $q\xi_{ox}$. The physical necessity of ξ_{ox} is due to the fact that its gradient across the insulator layer provides the driving force for the minority carriers to cross this layer. Thus one would expect that as the thickness of the oxide layer (δ) increases, ξ_{ox} would increase if it is required that the same number of photogenerated carrier should cross the insulating layer. But note that ξ_{ox} increases, the number of minority carriers at the interface increases, which in turn increases the number of minority carriers at the semiconductor edge of the depletion region. This then modifies the boundary condition for the solution of the diffusion equation needed to obtain the profile of photogenerated carriers. The net effect of this modification

is to reduce the short circuit current J_{SC}. This happens because with E_{Fp} constant through the depletion region one gets $E_{Fp}(b) = \xi_{ox}$, which when used in eqn. (1.11b) of J_{diff}, shows the J_{diff} increases with increasing δ. Since J_{diff} subtracts from J_L, J_{SC} decreases with increasing δ.

(iv) Let us now consider the position-dependence of $E_{Fn}(x)$ and $E_{Fp}(x)$ in the depletion region. If the transport of the majority carriers is governed by thermionic emission then $E_{Fn}(x)$ remains constant in the depletion region [19]. The nature of $E_{Fp}(x)$ can be obtained by recalling the behaviour of eqn. (1.9b), which we rewrite in a modified form for N type semiconductor.

$$\exp \left[-\left(\frac{E_{Fp}(b) - E_{Fp}(o)}{kT} \right) \right] - 1$$

$$= J_p \, N_d^{\frac{1}{2}} \, (1/n_i^2 \, \mu \, p)(\pi \varepsilon_s/2q^2 kT)^{\frac{1}{2}} \, \exp(E_{Fp}(o)/kT)$$

$$(2.4)$$

Note that $E_{Fp}(o) = q \xi_{ox} < 0$. It is apparent from eqn. (2.4) that as ξ_{ox} increases, the difference between the Fermi level at $x = 0$ and $x = b$ would decrease. Thus $E_{Fp}(x)$ becomes flatter and flatter in the depletion region as ξ_{ox} increases. In Sec. 2.3.1, we would show that the range of our calculations is such that taking $E_{Fp}(x)$ constant in the depletion region becomes valid.

(v) The potential difference V at the terminals of the cell is equal to $| E_{Fs} - E_{Fm} | /q$, where $E_{Fs} = E_{Fh}$ in the bulk of the semiconductor. In the conventional situation where $\xi_{ox} = 0$

note that $|E_{Fn}-E_{Fp}|/q = V$. Since the split $E_{Fn}-E_{Fp}$ is controlled by photogeneration of carriers, it is obvious that a non-zero value of ξ_{ox} entails a loss in available V. Thus ξ_{ox} is a "necessary" evil for $\delta < \delta_{SC}$ in as much as it keeps J_{SC} constant with increasing δ but entails a loss in the developed voltage available at the external terminals. In the case that $\delta > \delta_{SC}$ such that J_{SC} starts falling with δ the presence of ξ_{ox} becomes completely disadvantageous.

2.2.3 Charge Balance Equation

The relation $\phi_B^* = \phi_B + V_i$ given by eqn. (2.3) exhibits that to know ϕ_B^* one has to know ϕ_B and V_i. An expression for ϕ_B is given in eqn.(2.1). Here we setforth to obtain an expression for V_i. This can be obtained by considering the charge balance equation in dark,

$$Q_M + Q_{OX} + Q_i + Q_{SC} = 0 \qquad (2.5a)$$

and under illumination

$$Q_M^* + Q_{OX}^* + Q_i^* + Q_{SC}^* = 0 \qquad (2.5b)$$

Here Q_M, Q_{OX}, Q_i and Q_{SC} are the charges per unit area in the case of thermal equilibrium respectively in the metal, the oxide layer, the surface states and the space charge region of the semiconductor. Those with asterisk superscripts are the corresponding charges under illumination. In the following discussion we would consider $Q_{OX} = \rho\delta$, $Q_{OX}^* = \rho^*\delta$, where ρ and ρ^* are the charge densities in the oxide in

thermal equilibrium and under illumination, respectively, and are assumed to be constants. The functional dependence of Q_i, Q_i^*, Q_{SC} and Q_{SC}^* has been given in Appendix B.

Here we proceed to obtain an expression for V_i in terms of ρ, ρ^*, Q_i, Q_i^*, Q_{SC} and Q_{SC}^*, so that when the functional dependences of these are determined, a value of V_i may be obtained. The first task is the determination of the potential drop Δ across the oxide layer in thermal equilibrium.

Solving the Poisson's equation in the oxide,

$$\frac{d^2 \Psi}{dx^2} = - \frac{\rho}{\varepsilon} \; ; \text{ one obtains}$$

$$\Delta = \Psi(o) - \Psi(-\delta)$$

$$= \frac{\delta}{\varepsilon_i} [\tfrac{1}{2} \delta \rho + Q_i + Q_{SC}] \tag{2.6}$$

Since Δ is the difference of potentials at two points, only one boundary condition $\varepsilon_i \frac{d\Psi}{dx} = (Q_i + Q_{SC})$ at $x = 0$ has been utilized in deriving eqn. (2.6). Following a procedure similar to the one used for the derivation of eqn. (2.6), under illumination one obtains the potential drop across the oxide $(\Delta - V_i)$ as:

$$\Delta - V_i = \frac{\delta}{\varepsilon_i} [\tfrac{1}{2} \delta \rho^* + Q_i^* + Q_{SC}^*] \tag{2.7}$$

From equations (2.6) and (2.7) one obtains

$$- V_i = \frac{\delta}{\varepsilon_i} [\tfrac{1}{2}(Q_{OX}^* - Q_{OX}) + (Q_i^* - Q_i) + (Q_{SC}^* - Q_{SC})] \tag{2.8}$$

Once V_i is known V_s can be obtained from eqn.(2.2) for a
given value of voltage V developed under illumination for
a given load.

So far we have considered V_i under illumination.
In the case that the diode is not illuminated but is
forward biased by an applied voltage, let us replace V_i by
a corresponding V_i^f; the expression for which can be written
in analogy with eqn.(2.8) as

$$-V_i^f = \frac{\delta}{\epsilon_i} [\tfrac{1}{2}(Q_{OX}^f - Q_{OX}) + (Q_i^f - Q_i) + (Q_{SC}^f - Q_{SC})] \qquad (2.9)$$

Here Q_{OX}^f, Q_i^f and Q_{SC}^f are the respective charge density in
the oxide, surface states and depletion layer under forward
bias.

Thus if the expressions for Q_i, Q_i^*, Q_i^f, Q_{SC}, Q_{SC}^*
and Q_{SC}^f are developed, one can obtain the values of V_i and
V_i^f. These expressions have been given in Appendix B. Note
that here we have taken a constant charge in the oxide layer.
In the case that this is not true, one would also require the
expressions for Q_{OX}, Q_{OX}^* and Q_{OX}^f. To summarize, it is now
possible to obtain the distribution of a developed voltage
V in the oxide region (V_i) and in the semiconductor depletion
region (V_s). With this distribution known, we can now
proceed to consider the current voltage relation of the
Schottky (MIS) solar cell. Before concluding let us also
note that the expressions for charges may themselves depend

upon the current voltage characteristics in which case an iterative analysis would be required. Two cases where this iteration is simpler correspond to the short-circuited and open-circuited conditions of the diode. Since the analysis in these two cases is simpler and provides physical insight in the operation of the device, we have considered them in detail in the following sections.

2.3 I-V Characteristics

Our interest is in the calculation of the illuminated I-V characteristics of an MIS solar cell. Particular attention has been paid to two specific cases corresponding to the open circuited and short circuited conditions of the cell. But before considering these, let us consider the mechanism of current transport through an MIS solar cell made on an N type semiconductor. Let $J_n(x)$ and $J_p(x)$ be the majority and minority carrier current densities, respectively, flowing through an illuminated cell. The majority carrier current density J_n is governed by the same equation as in electrically biased case under dark and has been discussed by Card and Rhoderick [19]. They obtain:

$$J_n = A_n^{**} T^2 \alpha_n \exp(-q\phi_B^*/kT) [\exp(qV/kT) -1] \qquad (2.10)$$

where A_n^{**} is the Richardson constant, $\alpha_n = \exp[-\chi_{CB}(\delta)^{\frac{1}{2}}\delta]$, $\chi_{CB}(\delta)$ is the barrier height for majority carrier across the oxide layer as shown in Fig. 2.2, V is the developed

voltage and $\emptyset_B^*$ is the barrier height under illumination. Note that in the case of a dark but forward biased diode, $\emptyset_B^*$ is replaced by $\emptyset_B^f$.

The minority carrier component is given as

$$-J_p = J_L - J_{diff} - J_{R1} - J_{R2} \tag{2.11}$$

The component J_L is the light generated current density and is the same as in the case of SBSC as given in eqn.(1.13). Note that J_L contains the sum of the effect of photo-generated carriers in the depletion layer and the quasi-neutral region. The component J_{diff} is due to the flow of some of the photo-generated minority carriers in a direction opposite to the flow of J_L as explained in Sec. 1.2.2. There the expression for J_{diff} is given by eqn. (1.11b) which we rewrite for convenience:

$$J_{diff} = J'_{diff} \left[\exp \left\{ \frac{q(V - \xi_{OX})}{kT} \right\} - 1 \right] \tag{2.12}$$

where

$$J'_{diff} = qD_p\, p_{nO}/L_p \tag{2.12a}$$

Note that we have used the relation $E_{Fp}(b) = \xi_{OX}$ and have also introduced the effect of the developed voltage in this expression.

The component J_{R1} is due to the recombination at the interface layer and an expression for this, using Schockley-Read-Hall (SRH) theory [20,21], has been developed by Landsberg and Klimpke [12]. The steps of its derivation has been outlined in Appendix B and lead to the expression

$$J_{R1} = J_R' \, [\exp\{\, q(v- \xi_{OX})/kT\,\} -1\,] \qquad\qquad (2.13)$$

where

$$J_R' = n_i^2 \, \frac{kT\, D_s H(o)}{n_o(o)(A-B)} \; \ln\left[\frac{\{\exp(\frac{q\varnothing_B^*}{kT})-A\}\{\exp(\frac{q\varnothing_B^* - E_G}{kT})-A\}}{\{\exp(\frac{q\varnothing_B^*}{kT})-B\}\{\exp(\frac{q\varnothing_B^* - E_G}{kT})-B\}} \right]$$

$$(2.14a)$$

and

$$\left.\begin{matrix}A\\B\end{matrix}\right\} = -\left[\frac{G(o)\, n(o) + H(o)\, p(o)}{2G(o)n_o(o)} \right] \pm \left\{ \left[\frac{G(o)n(o) + H(o)p(o)}{2G(o)n_o(o)}\right]^2 - \frac{H(o)P_o(o)}{G(o)n_o(o)} \right\}^{\frac{1}{2}}$$

$$(2.14b)$$

where

$$G(o) = T_1^S + T_1 \, n(o) + T_2 \, p(o)$$

$$H(o) = T_2^S + T_3 \, n(o) + T_4 \, p(o)$$

The reaction constants T_1^S, T_2^S, T_1, T_2, T_3 and T_4 are defined in Appendix B and will be taken to be the same for all interface states [12]. $n(o)$ and $p(o)$ are respecively electron and hole concentration at $x = 0$ and expressions for them are given later in eqns. (2.17a) and (2.17b). $n_o(o)$ and $p_o(o)$ are relevant carrier concentrations in thermal equilibrium.

The component J_{R2} is due to the recombination of the photogenerated carriers in the depletion region and its expression is well known [17]. It varies as $\exp[\, q(V-\xi_{OX})/2kT\,]$ as compared to the $\exp[\, q(V- \xi_{OX})/kT\,]$ variation of J_{R1}. Also the values of preexponential factors in J_{R1} and J_{R2} are such that for the range of our calculations $J_{R1} \gg J_{R2}$. Hence the effect of J_{R2} has been ignored in the following analysis.

Before concluding the considerations of the current components, it is important to note that the minority carrier density J_p given by eqn. (2.11) must also be the minority carrier current density that tunnels through the oxide layer, i.e. J_p can also be written as

$$-J_p = A_p^{**} T^2 \; \alpha_p \; \exp[\; \frac{-E_g + q\emptyset_B^* - q\xi_{OX}}{kT} \;] \; [1 - \exp(\frac{q\xi_{OX}}{kT}) \;] \qquad (2.15)$$

$$= J'_{tunnel}[\; \exp(-q\xi_{OX}/kT) \; -1] \qquad (2.15a)$$

where

$$\alpha_p = \exp \; [-\chi_{VB}(\delta)^{\frac{1}{2}} \; \delta \,] \qquad (2.15b)$$

and

$$E_g - q\emptyset_B^* + q\xi_{OX} = E_{Fp} - E_v \qquad (2.15c)$$

Here $\chi_{VB}(\delta)$ is the barrier height across the oxide for the minority carriers as shown in Fig.2.2. In the following sections we use these equations of current transport to obtain the short circuit current, the open circuit voltage and then the I-V characteristics of the MIS cells. The values of parameters that have been used are given in Appendix B.

2.3.1 Variation of I_{SC} with δ :

The experimental features of $I_{SC}(\delta)$ in an MIS solar cell is that it remains constant upto some $\delta < \delta_{SC}$ and then starts falling off [1]. In the following, we have attempted to explain this feature.

The short circuit current for an MIS cell on N type semiconductor is given as $I_{SC} = aJ_p$ where a is the area of the cell and taken as 1 cm^2, and J_p is the minority carrier current density given by eqn. (2.11), which we rewrite for convenience

$$-J_p = J_L - J_{diff} - J_{R1} - J_{R2} \qquad (2.11)$$

In the following we have neglected the term J_{R2} due to the reasons given earlier. The expression for J_L is the same as in the case of Schottky barriers and is given by eqn.(1.13). We take the value $J_L = 25$ mA/cm^2 in the present calculations. To evaluate J_{diff} and J_{R1} one needs the value of ξ_{OX} for the short circuited case. The general expression for ξ_{OX} can be obtained by using eqn. (2.12) and (2.13) in eqn. (2.11) and then equating it to eqn. (2.15). The resulting expression for ξ_{OX} is

$$- \xi_{OX} = \frac{kT}{q} \ln[\frac{J_L + J'_{diff} + J'_R + J'_{tunnel}}{(J'_{diff} + J'_R)\exp(\frac{qV}{kT}) + J'_{tunnel}}] \qquad (2.16)$$

In the case of short circuit, i.e. $V = 0$, one gets,

$$- \xi_{OX} = \frac{kT}{q} \ln[1 + (\frac{J_L}{J'_{diff} + J'_R + J'_{tunnel}})] \qquad (2.16a)$$

Here J'_{diff}, J'_R and J'_{tunnel} are defined by eqns. (2.12a), (2.13a) and (2.15a), respectively.

We would start the calculations by making two simplifications:

(i) The effect of the component J_{R1} due to recombination at the interface is initially neglected. The effect of its inclusion is discussed later.

(ii) The simplified expression for the barrier height $\emptyset_B$ in thermal equilibrium, as given by Cowley and Sze [16], is used:

$$\emptyset_B = C_2(\emptyset_M - \chi) + (1-C_2)(\frac{E_G}{q} - \emptyset_o) \qquad (2.1b)$$

where

$$C_2 = (1 + q^2 \delta D_s/\epsilon_i)^{-1}$$

The effect of taking the more general expression for $\emptyset_B$ as given by eqn.(2.1a) has also been discussed later.

We note from eqn.(2.1b) that for the range of δ considered and for $D_s \approx 2 \times 10^{11}$ per eV per cm^2 one gets $q\emptyset_B \simeq \emptyset_M - \chi$. We have chosen $(\emptyset_M - \chi) = 0.69$ eV and 0.5 eV; a comment on this choice is given later. ξ_{OX} is plotted from eqn.(2.16a) and is shown in Fig. 2.4(c). In short circuited case J_p^{SC} (or J_{SC}) represents the total current density and has been calculated using the values of ξ_{OX}^{SC} (i.e. ξ_{OX} at short circuit) in eqn.(2.11). The plot of J_{SC} versus δ is given in Fig.2.3(a) for $\emptyset_M - \chi = 0.5$ eV and 0.69 eV. Note that starting from $\delta = 20$ A° a drop in current takes place for $(\emptyset_M - \chi) = 0.5$ eV but not for $(\emptyset_M - \chi) = 0.69$ eV. The physical reason for this can be seen as follows.
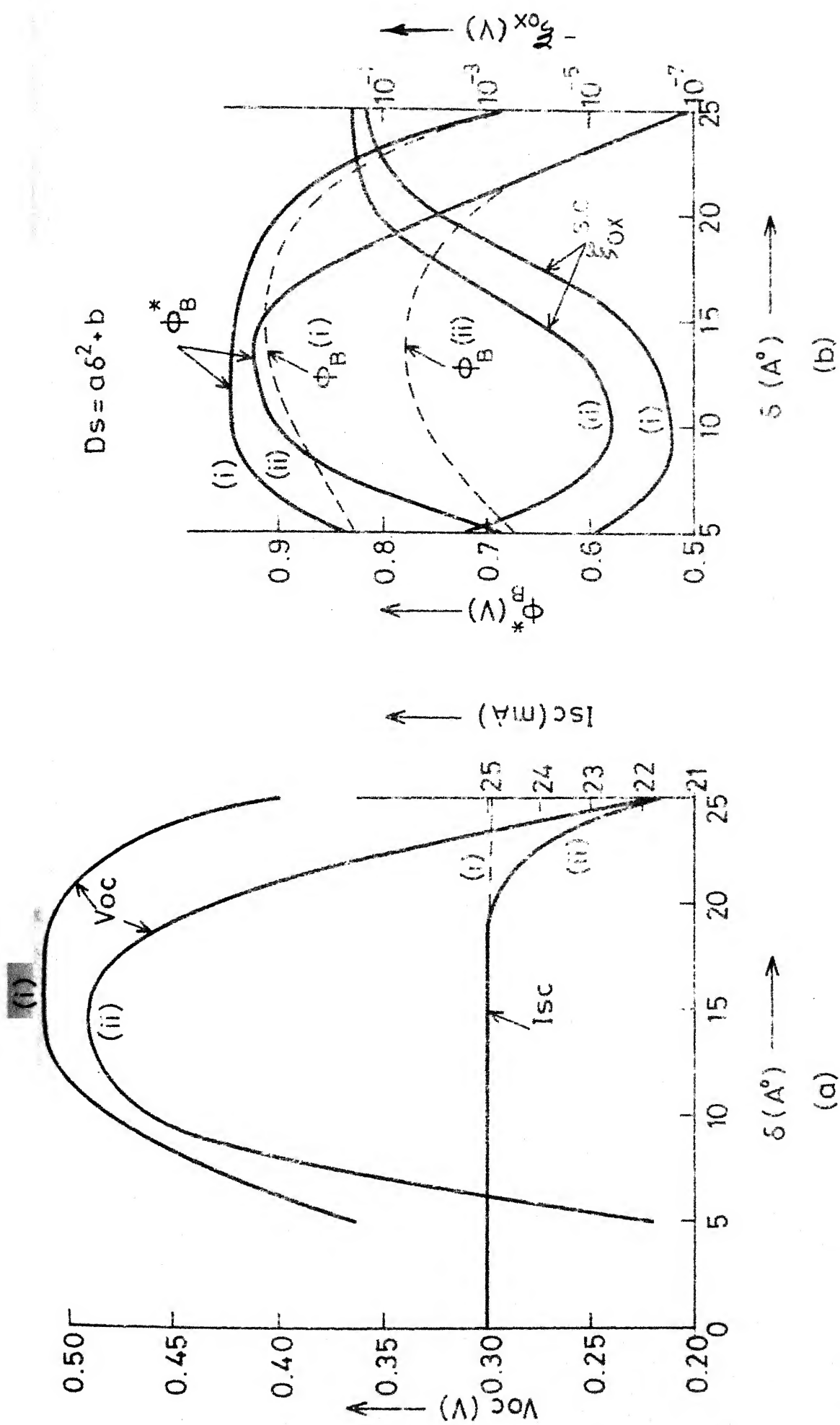
Fig 2.3 Label (i) Corresponds to $(\phi_M - \chi) = 0.69\ eV$ and label (ii) to $(\phi_M - \chi) = 0.5\ eV$.

50
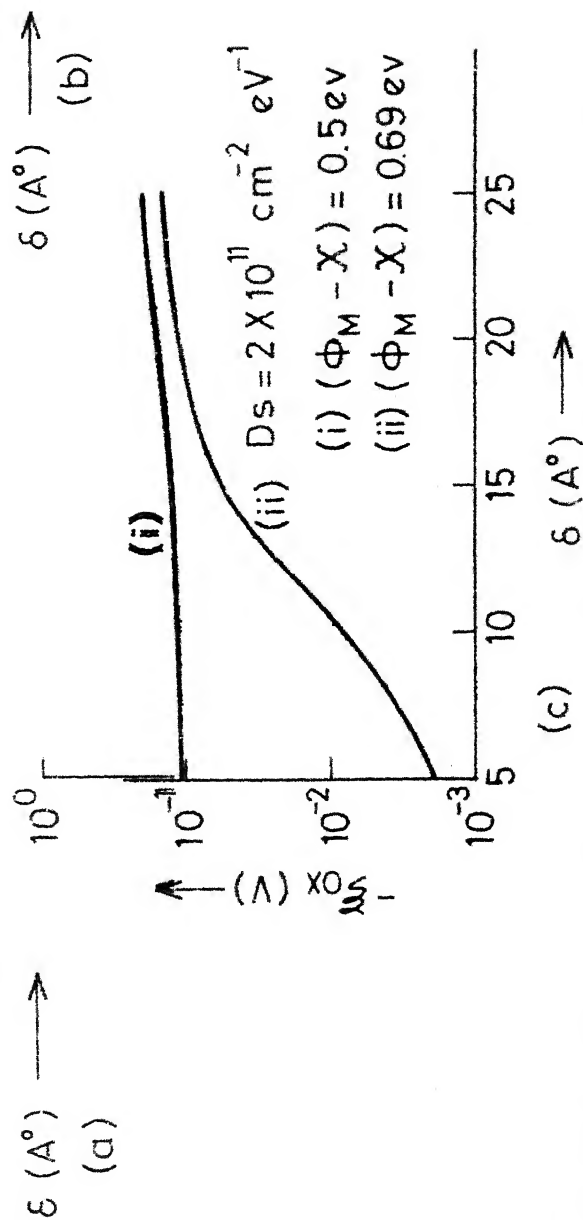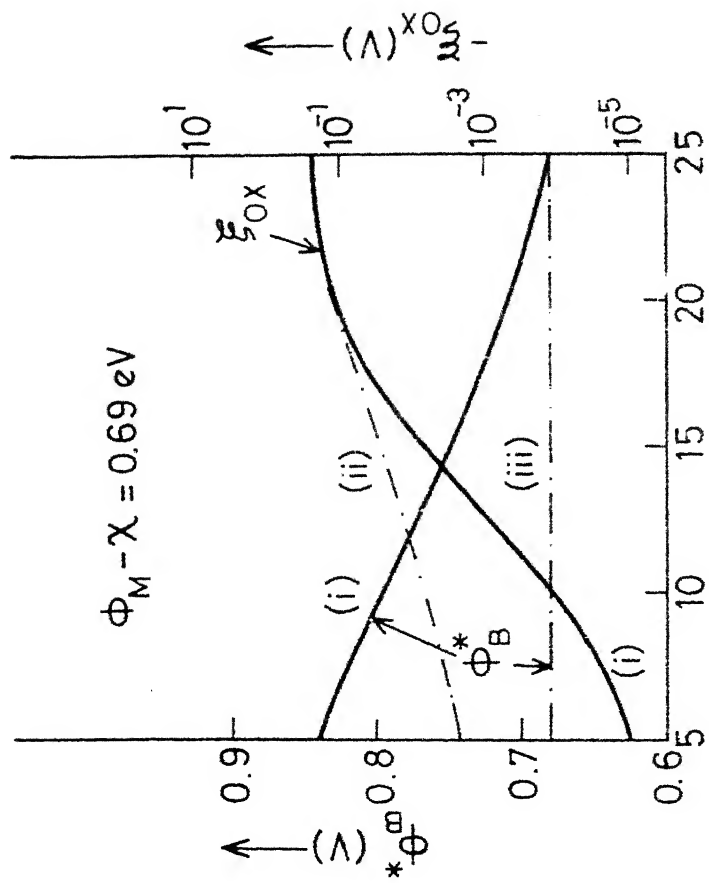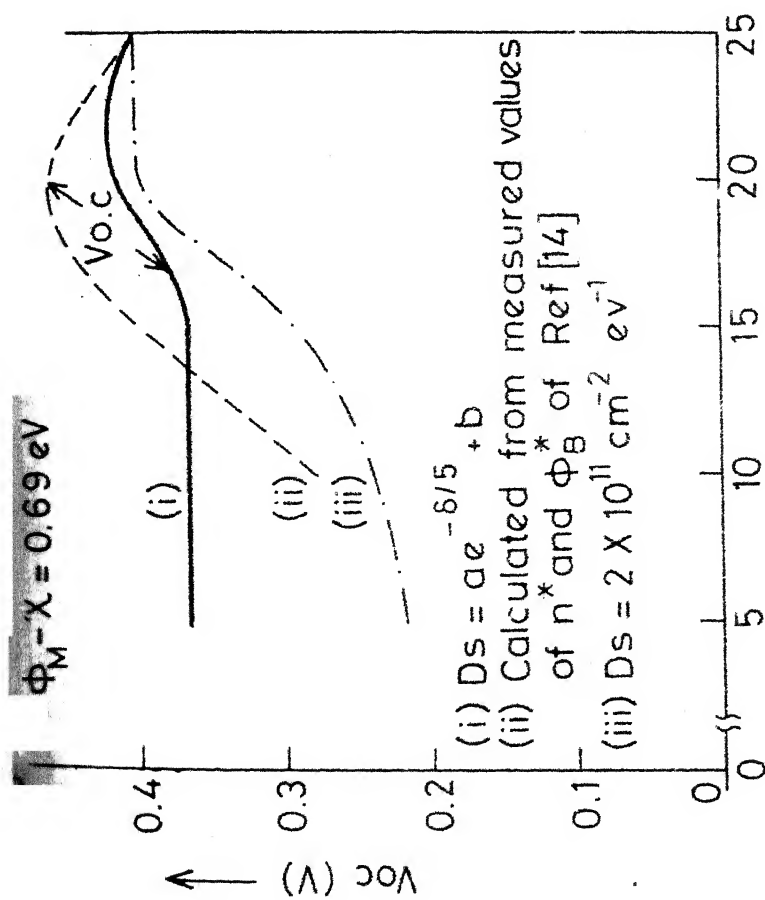
Fig. 2.4 Plots of the open circuit voltage Voc versus δ. & Plots of the barrier height ϕ_B^*, and ξ_{OX} versus δ

(i) Let us consider the behaviour of $J_{diff}(\delta)$ defined in eqn.(2.12) for $V = 0$. To start the discussion let us calculate the value of $\xi_{OX}(\delta)$ that is needed to to get, say, $J_{diff}(\delta) = 1$ mA/cm^2. For the parameters chosen one gets $-q\,\xi_{OX} = 0.434$ eV. We reiterate that as long as $-q\,\xi_{OX} < 0.434$ eV, the value of $J_{diff}(\delta)$ will not exceed 1 mA/cm^2. Note from Fig.2.4(c) that ξ_{OX}, for $(\emptyset_M - \chi) = 0.69$eV and in the range $0 < \delta < 25$ A°, remains below $-q\,\xi_{OX} = 0.434$ eV, resulting in almost constant value of $J_{SC}(\delta)$. In the case of $(\emptyset_M - \chi) = 0.5$ eV, $-q\,\xi_{OX}$ reaches a value of 0.434 eV at $\delta = 22\cdot 5$Å giving $J_{diff}(\delta_{SC}) = 1$ mA. This choice of δ_{SC} defined above is arbitrary. Here we take it to be that values of δ where current has falled by 1 mA/cm^2. Also note that in this case at $\delta = 25$A°, $J_{diff} = 4$ mA/cm^2, which is comparable to the drop experimentally obtained by Lillington and Townsend [1].

(ii) The discussion in (i) has exhibited the sensitivity of the fall of $J_{SC}(\delta)$ to the value of $\emptyset_B$, which in the present case of low value of D_S is given by $(\emptyset_M - \chi)$. The value of $q\emptyset_B = 0.69$ eV corresponds to the workfunction $\emptyset_M = 4.7$ eV for gold vacuum interface and electron affinity $\chi = 4.01$ eV for silicon. The value $(\emptyset_M - \chi) = 0.5$ eV has been chosen to match the experimental results of barrier height for $\delta > 20$ A° in the case of Au-SiO$_2$-nSi diodes [14].

It is obvious that it is desirable that J_{SC} should not fall with δ. The discussion given above points out that for this to happen, $\phi_B(\delta)$ should be larger than a certain threshold value. This can be obtained by either choosing larger value of $(\phi_M - \chi)$ and/or large value of $D_s(\delta)\delta$ product. In order to meet the requirement of large barrier height at a chosen δ a large value of $D_s(\delta)$ is desirable if high values of $(\phi_M - \chi)$ can not be obtained. Care, however, has to be taken in choosing a large value of $D_s(\delta)$ because it also affects the current J_{R1} due to recombination at the interface, which adversely affects the open circuit voltage [12]. Hence, we would return to the choice of $D_s(\delta)$, after discussing the behaviour of the open circuit voltage.

In the beginning we have ignored the effect of J_{R1}. Let us now include it and see its effect on $J_{SC}(\delta)$. To include the effect of J_{R1} from eqn.(2.13), the value of $J_R^!$ is needed. $J_R^!$ is evaluated from eqn. (2.14a). This needs evaluating $n(o)$, $p(o)$, $n_o(o)$, $p_o(o)$ and the values of n_i, T, $G(o)$ and $H(o)$. The expressions used for $n(o)$ and $p(o)$ are

$$n(o) = N_C \exp\left[-\frac{q(\phi_B^* - V)}{kT} \right] = N_C \exp\left[-\frac{E_C - E_{Fn}}{kT} \right] \quad (2.17a)$$

$$p(o) = N_V \exp\left[\frac{-E_G + q(\phi_B^* - \xi_{OX})}{kT} \right] = N_V \exp\left[\frac{E_V - E_{Fp}}{kT} \right] \quad (2.17b)$$

$n_o(o)$ and $p_o(o)$ are obtained, respectively, from eqns.(2.17a)

and (2.17b) by putting $\xi_{OX} = 0$ and replacing $\emptyset_B^*$ by $\emptyset_B$. Note that $\emptyset_B^*$ with illumination but for V=0 is almost equal to $\emptyset_B$. n_i is the intrinsic concentration in silicon at T = 300°K. We have assumed G(o) = H(o) following Landsberg etal [12]. The expression for G(o) is given in Appendix B. The calculation of $J_R^!$ is started by taking $\xi_{OX} = 0$. With this value of $J_R^!$, ξ_{OX} is calculated from eqn. (2.16a). This value of ξ_{OX} is now used to calculate $J_R^!$, and the iteration is continued till ξ_{OX} converges within a limit of error. Using the values of $\emptyset_B$ and ξ_{OX} at V=0, $J_{R1}(\delta)$ at short circuit is calculated. The maximum value of $J_{R1}(\delta)$ under short circuit is of the order of 10^{-6} amps/cm^2, hence it is justified to ignore its effect on $J_{SC}(\delta)$ since it contains $J_L(\delta)$ which has been taken to be 25 mA/cm^2. Also note that when the more general expression for $\emptyset_B$ given by eqn.(2.1a) was used, instead of eqn. (2.1b), no significant change in $J_{SC}(\delta)$ was found.

While discussing the behaviour of the energy band profile at the beginning of this chapter, we had assumed that the minority carrier quasi-Fermi level $E_{Fp}(x)$ would remain constant throughout the depletion region. We now set out to seek the justification for this assumption. Let us rewrite eqn. (2.4) in a modified form as

$$-E_{Fp}(b) = -q\,\xi_{OX} + kT \ln [\, 1+M \exp(q\,\xi_{OX}/kT)\,] \qquad (2.4)$$

$$\text{where } M = J_p N_D^{\frac{1}{2}} \left(\frac{1}{n_i^2 \mu_p}\right)\left(\frac{\pi \varepsilon_s}{2q^2 kT}\right)^{\frac{1}{2}}$$

We consider the following cases:

(i) If $M \exp(q\, \xi_{OX}/kT) \ll 1$, then $E_{Fp}(b) = \xi_{OX}$; thus $E_{Fp}(x)$ is flat in the depletion region. To get the limit on ξ_{OX} for this to be true, we can use the relation $\xi_{OX} = \frac{kT}{q} \ln(k/M)$ where $k \ll 1$. Taking $k = 1$ and M calculated for the parameters mentioned above, we get a typical value of $q\xi_{OX} = -0.036$ eV, above which E_{Fp} becomes flat.

(ii) If $M \exp(q\, \xi_{OX}/kT) \gg 1$, the $E_{Fp}(b) = -kT \ln(M)$, which is the case of SBSC (where $\delta = 0$). There we have found $E_{Fp}(b) = -0.33$ eV; which is the worst case of the bending of $E_{Fp}(x)$. We have already noted an important fact that for $J_{diff}(\delta)$ to equal 1 ma/cm^2, the amount of $E_{Fp}(b)$ needed is -0.434eV. This leads us to the conclusion that in this case though $E_{Fp}(x)$ is not constant, the worst case value is such that it does not affect our calculation.

2.3.2 The Open Circuit Voltage (V_{OC}):

In this particular case the sum of the majority and minority carrier components of current densities has to be zero, i.e.

$$J_n(x) + J_p(x) = 0 \qquad (2.18)$$

In order to use eqn.(2.18) to obtain V_{OC} one needs to get an expression for ξ_{OX}. This is given by eqn.(2.16) with $V = V_{OC}$. Note that $J_R^!$ in eqn. (2.16) depends on ξ_{OX}, hence the value of ξ_{OX} can only be obtained by iteration. The

next task is to obtain V_{OC}. This is done by using eqn.(2.18) with $J_n(x)$ taken from (2.10) and $J_p(x)$ taken from (2.15) and ξ_{OX} taken from (2.16). This results in a quadratic equation in $\exp(qV_{OV}/kT)$ given as follows:

$$\exp(2qV_{OC}/kT) + \mu_1 \exp(qV_{OV}/kT) - \frac{J_L \,\alpha_p \exp(\frac{-E_g+2q\emptyset_B^*}{kT})\,A_p^{**}}{(J'_{diff} + J'_R)\,\alpha_n\,A_n^{**}} = 0 \qquad (2.19)$$

where

$$\mu_1 = \frac{J_{tunnel}}{(J'_{diff}+J'_R)} + \exp(\cdot\frac{-E_G+2q\emptyset_B^*}{kT})\,\frac{\alpha_p\,A_p^{**}}{\alpha_n\,A_n^{**}} \qquad (2.20)$$

Hence one obtains

$$V_{OC} = \frac{kT}{q} \ln [-\frac{\mu_1}{2} + \frac{1}{2}\{ \mu_1^2 + \frac{4J_L\,\alpha_p \exp(-\frac{E_G+2q\emptyset_B^*}{kT})\,A_p^{**}}{(J'_{diff} + J'_R)\,\alpha_n\,A_n^{**}} \}^{1/2}] \qquad (2.21)$$

Before using eqn. (2.21) for determining V_{OC}, let us digress to simplify this expression and compare the simplified expression with the results existing in the published literature.

Let us consider the case where the currents J_{diff} and J_R are negligible. In this case eqn. (2.19) simplifies to

$$\exp(qV_{OC}) [J'_{tunnel} \exp(-q\emptyset_B^* /kT)] = \frac{\alpha_p\,J_L}{\alpha_n} \exp(\frac{-E_g+q\emptyset_B^*}{kT}) \frac{A_p^{**}}{A_n^{**}} \qquad (2.22)$$

or

$$V_{OC} = \phi_B^* + \frac{kT}{q} \ln\left(\frac{J_L}{A_n^{**}T^2\alpha_n}\right) \qquad (2.23)$$

Using $\phi_B^* = \phi_B + V_i$, and the relation $n = V_{OC}/(V_{OC}-V_i)$, which is the value of the ideality factor for the open circuit case; one can rewrite eqn. (2.23) as

$$V_{OC} = n\phi_B + \frac{nkT}{q} \ln\left(\frac{J_L}{A_n^{**}T^2\alpha_n}\right) \qquad (2.24)$$

If α_n is taken to be unity, eqn. (2.24) is the same equation as the one given by Anderson etal[22]which they have correlated with several expressions of V_{OC} available in literature at that time. Before proceeding further, let us consider the nature of variation of V_{OC} with δ as prediced by eqn. (2.23). Here ϕ_B^* and α_n are functions of δ. As δ increases α_n monotonically decreases, thereby the second term on right side of eqn. (2.23) monotonically increases. If one now demands that V_{OC} fall with δ, in any range of δ it becomes necessary that ϕ_B^* must decrease with δ in that range; the rate of change being of proper amplitude to annul the effect of the increase in the second term. We know that $\phi_B^* = \phi_B + V_i$, and one possibility for decrease of ϕ_B^* with δ is that both ϕ_B and V_i decrease with δ. Perusal of eqn. (2.1a) and (2.8) for ϕ_B (for $(\phi_M-\chi) < (E_G/q-\phi_0)$)and V_i (for $Q_{SC}=Q_{SC}^*$),respectively leads to the following conclusions.

(A) If $(\phi_M-\chi)$ is constant with δ then both ϕ_B and V_i would decrease if the product $D_s\delta$ decreases with increasing δ.

This leads to a very important conclusion, that D_S with constant value, under this model, cannot explain the experimental feature that V_{OC} decreases with increase of δ for $\delta > \delta_{OC}$; rather it is incumbent that a $D_S(\delta)$ function be chosen which decreases faster than linearly, for $\delta > \delta_{OC}$. It is also important to note that to explain the experimentally observed initial increase of V_{OC} with δ, the product $D_S(\delta)\delta$ must increase in this range. These then are the guide lines for choosing a proper variation of $D_S(\delta)$. The experimentally observed fact that D_S is lower for $Si-SiO_2$ system than for bare silicon [23] is conductive to physical existance of such $D_S(\delta)$. The only problem is in choosing the proper functional variation, since to the best of our knowledge no experimental results in this direction are available. To get a physical feel·we have decided to study two functional dependences (i) $D_S = a\ \delta^2 + b$ and (ii) $D_S = C\ exp(-\delta/\delta') + d$ which, as is obvious, have two extreme natures of variation of $D_S(\delta)\delta$. For the sake of comparison the results for a constant value of D_S ($= 10^{11}/eV/cm^2$) have also been calculated and are given in Fig.2.4(a).

(B) So far we have considered $(\emptyset_M - \chi)$ to be constant with δ and required D_S to be a function of δ. The values of $\emptyset_B$ and V_i would also decrease if $D_S = 0$, but $(\emptyset_M - \chi)$ be a function of δ. However, this model would require that $(\emptyset_M - \chi)$ initially increases with δ and then starts decreasing, which seems rather

contrary to the physical situation. In an actual situation, both $(\emptyset_M - \chi)$ and D_S can become monotonically decreasing function of δ , such that the initial increase of V_{OC} with δ is governed by the increase in $D_S(\delta)\delta$ and constancy of $(\emptyset_M - \chi)$, whereas the fall of V_{OC} for $\delta > \delta_{OC}$ is due to a combined effect of fall of $D_S(\delta)\delta$ and $(\emptyset_M - \chi)$. However, for the sake of simplicity we have only concentrated on the case where $(\emptyset_M - \chi)$ is constant and $D_S(\delta)\delta$ varies in the fashion mentioned earlier.

To obtain a plot of V_{OC} versus δ, using eqn.(2.21) one needs to know J_L, J_R', J'_{tunnel} and $\emptyset_B^*$. For this an iterative process has been used using the following steps:

(i) J_L and J'_{diff} have the same values as in the case of the calculation of I_{SC} in Sec. 2.3.1.

(ii) Taking $\emptyset_B$ and ξ_{OX} at $V = 0$, as calculated in Sec. 2.3.1, J_R' and J'_{tunnel} are calculated. Using these values in eqn. (2.21) a value of V_{OC} is obtained.

(iii) Using this value of V_{OC} for V, V_i is calculated from eqn. (2.3) and the relevant expressions of Appendix B. Thus $\emptyset_B^*$ for this value of V_{OC} is obtained.

(iv) n(o) and p(o) are calculated from eqns.(2.17a) and (2.17b) for this new $\emptyset_B^*$.

(v) ξ_{OX} at this $V = V_{OC}$ is obtained from eqn. (2.16). Then step (iv) is repeated for this new ξ_{OX} until p(o) converges within given accuracy.

(vi) $J_R^!$ and $J_{tunnel}^!$ are calculated for $\emptyset_B^*$ and ξ_{OX} obtained from step(iii) and (v) and used in eqn. (2.22) to obtain V_{OC}. Steps (iii) to (v) are repeated until desired accuracy is obtained.

The plots of V_{OC} versus δ using this procedure are given in Figs.2.3(a) and 2.4(a).Let us note the following features.

(i) First of all let us consider the cases for $(\emptyset_M - \chi)$ = 0.69 eV with $D_s = a \delta^2 + b$, $D_s = C \exp(-\delta/\delta') + d$ and $D_s = 10^{11}/eV/cm^2$ which have been shown in Fig. 2.3a(i), Fig. 2.4a(i) and (iii), respectively. Note that whereas in the first two cases V_{OC} falls off at large values of δ, in the third case there is no such fall off as would be antici-pated from the discussion following eqn.(2.24). Also note that these features are supported by the respective plots of $\emptyset_B^*$ versus δ, given in Fig. 2.3(b) and Fig. 2.4(b).

(ii) The values of V_{OC} have also been calculated for $(\emptyset_M - \chi)$ = 0.5 eV and different distributions of $D_s(\delta)$. The features of the results are very similar to the previous case (e.g. see 2.3(ii)); thus from the consideration of V_{OC} alone one may not realize the importance of choosing the proper value of $(\emptyset_M - \chi)$. However, if the choice of parameters is to be such that the experimental nature of both $I_{SC}(\delta)$ and $V_{OC}(\delta)$ is simultaneously explained, as they must be, there is no choice but to discard the value of $(\emptyset_M - \chi)$ = 0.69 eV.

(iii) Regarding the choice between the variation $D_s = a \delta^2 + b$ and $D_s = C \exp(-\delta/\delta') + b$, one notes that from Fig. 2.3a(i) and Fig.2.4a(i), that the variation of $V_{oc}(\delta)$ in the previous case is more akin to the experimental results [1] than the latter one. This suggests, based on the experimental results of Lillington and Townsend [1] that there is a great likelihood that $D_s(\delta)$ would be nearer to a parabolic variation in this case. We have also calculated $I_{sc}(\delta)$ with different functional dependences of $D_s(\delta)$ and have found that there is no perceptible difference between the different cases. Hence while discussing $I_{sc}(\delta)$, only the case with constant D_s was mentioned.

2.3.3 Illuminated I-V Characteristics:

So far we have concentrated on two particular cases, the short circuited and open circuited conditions, of the illuminated I-V characteristics of an MIS cell. But from the point of view of efficiency a knowledge of the complete I-V characteristics is needed. The basic equations needed for this calculation have already been developed in the earlier sections; as a matter of fact these have been used in the calculation of I_{sc} and V_{oc}. While calculating the complete I-V characteristics, the difference from the calculation of I_{sc} and V_{oc} appears in the form of more elaborate iterative procedure. This is given below.

i) Consider a given V at which I is desired. Assume $\xi_{ox} = 0$.

ii) Calculate $\phi_B^* = \phi_B + V_i$, by obtaining ϕ_B from eqn.(2.1a) and V_i from eqn. (2.8). Since $V = V_i + V_s$, V_s is now known.

iii) Calculate J_L from the method of Chapter 1 and J_{diff}, J_{R1} and J_{tunnel} using eqns. (2.12), (2.13) and (2.14). Thus the minority carrier component of current is known.

iv) Calculate ξ_{OX} from eqn.(2.16).

v) Repeat steps (ii) to (iv) till convergence within required limit of error is obtained.

vi) Obtain the minority current from step (iii) and the majority carrier one from eqn. (2.10). Thus the total current is known for the given V.

vii) At each V repeat the steps from (i) to (vi).

Also, note that if ξ_{OX} is taken to be zero, then, obviously no iteration is needed for ξ_{OX} and this is the case treated by Landsberg and Klimpke [12] for computing the efficiency in an MIS solar cell. In the case that there is interest in the efficiency for the non-zero value of ξ_{OX}, the iterative procedure given here can be pursued, but we have not carried out this calculation.

2.4 Summary:

In this chapter an analysis of Schottky (MIS) solar cell has been given. The effect of charges due to interface states and the effect of the splitting of the minority carrier quasi-Fermi level from the metal Fermi level have been

included in the model. This has been utilized to explain
the experimentally observed features of an MIS cell (taking
$Au-SiO_2-nSi$ cell as example) that the short circuit current
remains constant upto some δ and then starts falling, and
that the open circuit voltage initially increases with δ,
reaches a maximum, flattens out and then starts dropping.
It is worthwhile to compare the present analysis with that
of Buxo etal [13]. They have found that in the range of
where I_{SC} is falling with δ, V_{OC} remains constant (see
Fig.3 and 4 of [13]). This result seems to be unphysical
because this can only happen if $\emptyset_B^*$ increases with δ at
a required rate; but this is the region where Buxo etal [13]
have, in essence, assumed $\emptyset_B^*$ to be independent of δ. This
discrepancy has been removed in the present chapter. In the
next chapter we undertake to study an alternate method for
increasing the open-circuit voltage of a Schottky-barrier-
based solar cell.

CHAPTER 3

SCHOTTKY BARRIERS WITH OPPOSITELY DOPED INTERFACE LAYER

A method for increasing the open-circuit voltage of
a Schottky barrier solar cell (SBSC) is to introduce a thin
insulating layer between the metal and the semiconductor
resulting in an MIS solar cell. This has already been
described in the previous chapter. In this chapter we
consider another recent technique which increases the open-
circuit voltage of a SBSC, but as yet has not found wide
prevalence in the solar cell literature. Due to this reason
we would elaborate the basic principles of the method in some
detail. The method consists of oppositely doping a thin
layer of the semiconductor substrate before depositing the
metal, thus giving rise to a metal-P-N or metal-N-P structure.
Of course, one can extend the idea to jointly incorporate
this thin oppositely doped layer along with a thin insulating
layer resulting in a metal-(thin) insulator-P-N or metal(thin)
insulator-N-P structure. A perusal of the published literature
shows that so far there has been only one experimental attempt
in this direction by Pai et al [1], where they have obtained
the oppositely doped layer by ion implantation and then grown
thin SiO_x before evaporating a thin layer of metal. This
cell provides some unique advantages which have been described
later.

Before proceeding further, it is important to note that the usefulness of the M-P-N or M-N-P structures, which arises due to their ability to increase the effective barrier height, is not limited to solar cells only. As a matter of fact, they form a part of the class where an effective control, either decrease or increase of the barrier height is desired. Hence, in this chapter, we would keep the initial discussions at a general level so that these are applicable to many devices and later return to solar cells.

Schottky barriers are employed in a variety of semiconductor devices (for example, Schottky-gate field effect transistor [2], Schottky-barrier solar cells [3,4], injection controlled transferred electron devices [4] etc.) and in all of these it is desirable to control the height of the barrier to optimize the device performance. However, it is well known that in commonly employed semiconductors like Si, GaAs etc., this control becomes difficult because the barrier height cannot be appreciably varied by choosing metals with different work functions; rather it is largely controlled by the interface surface-state-density which is fixed. To obviate this limitation, several workers [5-10] have experimentally as well as theoretically demonstrated that the presence of a thin doped semiconducting layer at the interface can be used to control the effective barrier height. If the surface layer is of the same type as the

bulk semiconductor (e.g. metal-N^+(thin)-N structure) then a decrease in effective barrier height is obtained [5,8]. A limiting case of this is obtained when the doping and thickness of interfacial layer are large so that ohmic contact is formed [5]. On the other hand, for structures like metal-(thin)P-N where the interface layer is oppositely doped to the bulk, an increase in the barrier height ensues. Shannon has obtained the thin interfacial layer, for both these cases by ion-implantation [6,7] and has compared the experimental and theoretical results [8]. Recently, Van-der-Ziel [9] has theoretically calculated the barrier height for epitaxial metal-P-N structure. The purpose of the analysis in the present chapter is to obtain the potential profile and thereby the range of geometrical and material parameters which would provide the control of the barrier height and then apply these to the case of solar cells. The calculation includes the effect of mobile carriers which allows the determination of some of the parameters which would not have been possible otherwise. But before doing this, in the next section we give a physical description of the role of the interface layer in changing the potential profile, briefly review the work of Van-der-Ziel [9]; and then give the potential profile calculation including the effect of mobile carriers.

3.1 Potential Profile of Doped Interface-Layer Structure

Let us consider a metal-semiconductor Schottky diode which is characterized by the barrier height $\emptyset_{Bo}$ and the type and doping of the bulk semiconductor. In the following we take the bulk semiconductor to be of N type with a doping density N_d. The calculations can be easily modified for P-type bulk semiconductor. When an interface-layer (P or N type) is metallurgically interposed between the metal and the bulk semiconductor, the potential profile $\Psi(x)$ in the vicinity of the metal contact is modified as shown in Fig.3.1. If the interfacial layer is of opposite type to the bulk and its doping and width are suitably chosen (as discussed in Sec. 3.2), a minimum Ψ_m in potential appears at a distance x_m from the metal (Fig. 3.1b). Thus an effective increase in the barrier-height is obtained. If the width of the interfacial layer, keeping the doping constant, is further increased, there is a flattening of the potential profile at the minimum point and the structure behaves as a metal-P-semiconductor Schottky diode in series with a P-N junction (Fig. 3.1c). It is also possible that the width and doping of the interfacial layer is such that a minimum in potential profile does not appear, i.e. no barrier height increase takes place, as is the case in Fig. 3.1(d). When the interfacial layer is of the same type as the bulk, but is more heavily doped, then depending upon the width and doping of
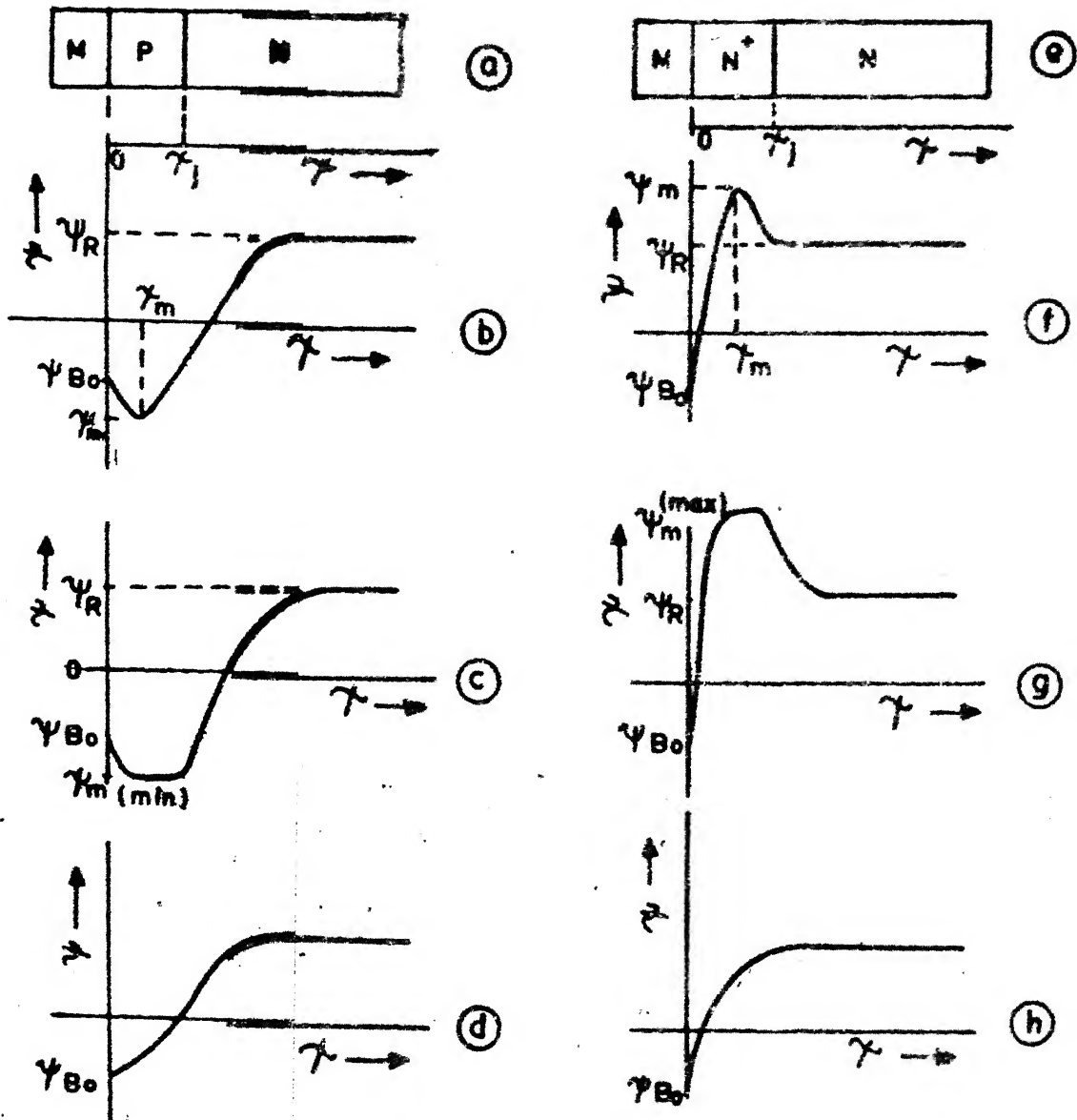
Fig.3.1 Metal-P-N and Metal-N⁺-N structures and the
potential profiles (see text for description).

this layer one may obtain an ohmic or an injecting contact.
This distinction depends on two features, the first being
the condition whether the space-charge at the high-low
interface is wiped out or not, and the second being the
mechanism of current transport, field-emission or thermionic-
field emission, at the metal contact as discussed in [5]. When
the interfacial layer is heavily doped and is sufficiently
thick such that potential profile of Fig.3.1(g) ensues then
the contact behaves as ohmic. If keeping the doping constant,
the width of this layer is reduced to an optimum value, then
the flattening at the maximum of the potential profile
vanishes as shown in Fig. 3.1(f). This width of the inter-
facial layer is the minimum width which must be exceeded to
form an ohmic contact. In the case that the potential
profile is monotonic and the doping of interfacial layer is
such as to lead to thermionic field-emission, an injecting
contact is obtained.

We would calculate the general profiles including
the effect of mobile carriers in Sec. 3.1.2. In the
following section we consider an M-P-N structure and
follow the treatment of Van-der-Ziel[9] where the effect
of mobile carriers has been ignored.

3.1.1 Potential profile of M-P-N diode in depletion approximation

An M-P-N structure is shown in Fig. 3.1(a). Let
the width of the p layer be W_p and W_n be the width over

which the space charge region extends into the n-region and let x = 0 be at the metal contact. Further, assume that an abrupt junction has been made. Then in the depletion approximation Poisson's equation are

$$\frac{d^2\Psi}{dx^2} = \frac{qN_a}{\varepsilon_s \varepsilon_o} \quad \text{for} \quad 0 < x < W_p \tag{3.1a}$$

and

$$\frac{d^2\Psi}{dx^2} = -\frac{qN_d}{\varepsilon_s \varepsilon_o} \quad \text{for } W_p < x < (W_p + W_n) \tag{3.1b}$$

where q is the charge of the electron, ε_s is the dielectric constant of the semiconductor and ε_o is the permittivity of the free space.

The initial conditions are:

(a) $\Psi(o) = 0, \Psi(W_p + W_n) = \emptyset_{m1} - \emptyset_n - V$ (3.2)

where $\emptyset_{m1}$ and $\emptyset_n$ denote the work functions of the metal electrode and the n type semiconductor and V is the applied voltage.

(b) $\Psi(x)$ and $d\Psi/dx$ are continuous at $x = W_p$.

(c) $\left.\frac{d\Psi}{dx}\right|_0 = \frac{qN_d W_n - qN_a W_p}{\varepsilon_s \varepsilon_o}$ (3.3)

$\left.\frac{d\Psi}{dx}\right|_{(W_p + W_n)} = 0$ (3.4)

The solution for $0 \leq x \leq W_p$ is

$$\Psi(x) = \Psi_1(x) = \frac{qN_a}{\varepsilon_s \varepsilon_o}\left(\frac{1}{2}x^2 - x W_p\right) + \frac{qN_d}{\varepsilon_s \varepsilon_o} W_n x \tag{3.5}$$

whereas for $W_p \leq x \leq W_p + W_n$.

$$\Psi(x) = \Psi_2(x) = -\frac{qN_d}{\varepsilon_s \varepsilon_0}[\tfrac{1}{2}x^2 - x(W_n + W_p)] - \tfrac{1}{2}\frac{q(N_a + N_d)}{\varepsilon_s \varepsilon_0}W_p^2$$

(3.6)

The width of the space-charge in the N-region is obtained from the second boundary condition of eqn. (3.2a), that is

$$\emptyset_{m1} - \emptyset_n - V = \tfrac{1}{2}\frac{qN_d}{\varepsilon_s \varepsilon_0}(W_p + W_n)^2 - \tfrac{1}{2}q(\frac{N_a + N_d}{\varepsilon_s \varepsilon_0})W_p^2$$

(3.7)

When $N_d W_n < N_a W_p$, a potential minimum exists in front of the metal electrode. The position x_m follows from the condition $d\Psi/dx = 0$ at $x = x_m$, which gives

$$\frac{qN_a}{\varepsilon_s \varepsilon_0}(x - W_p) + \frac{qN_d}{\varepsilon_s \varepsilon_0}W_n = 0$$

or
(3.8)
$$x = x_m = W_p - \frac{N_d}{N_a}W_n$$

whereas its depth $\Delta\emptyset_B(V)$ is determined by substituting $x = x_m$ in eqn. (3.5).

Using some assumed values of the relevant parameters, Van-der-Ziel [9] has computed the amount of increase of barrier height which gives physical results. However, we have found that though the computations of [9] are valid for the range of parameters given in that paper, great caution must be exercised when extending this to a different combination of the values of parameters. This is mainly because of the reason that in [9] only a necessary condition

for the increase of barrier height has been taken into account, whereas another condition needed for sufficiency of this has been ignored. This would be discussed in Sec.3.2. Further, note that Van-der-Ziel has noted that in order to get meaningful results for a given N_a and N_d, the width of the P-layer should have a lower bound $W_p(min)$ and an upper bound $W_p(max)$. But his analysis not amenable to direct calculations of $W_p(min)$ and $W_p(max)$, rather a trial and error method has to be adopted. A method which includes the effect of mobile carriers and allows the direct calculation of $W_p(min)$ and $W_p(max)$ has been developed in this thesis and is given in Sec. 3.2. But before giving this the general calculations including the effect of mobile carriers (but in thermal equilibrium) for both $M-N^+-N$ and $M-P-N$ are given in the following section.

3.1.2 Potential profiles of M-P-N and M-N$^+$-N Structures:

The potential profile $\Psi(x)$ can be obtained by solving the Poisson's equation:

$$\frac{d^2\Psi}{dx^2} = -\frac{q}{\epsilon_0 \epsilon_s} [\ N(x) + p - n\ ] \qquad (3.9)$$

where $N(x)$ is net doping density and n and p are, respectively the electron and the hole concentrations. The symbols q, ϵ_s, ϵ_0 have been described in the previous section. The following cases where a solution of eqn. (3.9) can be obtained are of our interest.

(a) The effect of mobile carriers is ignored, i.e. p=n=0. This is the case discussed in the previous section. The calculations done there has inherent limitations as would become clear from the following discussion. As barrier height increases, for a P-type interface the valence band approaches the Fermi level and the number of minority carrier increases. Thus a limit is reached where the calculations done under depletion approximation become meaningless. One would be interested in knowing this limit below which the depletion approximation can be used. It is obvious that this limit can only be obtained if minority carriers are included in the calculation and the point where departure from the results of depletion approximation occurs, is noted. This has been our motivation for including the effect of mobile carriers in the calculation given below. To the best of our knowledge such an approach has not been taken earlier.

(b) The effect of mobile carriers are included but only thermal equilibrium condition is considered. In this case a closed-form expression for n and p can be obtained either by making Ehrenburg's [11,12] or Boltzman's approximation to the Fermi-Dirac distribution function. In the case that one makes Ehrenburg's approximation, one gets [11,12]

$$p = 4N_V \ [4\exp(\frac{E_G}{2} + q \ \Psi)/kT+1 \ ]^{-1} \tag{3.9a}$$

and

$$n = 4N_C \ [4\exp(\frac{E_G}{2} - q\Psi)/kT+1 \ ]^{-1} \qquad (3.9b)$$

where E_G is the bandgap, and N_C and N_V are, respectively, the effective density of states of the conduction and valance band. These expressions for p and n are valid even for degenerate semiconductors in case the excursion of the Fermi-level in the bands does not exceed 2kT. Hence these equations are to be used if any of the semiconductors are degenerately doped. Here the reference potential corresponds to the Fermi-level in the metal.

In the case that Boltzmann approximation is used to express p and n, one obtains

$$p = n_i \ \exp(-q\Psi/kT) \qquad (3.9c)$$

$$n = n_i \ \exp(q\Psi/kT) \qquad (3.9d)$$

where n_i is the intrinsic carriers concentration. Here the reference of Ψ is the point where $p = n = n_i$. The solutions of eqn. (3.9) with Ehrenburg's approximation are given in this section. Those with Boltzmann approximation can be easily obtained following similar analysis.

(c) The effect of mobile carriers are included and either reverse biased or forward biased devices are considered. In these cases, ideally, the current continuity equations and the Poisson's equation should be simultaneously solved. However, since the equations are coupled and nonlinear, it becomes extremely difficult to get closed form or simple

numerical methods of solution. A simplification can be brought in by considering the reverse-biased case where negligible current flows. Since in this case the potential profile can be obtained by solving Poisson's equation alone. Furthermore, one can simplify the situation by considering either only p or n and not both; for an example in the case of M-P-N diode, in the depletion region only p, and not n, need be considered. This point would be further elaborated at the end of Section 3.2. In the case that a diode is forward biased there is no choice but to solve the coupled equations mentioned earlier. The only exception is the case of an open circuited solar cell, using this structure, since in this case again no current flows.

Let us now solve eqn. (3.9) using (3.9a) and (3.9b) for the case of thermal equilibrium. We would take the doping to be abrupt such that $N(x) = N_1$ for $x < x_j$ and $N(x) = N_2$ for $x > x_j$, where x_j denotes the metallurgical junction. Eqn. (3.9) is normalized such that $\psi = (q\Psi/kT)$, $X = x/L_D$ where L_D is the Debye length for doping N_1, i.e. $L_D = [kT \, \epsilon_s \, \epsilon_o/(q^2 \, N_1)]^{\frac{1}{2}}$ and the impurity and carrier densities are normalized with respect to N_1. We now restrict our attention exclusively to the potential profiles of the form of either Fig. 3.1(b) or 3.1(f). In these cases, to the right of X_j the electric field is zero for $\psi = \psi_R$ and to the left of X_j it is zero at $\psi = \psi_m$. Using these values to

eliminate the constant of integration, we integrate the normalized form of eqn. (3.9) for $\chi < \chi_j$ and $\chi > \chi_j$ to obtain

$$\frac{d\psi}{d\chi}\bigg|^2_{\chi<\chi_j} = \pm\, 2^{\frac{1}{2}} \left[-\frac{N_2}{N_1}(\psi - \psi_m) - 4\left(\frac{N_v}{N_1}\right)\ln\frac{F(\mu=\psi_m)}{F(\mu=\psi)} \right.$$
$$\left. - 4\left(\frac{N_C}{N_1}\right)\ln\frac{F(\mu=-\psi_m)}{F(\mu=-\psi)} \right]^{\frac{1}{2}} \tag{3.10}$$

$$\frac{d\psi}{d\chi}\bigg|_{\chi>\chi_j} = \pm\, 2^{\frac{1}{2}} \left[-(\psi - \psi_R) - 4\left(\frac{N_v}{N_1}\right)\ln\frac{F(\mu=\psi_R)}{F(\mu=\psi)} \right.$$
$$\left. - 4\left(\frac{N_C}{N_1}\right)\ln\frac{F(\mu=-\psi_R)}{F(\mu=-\psi)} \right]^{\frac{1}{2}} \tag{3.11}$$

where

$$F(\mu) = 1 + 0.25 \exp\left(-\frac{E_G}{2kT} - \mu\right) \tag{3.12}$$

and ψ_R is obtained by solving $N_1 + p - n = 0$ in the normalized notation and is given as

$$\psi_R = \ln\left[(A_2 + (A_2^2 + 4A_1A_3)^{\frac{1}{2}})/2A_1 \right] \tag{3.13}$$

where $A_1 = 4\exp(+E_G/2kT)[1 + (4N_v/N_1)]$

$$A_2 = 16\,\exp(+E_G/2kT) + 1 + (16/N_1)(N_v - N_C)$$

$$A_3 = 4\,\exp(+E_G/2kT)[(4N_C/N_1) - 1]$$

The signs in eqn. (3.10) are chosen as follows. For metal P-N diode (Fig. 3.1b) the negative sign is taken for $\chi_m < \chi < \chi_j$ and positive for $0 < \chi < \chi_m$. The case for metal N^+-N diode (Fig. 3.1f) is just opposite. In eqn. (3.11), the negative sign is taken for metal-P-N diode and positive one for metal-N^+-N diode. Using the proper signs and noting that the

electric field and the potential are continuous at metallur-
gical junction $X = X_j$, one obtains the potential ψ_j at X_j
by equating eqns. (3.10) and (3.11) as:

$$X_j = \left(\frac{N_2}{N_1} - 1\right)^{-1} \left[\left(\frac{N_2}{N_1}\psi_m - \psi_R\right) + \left(\frac{4N_\nabla}{N_1}\right)\ln\frac{F(\mu = \psi_R)}{F(\mu = \psi_m)} \right.$$

$$\left. + (4N_C/N_1) \ln\frac{F(\mu = -\psi_R)}{F(\mu = -\psi_m)} \right] \qquad (3.14)$$

The use of eqns. (3.9) to (3.14) allows the determination of
the potential profile in the following manner:

(i) If the doping N_1 of the bulk semiconductor is known
then ψ_R is determined from eqn. (3.13). Note that N_1 is a
positive quantity for donor impurities.

(ii) A knowledge of N_2 and ψ_m, along with the value of
ψ_R, allows the determination of ψ_j from eqn. (3.14). Here
N_2 is a positive quantity for donor impurities and a negative
quantity for acceptor impurities. Methods for choosing the
value of ψ_m in particular cases are given in Sections 3.2
and 3.3.

(iii) Starting from the value of ψ_j, the next step is to
use the Taylor-expansion:

$$\psi_{i+1} = \psi_i + (X_{i+1} - X_i)\psi_i' + \frac{(X_{i+1} - X_i)^2}{2!}\psi_i'' + \cdots$$

$$(3.15)$$

where the primes denote differentiation with respect to X.
It is to be noted that the expansion eqn. (3.15) also
determines the optimum step-size at each step to obtain a

desired amount of accuracy [13]. This is so because at each step ψ_i' is known from eqn. (3.10) or eqn. (3.11) and ψ_i'' is known from eqn. (3.9). Thus taking the ratio of the third term to the second one on the right of eqn. (3.15) and equating it to a fixed value, depending on desired accuracy, one can obtain the value of $(X_{i+1} - X_i)$ at that step.

(iv) Now the potential profiles in three different regions $0 < X < X_m$, $X_m < X < X_j$ and $X > X_j$ are obtained separately. Starting from ψ_j, eqn. (3.15) is used to the left till the chosen value of ψ_m is reached. This gives the potential profile for $X_m < X < X_j$. It is important to note that the distance $(X_j - X_m)$, which was unknown, has also been determined. Repeating the steps to the right of ψ_j till the potential reaches ψ_R, i.e. the neutral regions, the potential profile and the corresponding width of the space charge are obtained for $X > X_j$.

(v) The solution for the region $0 < X < X_m$ requires the value $\psi = \psi_{Bo}$ at $X = 0$. This can be obtained by knowing the barrier height $\emptyset_{Bo}$ without the interfacial layer. For the reference of potential chosen here, one obtains (see inset of Fig. 3.2):

$$\psi_{Bo} = (E_g / 2 - \emptyset_{Bo}) / kT \qquad (3.16)$$

Starting from ψ_{Bo} at $X = 0$, expansion in eqn. (3.15) is used to the right till the potential ψ_m is reached. Thus the

potential profile for the region $0 < \chi < \chi_m$, along with the unknown distance χ_m, is determined.

(vi) A knowledge of $(\chi_j - \chi_m)$ and χ_m allows the determination of χ_j, the metallurgical width of interface layer, for given values of N_1, N_2 and ψ_{Bo} so that a desired value of ψ_m is obtained. It is to be emphasized that the determination of this width is a significant advantage of the present method of calculation and is of help in designing the interfacial layer as is shown in the following sections.

So far we have considered the potential profiles which have an extremum but there is no flattening of the profile there. Next, let us consider the profiles given in Figs. 3.1(c) and 3.1(g). To determine the profiles in these cases the metallurgical width of the interface layer, along with the values of N_1, N_2 and ψ_{Bo}, should be known, because the present method cannot determine the width of the flat region near the extremum. The problem becomes basically of finding the potential-profile and the width of space-charge layer for Schottky barrier between the metal and the interface layer, and those of the high-low (or P-N) junction between the interface layer and the bulk semiconductor. All of these can be easily obtained by the present method. Subtraction of the sum of widths of space charge layers of Schottky-barrier and high-low (or P-N) junction from the metallurgical width of the interface layer determines the

width of the flat region at the extremum. Thus the potential profiles of the type shown in Figs. 3.1(c) and 3.1(g) can be determined. It should be mentioned here that this method, in a different context and with Boltzman's rather than Ehrenb rg's approximation of Fermi-Dirac integral, has been used earlier for high-low (or P-N) junctions with all the impurity atoms ionized [13] and with incomplete ionization of impurities [14]. However, in each of these cases the doping of high side is large enough that Boltzman approximation is not valid and the present method should be used to get accurate results.

The remaining profiles where there is no extremum but the interface layer is present cannot be obtained by the present method. This is because the constant of integration in obtaining eqn. (3.10) cannot be determined now.

In the following sections, use is made of the calculations given above to determine the parameters of the interface layer.

3.2 Barrier Height Increase in Metal-P-N Structures:

It has already been mentioned that an interfacial layer which is oppositely doped to the bulk semiconductor increases the barrier height, provided the width and doping of this layer are properly chosen. This is shown in the inset of Fig. 3.2. The considerations that help the determination
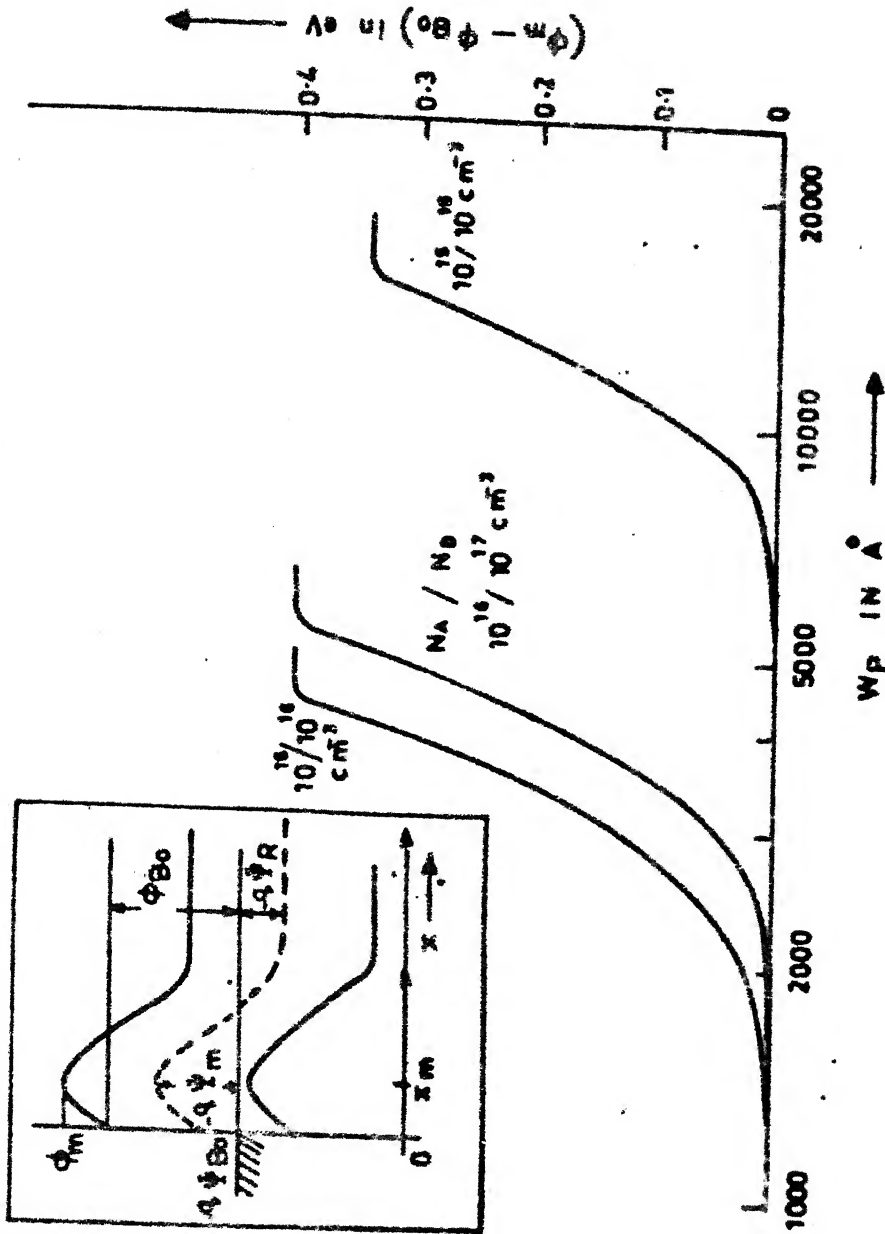
Fig. 3.2 $(\phi_m - \phi_{Bo})$ versus W_p for metal-p-n structures (in silicon), with dopings as parameters, $\phi_{Bo} = 0.504$ eV. Inset is energy band diagram corresponding to Fig.3.1(b).

of these parameters for a metal-P-N structure are discussed in this section. First we would consider the case of thermal equilibrium and then the cases with applied bias.

3.2.1 Thermal equilibrium conditions:

The aim is to determine the parameters such that a profile of the type of Fig. 3.1(b), and not of type of Fig. 3.1(c) where a P-N junction is formed or of type Fig. 3.1(c) where no barrier increase is available, is obtained. This constrains the value of ψ_m, which was taken as a parameter in Sec. 3.1 to lie between $\psi_{Bo} < \psi_m < \psi_m(min)$. The fact that ψ_m has to be less than ψ_{Bo} for barrier height increase is obvious. The value of $\psi_m(min)$ is shown in Fig. 3.1(c) and is determined only by doping N_a of the P-layer at a given temperature. It can be obtained by solving $(-N_a + p - n) = 0$ in the normalized notation and is given by eqn. (3.13) with N_1 replaced by $-N_a$. The fact that $\psi_m(min)$ is determined only by N_a at a given temperature leads to an important conclusion, i.e. the value of N_a corresponding to $\psi_m(min) = \psi_{Bo}$ is the minimum value, $N_a(min)$, which must be exceeded to obtain an increase in barrier height.

Theoretical calculations without recognising the existence of $N_a(min)$ can lead to misleading conclusions as would be evident from the following numerical example. Van-der-Ziel [9] has obtained the potential profile for a

metal-p-n structure without including the effect of mobile
carriers. He has concluded that for a barrier height increase
to take place, the inequality:

$$N_a W_p > N_d W_n \tag{3.17}$$

must be satisfied, where W_n is the width of the space-charge
layer on N-side of the metallurgical junction. For example,
silicon this is the case for $N_d = 10^{15}$ cm^{-3}, $\phi_{Bo} = 0.907$ eV,
$N_a = 10^{16}$ cm^{-3} and $W_p = 1000$ Å, where W_n from [9] is
8800 Å. For this case, Van-der-Ziel's calculation predicts
that a barrier height increase of 2 m eV would be obtained
and the peak in the potential-energy profile of electron
would be located 120 Å^o in front of the metal. Actually this
conclusion is misleading because for this case N_a(min), using
eqns. (3.16) and (3.13) with N_1 representing $-N_a$(min), is
1.29×10^{16} cm^{-3} which is larger than the value of N_a chosen
here; hence there is no possibility of obtaining a barrier
height increase. Thus the inequality $N_a > N_a$(min) along
with the inequality eqn. (3.17) forms the necessary and
sufficient condition for a barrier height increase to take
place. Note that the inequality (3.17)is useful when the
effect of mobile carriers is neglected, however, the require-
ment $N_a > N_a$(min) is valid in all the cases.

Let us choose a value of $N_a > N_a$(min). The considera-
tions that help in determination of N_a in a particular case
are given later. Presently our concern is to determine the

range $W_p(min) < W_p < W_p(max)$ of the width of p-layer, for a given N_a such that an increase of barrier height, but without the formation of a P-N junction, is obtained. This can be done by following the method of Sec. 3.1. The value of $W_p(min)$ is obtained when eqn. (3.9) is solved for $\psi_m = \psi_{Bo}$. Similarly, the value of $W_p(max)$ is obtained for $\psi_m = \psi_m(min)$ for given value of N_a. It is expected that the determination of $W_p(min)$ and $W_p(max)$ would be of help in the proper fabrication of these devices.

The general nature of the barrier height increase $\Delta\emptyset = \emptyset_m - \emptyset_{Bo}$, as a function of W_p with the doping N_a treated as a parameter for silicon at 300°K -. is shown in Fig. 3.2. The following features of this figure should be noted.

(a) For increasing value of N_a, the maximum attainable $\Delta\emptyset$ increases. However, the largest usable value of N_a may be limited by the solubility limit of the dopant, or by the fact that as N_a increases the required value of W_p gets smaller making the fabrication difficult, or that $(d\Delta\emptyset / dW_p)$ becomes sharper so that more precise control of thickness is needed.

(b) For $W_p > W_p(max)$, in each case, a constant value of $\Delta\emptyset$ has been shown. This is the region where P-N junction forms which is generally undesirable. In conventional calculations [9], this saturation cannot be obtained; rather a monotonic increase in $\Delta\emptyset$ would continue with increasing W_p.

This can be misleading, in as much as instead of improving the performance by increasing the barrier height the performance would deteriorate due to formation of P-N junction.

Before concluding this section, it should be mentioned that the general analysis given in the previous section which has been used to analyse M-P-N structures in the present section can also be used to analyse M-N$^+$-N structures. Here there are two cases of interest; one of ohmic contact and the other of injecting contact.

A. Ohmic Contacts: In this case the potential profile is that of Fig.3.1(g) where the space charge at the high-low junction is present and provides space-charge-limited current to the bulk semiconductor. Since the metal-N$^+$ depletion layer is separated by a flat potential from the high-low depletion region, the presence of the interface layer does not modify the barrier for tunneling, hence the value of doping required for field-emission would be the same as given in Ref. 15 . Regarding the width of the interface layer, it should be noted that it must be larger than a critical width, t_{min}, to ensure the separation of the depletion layer of metal-N$^+$ layer from that of the high-low junction by a flat profile. The width t_{min} corresponds to the case of Fig.3.1(e), where the flat region has just disappeared, i.e. the value of the peak in potential is still at Ψ_R corresponding to N_{d2}. It is expected that a knowledge of the value of t_{min} would be

of interest during the fabrication of Ohmic contacts,since
it must be exceeded to provide ohmic behaviour. The calcula-
tion of t_{min} is analogous to that of $W_p(max)$ in Sec. 3.2,
hence is not repeated here.

B. <u>Injecting Contacts</u>: To ensure injecting contacts, the
doping and the width of the interface layer are chosen so
that the effective barrier height is decreased by a controlled
amount. A systematic study of these contacts is of recent
origin [5,8] and experimental results to achieve injecting
contacts, particularly in N-InP by epitaxial growth [16] and
by controlled diffusion of sulfur [17] have been recently
reported. Unfortunately, the present method of calculation
of potential-profile fails in this particular case, which
corresponds to Fig. 3.1(h), as has already been mentioned in
Sec. 3.1.

Before concluding this section it must be mentioned
that the behaviour of the ohmic and injecting contacts alike
that of the MPN structure, is critically sensitive to the
applied voltage, hence the present method of analysis which
is only valid in thermal-equilibrium is of limited interest
in these cases. In the next section we give an approximate
method of analysis to study the MPN structure in non-equilibrium
situation. Similar analysis, with some changes, can also be
used for the study of ohmic contacts; but for reasons mentioned
earlier it cannot be used for injecting contacts.

3.2.2 Barrier Height increase in M-P-N structure in non-thermal equilibrium

The barrier height increase given in Fig. 3.2 would be only valid when no voltage is applied. In the case that the device is forward biased the following situation arises.

The barrier height would increase with increasing forward bias. Due to this the number of holes in the P-layer would increase and beyond a point one can no longer assume that the P-layer is completely depleted; rather a current due to minority current injection starts flowing. Thus the major advantage of a Schottky barrier diode of being a majority carrier device is lost. This limits its main advantage of fast switching in switching applications. In solar cell applications this means an increased forward current at a given voltage which would lead to deterioration in performance. Thus it is clear that the useful barrier height increase would be much less than the P-N junction limit given in the case of thermal equilibrium.

The quantitative information about this cannot be obtained by solving the Poisson's equation alone but current continuity also has to be solved. This gets to be an involved problem due to the coupling of these equations. A decoupling can be obtained in the case that the imrefs $\emptyset_p$ and $\emptyset_n$ are assumed to be constant in the space charge region. The constancy of $\emptyset_n$ follows from the assumption of majority

carrier current transport by thermionic emission and that for $\emptyset_p$ follows from the assumption of minority carrier current transport by diffusion model [18]. It is important to note that since the profiles of $\emptyset_p$ and $\emptyset_n$ are already assumed, the problem can be solved only by solving the Poisson equation and noting that $\emptyset_p - \emptyset_n = qV$.

The solution of Poisson equation itself can be simplified by further approximations that p >> n, which remains to be valid excepting at a distance of a few Debye lengths in the vicinity of the edge of the space charge layer. Thus eqn. (3.9), using Boltzmann approximation can be written as

$$\frac{d^2 \psi}{dx^2} = - \frac{q}{\varepsilon_0 \varepsilon_o} [\, N(x) + n_i \, \exp(-q \, \psi / \, kT)] \qquad (3.18)$$

It is important to note the simplicity of eqn. (3.18) which has resulted by taking the imref of minority carriers (holes) to be constant throughout the space charge region and coincident with the metal-Fermi level even when the bias is applied. The majority carrier (electron) imref is displaced from the metal Fermi level by qV, but since the relation p>> n has been used, the applied voltage does not appear in eqn. (3.18). The effect of applied voltage is taken by modifying the boundary condition in the bulk of the semiconductor.

Let us now solve eqn. (3.18) for an NPN diode where
the doping of P and N layers is taken to be abrupt such that

$$N(x) = -N_A \quad \text{for} \quad x < x_j$$
$$= N_D \quad \text{for} \quad x > x_j$$

where x_j is the metallurgical width of the P-layer taking
the metal semiconductor interface as the origin. Let us also
normalize eqn. (3.18) such that

$$\psi = q\Psi/kT \quad , \quad \chi = x/L_D$$

where

$$L_D^2 = (\frac{\varepsilon_s \, \varepsilon_o \, kT}{q^2 \, n_i}),$$

and the dopings are normalized with n_i, such that

$$N_1 = -N_A/n_i \quad \text{for} \quad \chi < \chi_j$$

$$N_2 = N_D/n_i \quad \text{for} \quad \chi > \chi_j$$

We assume a potential profile such that a minima ψ_m appears.
This gives a boundary condition $d\psi / d\chi = 0$ where $\psi = \psi_m$.
The other boundary condition is obtained in the bulk of the
semiconductor such that $d\psi/d\chi = 0$ where $\psi = \psi_R - V$, where ψ_R
is the diffusion potential in the bulk and is given by
eqn. (3.21). V is the applied voltage which is taken to be
positive for forward bias.

Integrating eqn. (3.18) once with ψ and using the above boundary conditions in the proper regions, one obtains:

for $\chi < \chi_j$;

$$\tfrac{1}{2}(d\psi/d\chi)^2 = [-N_1(\psi - \psi_m) + \exp(-\psi) - \exp(-\psi_m)] \quad (3.19)$$

for $\chi > \chi_j$;

$$\tfrac{1}{2}(d\psi/d\chi)^2 = [-N_2(\psi - \psi_R + V) + \exp(-\psi) - \exp\{-(\psi_R - V)\}]$$

$$(3.20)$$

The diffusion potential in the bulk can be determined from the charge neutrality condition as

$$\psi_R = \ln [\frac{N_2}{2} \{1 + (1 + \frac{4}{N_2})^{\tfrac{1}{2}} \}] \quad (3.21)$$

Using the fact that $d\psi/d\chi$ and ψ have to be continuous at $\chi = \chi_j$; also using eqns. (3.19) and (3.20) we get

$$\psi_j = \frac{N_1 \psi_m + N_2(V - \psi_R) + \exp -(\psi_R - V) - \exp(-\psi_m)}{(N_1 - N_2)} \quad (3.22)$$

Now all the relations for obtaining the potential profile have been obtained. The calculations can proceed exactly (see steps (i) to (v) after eqn. 3.14) as in the case of thermal equilibrium given in Sec. 3.1.2.

It has already been mentioned that the advantage of a barrier height increase using a P-layer in M-P-N structure gets nullified if minority carrier current gets

dominant. An idea about the range where the effect of
mobile carrier starts dominating can be easily obtained by
considering eqn. (3.19). Using this equation, we have
plotted $(d\psi/d\chi)^2$ at $\chi = 0$, versus ψ_m in Fig. 3.3. The
plot has been given for three values of $N_1 = -N_A$, which
along with other parameters of interest is given in Fig.3.3.
The solid curve is for the case when mobile carriers have
been ignored, i.e. the exponential terms in eqn.(3.19)
have been neglected. The dotted curves are with mobile
carriers taken into account and the points where they depart
from the solid curve demark the values of ψ_m above which
the neglect of mobile carriers would lead to erroneous
results. Also note that the points A(i), A(ii) and A(iii)
on the ψ_m axis denote the upper limits on ψ_m for the
respective dopings due to the formation of P-N junction.

3.2.3 Open circuit voltage of solar cells using MPN structure:

From the point of view of solar cells the main
advantage of M-P(thin)-N Schottky barriers over M-N Schottky
barriers is due to the increased open circuit voltage
ensuing from the increase in barrier height. The open
circuit voltage is obtained by equating the diode forward
current to the light generated current and solving for the
resulting voltage.

The diode current for M-P-N structure can be
written as:

dominant. An idea about the range where the effect of mobile carrier starts dominating can be easily obtained by considering eqn. (3.19). Using this equation, we have plotted $(d\psi/d\chi)^2$ at $\chi = 0$, versus ψ_m in Fig. 3.3. The plot has been given for three values of $N_1 = -N_A$, which along with other parameters of interest is given in Fig.3.3. The solid curve is for the ease when mobile carriers have been ignored, i.e. the exponential terms in eqn.(3.19) have been neglected. The dotted curves are with mobile carriers taken into account and the points where they depart from the solid curve demark the values of ψ_m above which the neglect of mobile carriers would lead to erroneous results. Also note that the points A(i), A(ii) and A(iii) on the ψ_m axis denote the upper limits on ψ_m for the respective dopings due to the formation of P-N junction.

3.2.3 Open circuit voltage of solar cells using MPN structure:

From the point of view of solar cells the main advantage of M-P(thin)-N Schottky barriers over M-N Schottky barriers is due to the increased open circuit voltage ensuing from the increase in barrier height. The open circuit voltage is obtained by equating the diode forward current to the light generated current and solving for the resulting voltage.

The diode current for M-P-N structure can be written as:

Fig. 3.3 Deviation from deplection approximation (solid line) with mobile carriers (dotted line): Note the scale change in both the cases

$$I = aA^{**} \, T^2 \, \exp[\, -q(\frac{\emptyset_{Bo} + \Delta \emptyset_B(V)}{kT})\,][\, \exp(qV/kT)-1\,] \qquad (3.23)$$

where $\emptyset_{Bo}$ is the barrier height of M-N structure and $\Delta\emptyset_B(V)$ is the barrier height increase at voltage V due to the presence of P-layer. Other symbols have their usual meaning. We assume that $V \gg (kT/q)$ so that unity can be neglected compared to $\exp(qV/kT)$. Let us Taylor expand $\Delta\emptyset_B(V)$ around $\Delta\emptyset_B(o)$, where $\emptyset_B(o)$ is the barrier height increase in thermal equilibrium due to the P-layer. One gets

$$\Delta \emptyset_B(V) = \Delta \emptyset_B(o) + \frac{d[\Delta \emptyset_B(V)]}{dV}\Big|_{V=0} V + \ldots \qquad (3.24)$$

Using equation (3.24) in (3.23) and rearranging one gets

$$I = aA^{**} \, T^2 \, \exp[\, - \frac{q(\emptyset_{Bo} + \Delta \emptyset_B(o))}{kT}\,] \, \exp(qV/kT) \qquad (3.25)$$

where

$$n = \frac{1}{1 - \dfrac{d(\Delta \emptyset_B(V))}{dV}\Big|_{V=0}} \qquad (3.26)$$

If the value of $\dfrac{d(\Delta \emptyset_B(V))}{dV}\Big|_{V=0}$ is small compared to unity such that $n \simeq 1$, one can use $\Delta \emptyset_B(o)$ calculated for thermal equilibrium to obtain the open circuit voltage. If I_L is the light generated current in this case one gets:

$$V_{OC} = \emptyset_{Bo} + \Delta \emptyset_B(0) + \frac{kT}{q} \ln(\frac{I_L}{aA^{**} \, T^2}) \qquad (3.27)$$

Using the values of $\Delta \emptyset_B(o)$ from Fig.3.2, the values of V_{OC} has been obtained for $\emptyset_{Bo} = 0.503$ V, $I_L = 25$ mA/cm^2, a = 1 cm^2,

$A** = 120$ Amp/cm^2/°K^2 and $T = 300$ °K. The plot of V_{OC} versus W_p, for $N_D = 10^{15}$ and 10^{16} cm^{-3} and $N_A = 10^{15}$ and 10^{16} cm^{-3} is given in Fig. 3.4(a).

Recently Card [18] has done an experimental study where he has done a 'solid-state-epitaxial' deposition of the thin P-layer on N-type silicon by heat treating evaporated aluminium layers. The experimental results of Card [18] are shown in Fig. 3.4(b). The abscissa is the temperature of heat treatment, which in effect determines N_A and W_p. Whereas a quantitative comparison of Figs. 3.4(a) and 3.4(b) is not possible due to lack of knowledge of the exact experimental parameters, the striking similarity of the plots is noteworthy.

3.3 Metal-(thin)Insulator-P-N Structures

A major disadvantage of the tunneling MIS solar cell discussed in the previous chapter is that its open circuit voltage varies critically with the thickness of the insulating layer. Thus the control of the open circuit voltage from the point of view of reproducibility from run to run needs stringent control on processing. It will be shown in this section that if thin oppositely doped layer is grown on the semiconductor substrate before growing the oxide, then the advantage of the increase of open circuit voltage is maintained but its critical dependence on the thickness of the insulating layer is obviated.
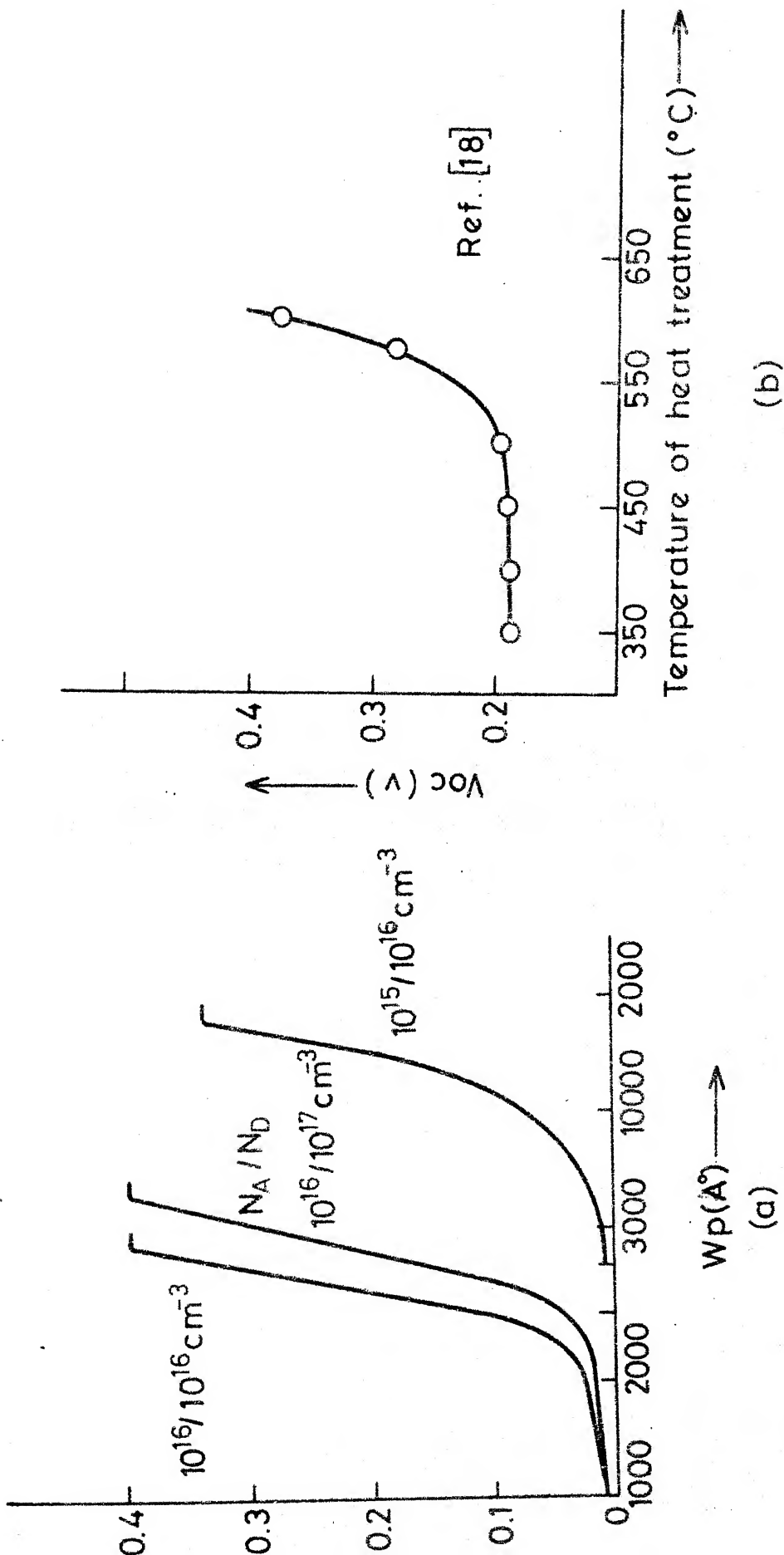
Fig.3.4 Effect of interfacial layer on Voc.

In the following we would consider a metal-(thin) insulator-P-N structure (MIPN); the considerations for a metal-(thin)insulator-N-P structure (MINP) are analogous and can be easily followed. A band diagram of MIPN solar cell is shown in Fig. 3.5(a).

It is obvious that there are two ways of analysing this type of cell. One can either start with MPN structure and study the effect of increasing the oxide layer or one can start with an MIS cell and study the effect of the width and doping of the P-layer. We have taken the latter approach, i.e. we have modified the equations of the MIS cells given in Chapter 2, but used the same analysis of MPN structure as given earlier in this chapter. While considering MPN structure, for simplicity, we have ignored the mobile carriers.

Let us consider the open circuit voltage of the cell shown in Fig.3.5 (a). This can be obtained by solving for V from $J_n + J_p = 0$, where J_n and J_p are the majority and minority carrier components of current. The modified expression for J_n is

$$J_n = A^{**} T^2 \alpha_n \exp(- \frac{q(\phi_B^* + \Delta \phi_B^*)}{kT}) [\exp(qV/kT)-1] \qquad (3.28)$$

Note that this equation is the same as in the case of MIS cell excepting the presence of the term $\Delta \phi_B^*$ which has been added to ϕ_B^*. The value of $\Delta \phi_B^*$ for a given doping and width

(a)

(b)

(c)

(d)
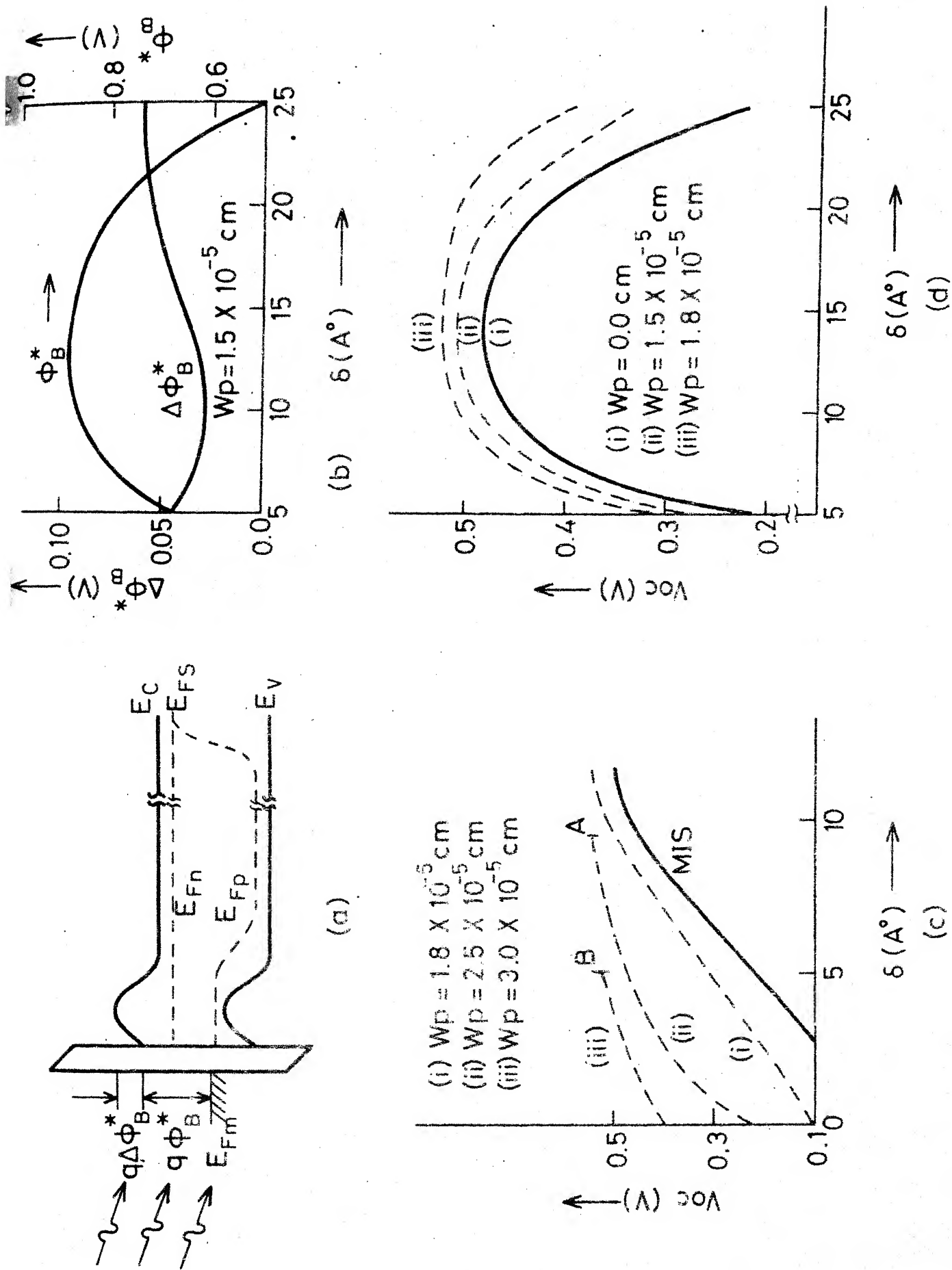
Fig. 3.5 For details see text.

Panel (b): ϕ_B^* (V), $\Delta\phi_B^*$ (V) versus δ (A°), $Wp = 1.5 \times 10^{-5}$ cm

Panel (c): Voc (V) versus δ (A°)
(i) $Wp = 1.8 \times 10^{-5}$ cm
(ii) $Wp = 2.5 \times 10^{-5}$ cm
(iii) $Wp = 3.0 \times 10^{-5}$ cm

Panel (d): Voc (V) versus δ (A°)
(i) $Wp = 0.0$ cm
(ii) $Wp = 1.5 \times 10^{-5}$ cm
(iii) $Wp = 1.8 \times 10^{-5}$ cm

of the P-layer can be obtained from Van der-Ziel's analysis given in Section 3.1.1. Regarding the minority carrier current J_p, we have assumed it to be the same as in the case of the MIS cell. The expression for the open-circuit voltage of the MIPN cell is now obtained following steps which are similar to those in the case of MIS cell. The resulting expression for V_{OC} is

$$V_{OC} = \frac{kT}{q} \ln \left[\frac{-\mu_3 + [\mu_3^2 + \dfrac{4J_L \alpha_p \exp\{(-E_g + 2q\emptyset_B^* + q\Delta\emptyset_B^*)/kT\}}{\alpha_n(J'_{diff} + J'_R)}]^{\frac{1}{2}}}{2} \right]$$

(3.29)

where $\mu_3 = \dfrac{\alpha_p}{\alpha_n} \exp[(E_g + 2q\emptyset_B^* + q\Delta\emptyset_B^*)/kT] + J'_{tunnel}/(J'_{diff} + J'_R)$ (3.30)

and all other terms excepting $\emptyset_B^*$ have been defined in Chapter 2. Note that if the diffusion and recombination components are small such that J_{diff} and J_R are negligible, then eqn. (3.29) reduces to

$$V_{OC} = \frac{kT}{q} \ln(J_L/A^{**}T^2 \alpha_n) + (\emptyset_B^* + \Delta\emptyset_B^*)$$

(3.31)

Computations have shown that the values of V_{OC} from eqns.(3.29) and (3.31) are in very good agreement for low values of δ.

The open circuit voltage of the MIPN structure as a function of the thickness of the insulating layer with width of the P-layer as a parameter is shown in Fig. 3.5 (c and d). The calculations have been done using eqn. (3.19) and the steps are given below.

Let us consider Fig. 3.4(d) first.

(a) The curve (i) with $W_p = 0.0A^O$ is the same as that of the MIS cell given in Fig. 2.3a(ii). The material and the geometrical parameters that have been used in the calculation of Fig. 2.3a(ii) have been also used in the following.

(b) The values of the doping N_a of the P layer and N_d of the N layer are taken to be 10^{16} cm^{-3} and 10^{15} cm^{-3} respectively. The width W_p of the P layer has been taken as a parameter and the values are shown in figure.

(c) $\emptyset_B$ at V = 0 is taken from Fig. 2.3. $\Delta\emptyset_B$ is calculated using eqn. (3.5), (3.7) and (3.8) for V = 0.

(d) V_{OC} is calculated using eqn. (3.29).

(e) Then $\emptyset_B^*$ at $V=V_{OC}$ from eqns. (2.3) and (2.8) and also $\Delta\emptyset_B^*$ (V_{OC}) from eqns. (3.5), (3.7) and (3.8) are calculated.

(f) Steps (d) is repeated to obtain V_{OC} for the new values of $\emptyset_B^*$ and $\Delta\emptyset_B^*$.

(g) Steps (e) and (f) are repeated until the desired accuracy is obtained.

Using this method the curves of Fig. 3.5(c) and (d) have been obtained. In Fig. 3.5(d) the values of W_p are low so that the limit of barrier height increase due to P-N junction formation is not reached. In these cases one observes that V_{OC} increases with increasing W_p for all values of δ. But the initial rise of V_{OC} is still sensitive to the value of δ. Thus the advantages of insensitivity of V_{OC} to δ has not been achieved.

The plots (ii) and (iii) of V_{OC} in Fig. 3.5(c) are for larger values of W_p, in which case it is apparent that the initial rise of V_{OC} has become less sensitive to δ as compared to the MIS cells; thus providing the technological advantages mentioned in the beginning of this section. But there is one more important point which should be noted here. As larger values of W_p are used, the limit of barrier height increase due to P-N junction formation is reached at lower values of δ (see point A on plot (ii) and point B on plot (iii) in Fig. 3.5(c)) thereby nulling the advantages of barrier height increase. A calculation of V_{OC} beyond this point will not be meaningful. The analysis given above provides an explanation and elaboration of the experimental observation of Pai et al [1] that V_{OC} becomes insensitive to δ if MINP or (MIPN) structures, instead of MIS structure, are used. Let us reiterate that this is only true for low values of δ. Pai et al [1] have obtained the N layer of MINP structure by ion-implantating a group V impurity in P type substrate and have formed the metallic contact using titanium.

3.4 Summary

In this chapter the role of an oppositely doped interface layer in increasing the barrier height of a Schottky barrier diode has been considered. This property would be of use in almost all the devices where Schottky barriers are employed e.g. power diodes, microwave diodes, MesFets, solar

cells etc. However, the advantage of the increase of barrier height is only available until the minority carrier effects start dominating. These limitations have been discussed.

From the point of view of solar cells, Schottky barriers have two disadvantages. One is due to the low open circuit voltage. This can be obviated by the use of (MIS) solar cells or by using structures like MPN or MIPN. These have been subject-matters of the previous and the present chapters. The other disadvantage of the Schottky barrier solar cells, which is also present in the case of MIS, MPN, MIPN and analogous cells, is due to the presence of a thin metallic layer through which light may pass. Thus the metallic layers have to be chosen to meet the conflicting optical, electrical, mechanical and metallurgical requirements. A design of the cell, so that some of these stringent requirements are relaxed would be discussed in the next chapter.

LATERAL SOLAR CELLS

In the previous chapters we have studied the
Schottky barrier, MIS, MPN and MIPN solar cells. The
difficulties inherent in them due to the presence of a
thin metallic layer (70 A^O) on the top has already been
mentioned earlier. In particular, deterioration of these
thin metal films due to temperature cycling in actual
operation may seriously affect the durability of these
cells, thereby more than offsetting the advantages offered
by them. Recently, a modified structure for SBSC has been
proposed by Green [1] in which the requirement of a thin
metal film has been obviated by using the structure shown
in Fig. 4.1. This structure is analogous to the grating
type of photovoltaic cells proposed by Loferski et.al.[2]
and analysed by other workers [3]. It consists of several
unit cells, each one of which has an exposed region of
semiconductor of width 2L and a metal strip of width
2B = (m-1)L. For brevity, the regions of width 2L and 2B
are called the lighted and the collecting regions respec-
tively. Carriers are photogenerated in the lighted region
and are laterally collected by the Schottky barrier in the
collecting region. Hence this structure is designated as
lateral SBSC. The intent of the present chapter is to
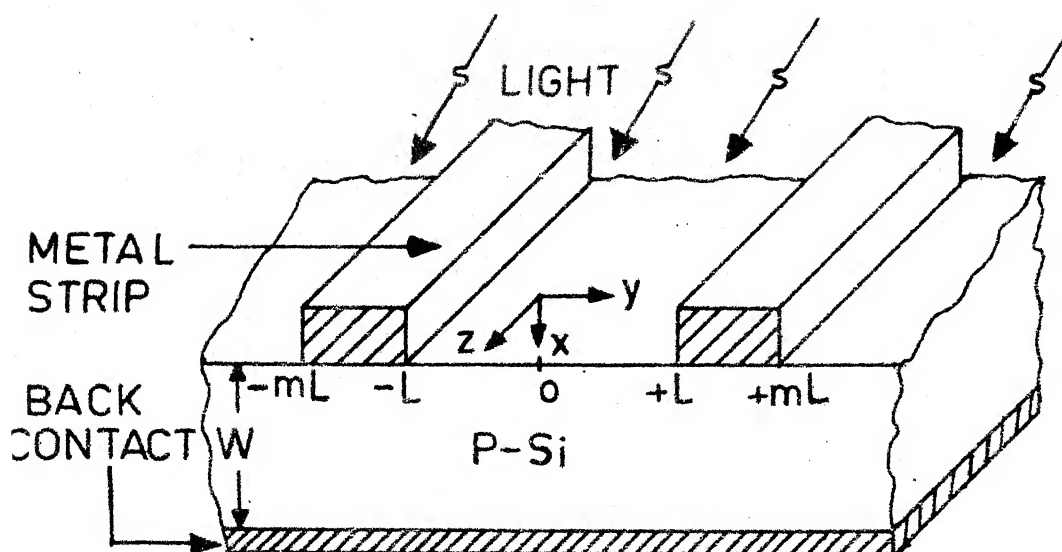
Fig.4.1 The schematic of lateral SBSC is shown. The width of the metal strip is $2B = L(m-1)$ and the extent of lighted region is $2L$. The cell consists of several units like this where the metallic strips are connected together.

calculate analytically the short circuit current by solving
a two-dimensional continuity equation and thereby obtain
the efficiency of this cell. The calculated results show
some interesting features. One of them is that the efficiency
does not increase monotonically with incrase in L/B as
reported earlier [1]. As a matter of fact, it has been
found that L/B is not a meaningful parameter for this cell,
rather both L and B have to be separately specified for
uniquely specifying the efficiency of the cell.

The calculation of efficiency proceeds in the following
manner. The two dimensional continuity equation for the minority
carriers in both the lighted and the collecting regions is
first solved. This is done in the following section.   These
solutions are then used to obtain the spectral response, the
short circuit current and the conversion efficiency of the
cell.

4.1 Continuity Equation

In this section the profile of photogenerated
minority carriers for the lateral SBSC, shown in Fig. 4.1
is determined. To do this let us consider the mechanism of
collection in a lateral SBSC, bringing out the assumptions
under which the present calculation has been done.

(i) Carriers are photogenerated in the lighted region.
In general, these are transported by drift and diffusion in
the presence of recombination to the edge of the space charge

region (below the metal) which is formed due to the Schottky-barrier. However, if it is assumed [4] that the electrostatic field is confined entirely to the narrow space-charge region, even in the presence of photogenerated carriers, then the rate-controlling process in current flow is the diffusion of minority carriers. In order to ensure this field-free diffusion, the non-equilibrium concentration of minority carriers must always be much smaller than the equilibrium concentration of majority carriers. This low-level generation needed to neglect the drift component of transport, is obtained in the case of irradiation of silicon by uncentrated solar light. We confine our attention to this case.

(ii) The carriers which reach the edge of the space-charge layer (below the metal) are transported to the metal by drift. Some of the carriers may also recombine in this region. We note, however, that [4] the width (W_{SC}) of this space charge region is negligibly small compared with the diffusion length (L) of minority carriers and with the width (W) of the cell. Typically, in a silicon solar cell W_{SC} is of the order of a few microns whereas L is of the order of a hundred microns and W is of the order of two hundred microns. Hence, on the scale of Fig.4.1, the edge of the space charge region below the metal has been taken at x=0 and any fringing of this region in the lighted region has been ignored. In other words, it has been assumed that all the photogenerated carriers

reaching the edge of the space charge layer are collected by the metal.

Under the assumptions given above the profile of photogenerated minority carriers (electrons), in the steady state, can be obtained by solving the two-dimensional continuity equations

$$D_n \left(\frac{\partial^2 n_j}{\partial x^2} + \frac{\partial^2 n_j}{\partial y^2} \right) - \frac{n_j}{\tau_n} = F(x, \lambda) \qquad (4.1)$$

where for the lighted region $n_j = n_L$ and

$$F(x, \lambda) = -Q(\lambda) \alpha(\lambda) \exp[-\alpha(\lambda)x] \qquad (4.2)$$

whereas in the collecting region $n_j = n_c$ and $F = 0$. Here the reflection losses have been neglected and the quantum efficiency has been taken to be unity. The boundary conditions (BC's) in both the lighted and the collecting regions are given in Table 4.1. The cell has been considered to be short-circuited giving rise to the condition $n_C = 0$ at $x = 0$ in the collecting region. The determination of the BC's in the y-direction poses some problems. This is due to the fact that at $y = L$, $-L$, mL and $-mL$ the BC's are not known. To obviate this, it is assumed that at these values of y one has $n_j = f(x)$, and the symmetry of the structure is utilized to put some restraining conditions given in Table 4.1. Use of these conditions allows one to solve eqn. (4.1) by standard method [5] as shown in Appendix C in terms of the coefficients which

Table 4.1

Table 4.1: Boundary conditions.

Serial Number	Boundary	Lighted Region	Collecting Region
(i)	x=0	$D_n \dfrac{\partial n_L}{\partial x} = Sn_L$ $(-L \leq y \leq L)$	$n_C = 0$ $-mL \leq y \leq -L$
(ii)	x=W	$n_L = 0$ $(-L \leq y \leq L)$	$n_C = 0$ $(-mL \leq y \leq -L)$
(iii)	Boundary condition in y-direction	$n_L = f(x)$ at $y = \pm L$	$n_C = f(x)$ at $y = -L$ and $-mL$
(iv)	Restraining condition	$\dfrac{\partial n_L}{\partial y} = 0$ at $y = 0$	$\dfrac{\partial n_C}{\partial y} = 0$ at $y = -(m+1)L/2$
(v)	Restraining condition	$\dfrac{\partial n_L}{\partial y} > 0$ at $y = -L$	$\dfrac{\partial n_C}{\partial y} > 0$ at $y = -L$
(vi)	Restraining condition	$\dfrac{\partial n_L}{\partial y} < 0$ at $y = L$	$\dfrac{\partial n_C}{\partial y} < 0$ at $y = -mL$

are to be iteratively determined. The solution in the collecting region is obtained as

$$n_C(x,y) = \sum_{q=1}^{\infty} C_q \sin(\beta_q x) \cosh(P_q(y+(m+1)L/2)/\cosh(P_q[(m-1)L/2])$$

$$(4.3)$$

where β_q are obtained from the solution of $\beta_q W = n\pi$, n being an integer and $P_q^2 = \beta_q^2 + L_n^{-2}$. To determine the coefficients C_q's in eqn. (4.3), one would need the solution of eqn. (4.1) in the lighted region.

The expression that satisfies eqn.(4.1) and the boundary conditions (ii), (iv), (v) and (vi) of Table 4.1 in the lighted region is:

$$n_L(x,y) = g_1(x) + g_2(x) - \sum_{p=1}^{\infty} B_p \sin X_p(x-W)[\cosh Q_p y/\cosh Q_p L]$$

$$(4.4)$$

$$g_1(x) = A \sinh[(x-W)/L_h]$$

$$g_2(x) = \frac{Q(\lambda)\alpha(\lambda)}{D_n(\alpha^2 - L_n^{-2})} [\exp(-\alpha W) \exp[-(x-W)/L_n] - \exp(-\alpha x)]$$

$$Q_p^2 = X_p^2 + L_n^{-2}$$

where X_p is the root of the equation:

$$X_p W \cot X_p W + (SW/D_n) = 0$$

The expression for A in $g_1(x)$ is obtained by substituting eqn. (4.4) in the boundary condition (i).

$$A = \{Q(\lambda)\alpha(\lambda)/[D_n(\alpha^2 - L_n^{-2})]\}(R/T) \quad (4.5)$$

where $R = [(D_n/L_n)+S] \exp [W(L_n^{-1} - \alpha)] - (S + \alpha D_n)$

$$T = (D_n/L_n) \cosh(W/L_n) + S \sinh(W/L_n)$$

The coefficients of expansion B_p, in eqn. (4.4) are determined by using the boundary condition (iii) in the following way.

The coefficients of expansion B_p in eqn. (4.4) and C_q in eqn. (4.3) are determined as follows. At $y = -L$, one has $n_C = n_L = f(x)$, i.e.

$$\sum_{q=1}^{\infty} C_q \sin \beta_q x = g_1(x) + g_2(x) - \sum_{p=1}^{\infty} B_p \sin \chi_p (x-W) \quad (4.6)$$

Multiplying both sides of eqn. (4.6) by $\sin \beta_n x$ and integrating between zero and W, we get:

$$C_n = (2/W) [-Z_1 + Z_2(Z_3 - Z_4) - \sum_{p=1}^{\infty} (B_p \beta_n \sin \chi_p W)/(\chi_p^2 - \beta_n^2)]$$
$$(4.7)$$

where $Z_1 = A \beta_n [\sinh(W/L_n)] /(L_n^{-2} + \beta_n^2)$

$\quad Z_2 = Q(\lambda) \alpha(\lambda) \beta_n / [D_n(\alpha^2 - L_n^{-2})]$

$\quad Z_3 = \{ \exp [W(L_n^{-1} - \alpha)] - (-1)^n \exp(-\alpha W) \} /(\beta_n^2 + L_n^{-2})$

$\quad Z_4 = [1-(-1)^n \exp(-\alpha W)] /(\alpha^2 + \beta_n^2)$

Thus equation (4.7) provides a relation between C_n and B_p's. An expression for B_t in terms of C_q's is obtained by using the relation

$$\partial n_j / \partial y = \partial n_C / \partial y \quad \text{at } y = -L$$

which gives

$$\sum_{p=1}^{\infty} B_p Q_p \sin X_p (x-W) \tanh(Q_p L) = \sum_{q=1}^{\infty} C_p P_q \sin \beta_q \, x \, \tanh(P_q (m-1)L/2)$$

$$\text{(4.8)}$$

Multiplying both sides of eqn. (4.8) by $\sin X_t (x-W)$ and integrating between zero and W, we get·

$$B_t = Z_6 \sum_{q=1}^{\infty} (C_p P_q \beta_q \sin X_t \, W/[X_t^2 - \beta_q^2]) \, \tanh[P_q (m-1)L/2]$$

$$\text{(4.9)}$$

where $Z_6 = -4 X_t / \{ (\sin 2 X_t \, W - 2 X_t W) Q_t \tanh[Q_t L] \}$

Equations (4.7) and (4.9) are iteratively solved to obtain the coefficients of expansion B_p and C_q in eqns. (4.4) and (4.3) respectively. For the range of parameters for which the calculations have been done it has been found necessary during the numerical calculation to keep five terms in B_p and fourteen terms in C_q for reasonable accuracy.

Once these coefficients are known, one can obtain the short-circuit current. But before doing this, we would digress to consider the case when the surface recombination velocity in the lighted region at $x = 0$ is infinite, i.e., $n_L = 0$ at $x = 0$. Boundary condition (i) for the lighted region in Table 4.1, for infinite surface recombination velocity, changes to $n_L = 0$ at $x = 0$ for $-L \leq y \leq L$. The expression that satisfies eqn. (4.1) and the boundary conditions is given by

$$n_L(x,y) = g_3(x) + g_2(x) - \sum_{q=1}^{\infty} B_q \sin \beta_q \; x \; \frac{\cosh P_q y}{\cosh P_q L} \qquad (4.10)$$

where $g_3(x) = A_1 \sinh(\frac{x-W}{L_n})$

and $A_1 = \dfrac{Q(\lambda) \alpha(\lambda)}{D_n(\alpha^2 - L_n^{-2})} \; [\dfrac{\exp(-\alpha W)\exp(W/L_n)-1}{\sinh(W/L_n)}].$

For infinite surface recombination velocity (i.e. for the case $n_L = 0$ at $x = 0$) the expansion of C_q can be obtained in closed form by using the boundary conditions:

$$n_C = n_L \quad \text{and} \quad \frac{\partial n_C}{\partial y} = \frac{\partial n_L}{\partial y} \; ; \quad \text{at } y = -L.$$

The expression for C_q thus obtained is

$$C_q = \frac{(2/W) \; [-Z_1 + Z_2(Z_3 - Z_4)] \tanh P_q L}{(\tanh P_q L + \tanh P_q \frac{L(m-1)}{2})}$$

Thus in this case no iteration is required, this simple calculation has been used as a check on the trends that have been obtained in the general case of finite surface recombination velocity in the lighted region at $x = 0$.

Before concluding this section, it should be mentioned that recently Hu and Edelburg [3] have also solved the continuity equation (4.1). They have used a method of Fourier expansion and their analysis has been briefly summarized in Appendix D. There we have also summarized a difference equation technique which has been used by Loferski et.al.[2] to numerically solve eqn. (4.1).

4.2 Short Circuit Current

The short circuit current $I_{SC}(\lambda)$ of a unit cell is calculated using the expression for n_C from eqn. (4.3) as follows:

$$I_{SC}(\lambda) = qD_n \int_{-mL}^{-L} \frac{\partial n_C}{\partial x}\bigg|_{x=0} dy \qquad (4.12a)$$

$$= 2qD_n \sum_{q=1}^{\infty} C_q(B_q/P_q)\tanh\{P_q(m-1)L/2\} \qquad (4.12b)$$

Here unit length in z-direction has been taken. Note that the symbol q has been used to denote charge of the electron as well as an index of summation. The derivative in the integral sign of (4.12a) should actually be evaluated at the edge of the depletion region in the collecting region rather than at x = 0. However, the evaluation at x = 0 has been done as a consequence of assumption (ii) of the previous section.

The spectral response of the unit cell as calculated from eqn. (4.2) is shown in Fig. 4.2 for 2B = 12 μm and 2L = 20 μm and 200 μm. The curve for 2L = 20 μm is shown for two values (10 and 10^4 cm/sec.) of the surface recombination velocity. The values of D_n, L_n and W for which the calculations have been done are also shown in Fig. 4.2. It is obvious from Fig. 4.2 that the surface recombination velocity at the front surface of the lighted region would play an important role in the performance of these cells.
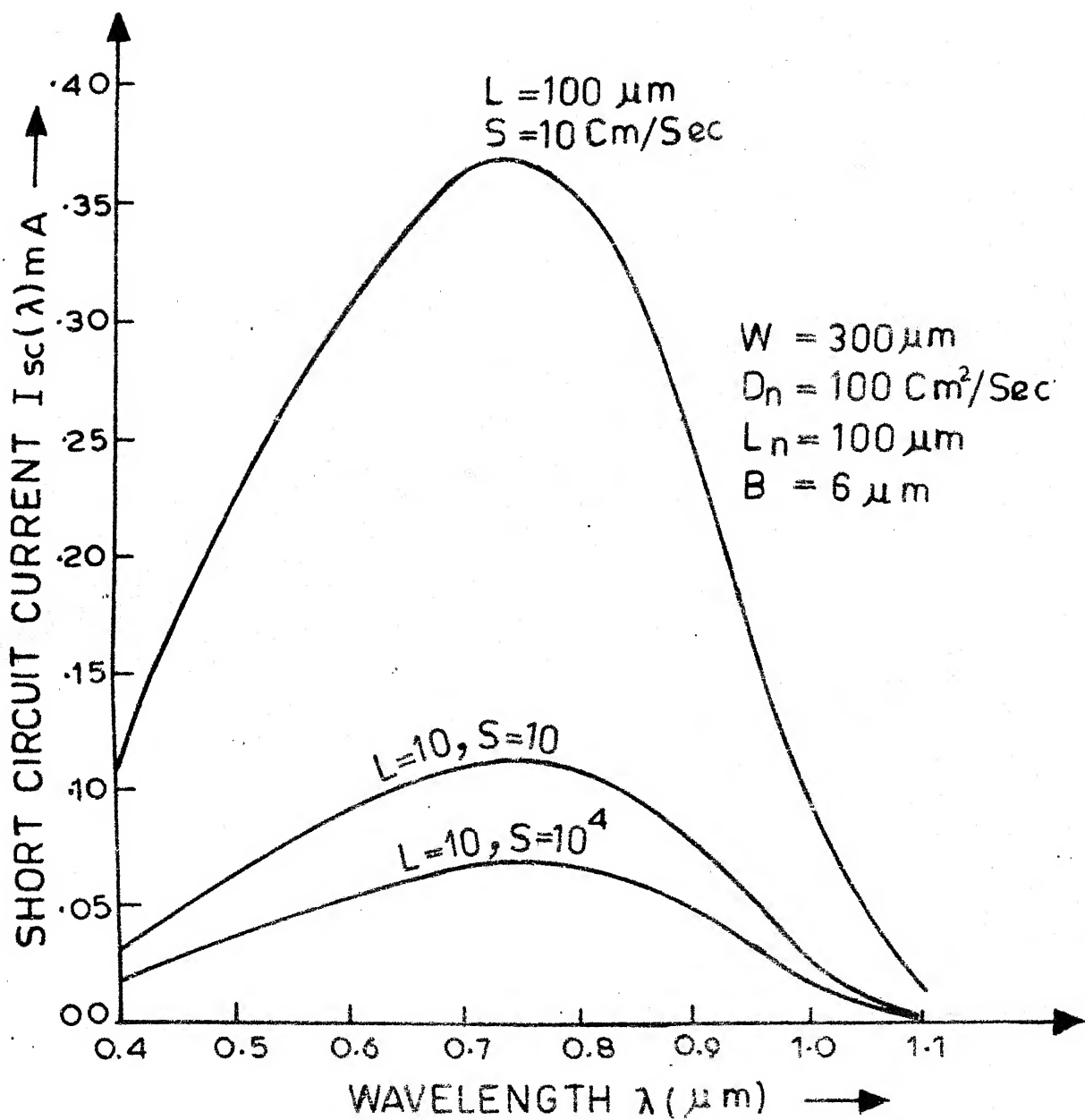
Fig. 4.2 Plot of the spectral response of lateral SBSC for
L = 10 μm and L = 100 μm both for B = 6μm. Note that
the areas of unit cell with L = 10 μm and L = 100 μm
are different.

To obtain the total short circuit current I_{SC}, of the unit cell, eqn. (4.12) is integrated for AMO sunlight using the data of Thekaekara[6]. A plot of I_{SC} versus the width 2B of the collecting region is shown in Fig. 4.3. Here L has been taken as a parameter for different plots. The values of D_n, L_n and W are the same as given in Fig. 4.2 and S=10cm/sec.

In the earlier literature [1], it has been implicitly assumed that I_{SC} is only dependent on L and not on B. This is at variance with the results shown in Fig.4.3 where I_{SC} is also dependent on B. This can be physically explained as follows. When B is zero, none of the photogenerated carriers are collected and obviously I_{SC} is zero. When B is small, for a given L, some but not all the photogenerated carriers are collected and I_{SC} increases. When B is sufficiently large so that all the photogenerated carriers can be collected, then any further increase in B does not increase I_{SC}.

So far we have considered L as fixed and have varied B. It is also of interest to consider the variation of I_{SC} with fixed B and varying L. This is shown as an inset in Fig.4.3. Initially, as L increases, I_{SC} increase because photogenerated carriers become available. Eventually I_{SC} saturates when L becomes of the order of or greater than the diffusion length of the minority carriers. These considerations of the results in Fig.4.3 and its inset would be of considerable help in explaining the behaviour of the conversion efficiency in the next section.
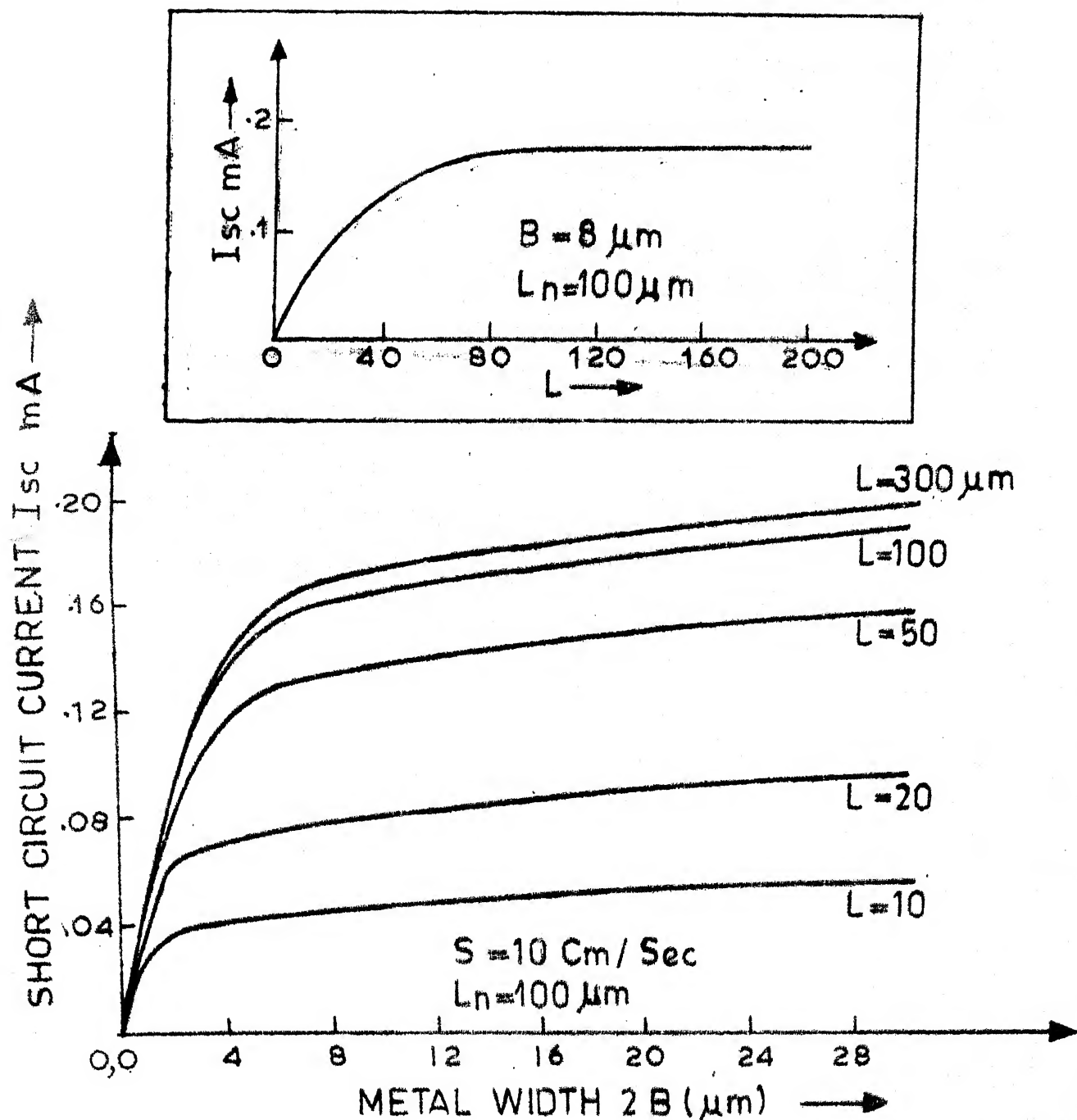
Fig. 4.3 Plot of the short-circuit current I_{sc} versus the width of metal for several values of L. In the inset I_{sc} versus L is plotted for a fixed B.

4.3 Conversion Efficiency

The conversion efficiency of the cell has been calculated in the conventional manner [7] as given in Chapter 1. The only care to be taken is that the area, for unit length in z-direction, for the calculation of the reverse saturation current per unit cell is 2B, whereas the total area of the unit cell is 2(L+B). Thus the conversion efficiency (η) at a load where maximum power is delivered is:

$$\eta = (V_{mp}I_{mp}) \text{ per unit cell}/((P_{in}2(L+B))) \qquad (4.13)$$

where for AMO solar radiation $P_{in} = 135.3$ mw/cm^2. V_{mp} is obtained from the solution of the transcendental equation

$$(1 + \frac{qV_{mp}}{nkT}) \exp(\frac{qV_{mp}}{nkT}) = (1 + \frac{I_{SC}}{I_S}) \qquad (4.14)$$

where the short circuit current I_{SC} has been calculated in Section 4.2, and

$$I_S = (2B) A^{**}T^2 \exp(-q\phi_B/kT) \qquad (4.15)$$

is the saturation current, per unit width, in the collecting region. The calculations have been done at room temperature and for P-type silicon where $A^{**} = 32$ amp/cm^2/°K^2. I_{mp} is the current of lighted SBSC at the voltage V_{mp}. The values of the barrier height ϕ_B and the diode quality factor n which are needed for the calculation cannot be precisely

determined because they depend on the method of fabrication. Hence these have been treated as parameters and several calculations have been done. A plot of the efficiency versus the width of the metal strip 2B for various values of L is plotted in Fig. 4.4 for $\emptyset_B = 1.1$ eV and n = 1.0.

In order to design a lateral SBSC one would like to choose the optimum value of L and B. In this regard the following reatures of Fig.4.4 should be noted:

1. For a fixed L and with increasing B, the efficiency increases, reaches a maximum and then falls off. The maxima is sharp for smaller values of L and broadens for higher value of L. It was thought earlier [1] that increasing L/B ratio would monotonically lead to higher effieiency. Thus for a given L one may think that it would be advantageous to reduce B as much as technologically feasible. Fig. 4.4 shows that this is only true in the region past the maxima; in the initial portion of the curves the behaviour is just the opposite. Thus, for a given L, there is a minimum value of B beyond which it should not be reduced even if technologically feasible. We consider that this is an important results of the present work. The general feature of this aspect of Fig.4.4 can be understood by considering the variation of I_{SC}, I_S and 2(L+B) with increasing value of B. When B is zero the conversion efficiency is zero because I_{SC} is zero. When B increases all the three quantities I_{SC}, I_S and 2(L+B) increase. Eqns.(4.13)
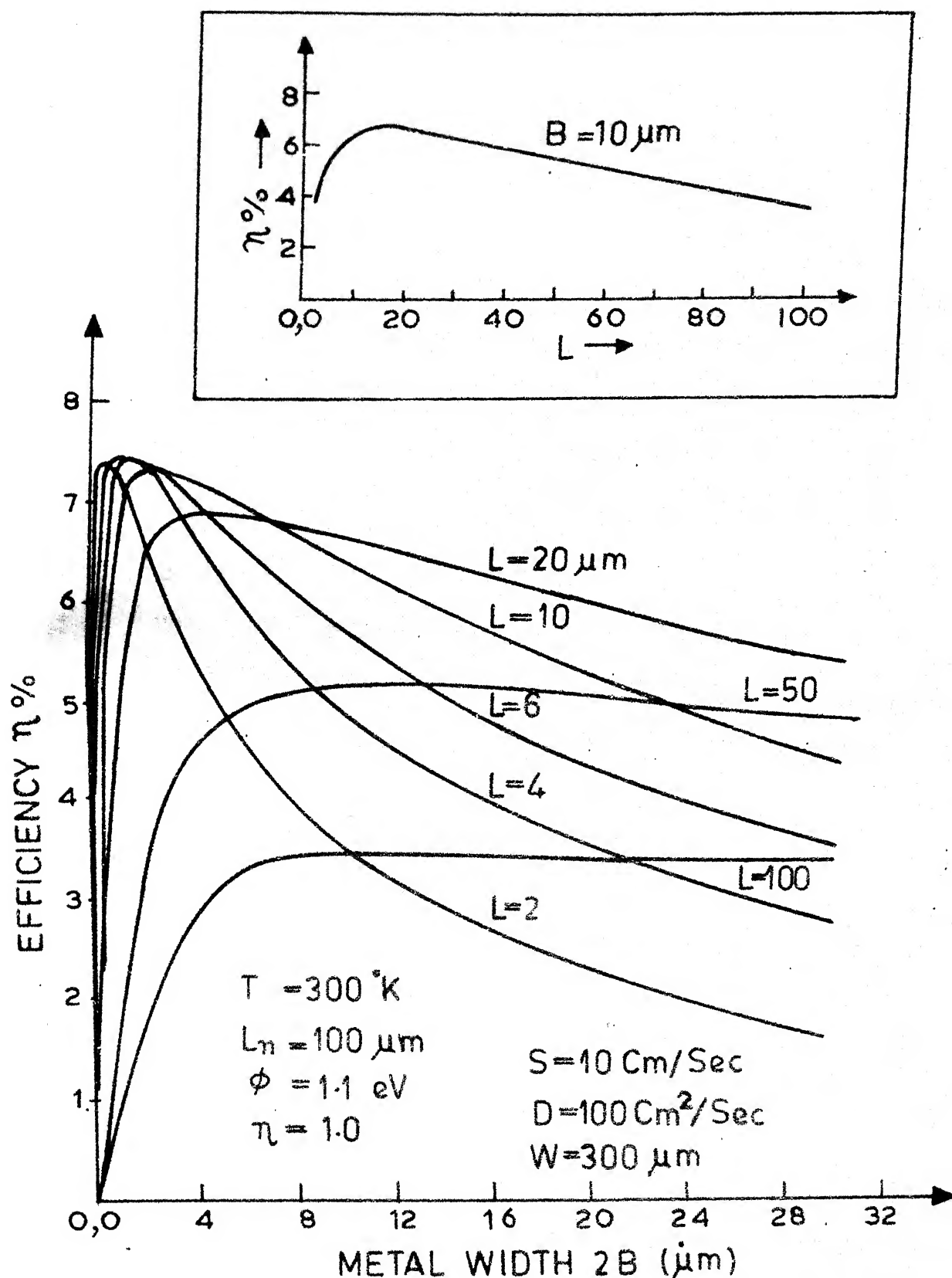
Fig. 4.4 Plot of the efficiency of the lateral SBSC versus the width of metal 2B = L(W_1), for several values of L. The plot of the efficiency versus L for a fixed B is shown in the inset.

and (4.14) show that an increase in I_{SC} is desirable whereas the increase in I_S and $2(L+B)$ lowers the efficiency. The variation of I_{SC} has been considered in Fig. 4.3 and shows a saturation, whereas both I_S and $2(L+B)$ increase linearly with B. These relative changes are such that the conversion efficiency, for a fixed L, shows a maxima as seen in Fig.4.4.

2. It is also of interest to consider the variation of efficiency with L. We confine our attention to that region of Fig. 4.4 where the efficiency decreases with increasing B. For a fixed B, the efficiency increases with increase in L, reaches a maximum and then falls off as shown in the inset of Fig.4.4. The physical reason for this behaviour can be understood by considering the nature of variation of I_{SC} with L as given in the inset of Fig.4.3 and by noting that the area $2(L+B)$ of the unit cell increases linearly with L. It should be noted that again there is a region where the efficiency decreases with increasing value of L/B, thus for a given B there is an upper limit on L for obtaining maximum efficiency. Earlier we have seen that for a given L there is a lower limit on B for getting the best efficiency. In general, Fig.4.4, provides a guideline for the choice of L and B while designing these cells and it has to be used keeping the technological constraints in mind.

It is worthwhile to compare the efficiency of lateral SBSC with those of conventional Schottky barrier solar cells discussed in Chapter 1. Before doing this, it should be

noted that in the published literature (for a summary see Landsberg and Klimpke [8]) there is a very wide range of effeciencies that have been reported for these conventional cells. For example, theoretically calculated values of efficiency for conventional silicon SBSC range between 5% to 20%. Such a wide variation is due to the choice of barrier height, inclusion or neglect of recombination in the calculation, and similar other factors. Hence any comparison between the efficiencies of two different types of cells should be done, as far as possible under similar conditions. This is done below.

Let us consider the lateral SBSC shown in Fig. 4.1. If the whole cell is covered by a very thin metallic coating instead of the gridded structure, then a conventional SBSC ensues. In this case the problem is one-dimensional and the solutions, taking recombination into account, have been given in Chapter 1. Considering all the relevant parameters to be the same as in Fig. 4.4 and assuming complete transmission through the thin metal film, the conversion efficiency of the conventional SBSC comes out to be approximately 6.5 percent. A comparison of this value with those given in Fig. 4.4 shows that in some ranges the efficiency of lateral SBSC is larger than that of the conventional cell, The physical reason for this is as follows [1]. In the lateral SBSC the light available for photogeneration of carriers is less because of the presence of opaque metallic layers. Also the total

recombination for carriers is high because of the longer collection path. These factors lower the efficiency. However, the reverse saturation current of the Schottky barrier is also lower because of the reduced metallic area and this effect enhances the efficiency. Thus it is possible that in some range the lateral SBSC has higher efficiency than the conventional SBSC.

Before concluding this section, let us consider two more effects which are of interest in the fabrication of these devices. (a) As already discussed in Chapter 2, the inclusion of a thin interfacial layer in conventional SBSC which in effect forms a MOS solar cell, gives rise to increased efficiency. If this is done during fabrication of lateral SBSC also, it may be possible to obtain experimental values of efficiency which are higher than those of Fig.4.4. In this case, the theoretical calculation would have to be modified to account for the presence of the interfacial layer as shown in Chapter 2. (b) The efficiency of a lateral SBSC is dependent on the value of the surface recombination velocity (s) at the front face of the lighted region. Care should be taken to keep this value as low as possible.

4.4 Summary

The conversion efficiency of lateral SBSC has been calculated and guidelines to choose the geometrical parameters of this cell have been provided. The deleterious effect of

the surface recombination velocity has been pointed out. Perhaps the main advantage of these cells as compared to the conventional SBSC would not be in providing better efficiency but in their greater durability. In conventional cell a very thin homogeneous metallic film is required which should have good optical properties, a large barrier height and should adhere well to the semiconductor. There are all the chances that a thin metallic film which has different lattice constant and temperature coefficient of expansion than the substrate would catastrophically deteriorate when subject to periodic temperature cycling in actual operation. In case of lateral SBSC the metallic film can be made quite thick, even an intimate contact using silicides can be utilized. These would also improve the series resistance. In the light of these observations, it is expected that lateral SBSC would be more useful than the conventional SBSC in terrestrial applications.

CHAPTER 5

CONCLUSION

The photovoltaic properties of metal semiconductor (Schottky barrier) and related devices like:

(i)   Metal-(thin)insulator-semiconductor tunneling MIS diodes,

(ii) Metal-(thin)P-N semiconductor and metal-(thin)N-P semiconductor devices,

(iii) Metal-(thin)insulator-(thin)P-N and metal-(thin)insulator -(thin)N-P semiconductor diodes, and

(iv) Lateral Schottky barrier solar diodes

have been studied in the previous chapters. An analysis of the short circuit current and the open circuit voltage for these cells has been given. From the knowledge of the complete I-V characteristics in the fourth quadrant (the fill factor) the efficiencies of the different cells can be calculated as has been demonstrated in some cases.

It has been pointed out that the temperature variation of the parameters of a solar cell are of importance from the point of view of actual operation of the cell. Therefore, the mechanisms that lead to this temperature variation have been studied. Attention has been first given to the study of temperature variation of the short-circuit current. It is commonly found that the short circuit current increases with temperature. Two mechanisms can be responsible for it.

(a) The energy band gap in commonly used semiconductors decreases with increasing temperature. Due to this decreased band gap some more long wavelength photons are absorbed and photogenerate electron-hole pairs thereby increasing the short circuit current. Note that this excess of photocarriers is due to long wavelength photons which get absorbed deep into the base of the semiconductor. Hence, this mechanism would only be operative if the diffusion length of the minority carriers are exceedingly large.

(b) The absorption coefficient of the semiconductor itself is a function of temperature and it increases with increasing temperature at all wavelengths in the case of silicon. Thus with increasing temperature, there is extra photogeneration of carriers at all the depths in the cell and this also causes the increase of short circuit current with increasing temperature. Since this mechanism is operative at all the sections of the cell, it would be important even in the case of materials with small diffusion lengths.

In actual situation, both the mechanisms mentioned above would contribute to the increase of short circuit current with temperature. However, in the case of a typical silicon solar cell, we have found that the contribution of the mechanism (a) is almost negligible. Since we have concentrated only on cells made of silicon, the above consideration is valid for all the cells studied in this thesis,

hence has not been given for each cell separately; rather the numerical results for only the Schottky barrier and lateral cells (Appendix D) have been given. Once the temperature variation of the short circuit current is known, that of the open circuit voltage can be computed by knowing the temperature variation of the ideality factor and the saturation current which depends on the barrier height. A review of the published literature has shown that the temperature variations of the ideality factor and the barrier height are extremely sensitive to the method of fabrication of the devices, hence the numerical computations have not been carried any further in th se cases.

A consideration of the Schottky barrier solar cells has shown that their biggest disadvantage is the low value of the open circuit voltage. This is obviated by using either the metal(thin)-P-N and analogous devices or tunneling MIS diodes. In the latter case one finds that both the open circuit voltage and the short circuit current, hence the efficiency are controlled by the thickness of the oxide-layer and fall when the thickness of the oxide layer exceeds a critical value.

An understanding of the mechanisms that cause these falls would suggest some methods to control the critical thickness mentioned above thus help in avoiding the low efficiency region. For example, it has been proposed that

the fall of the open circuit voltage for thicker diodes is primarily caused due to the decrease of the density-of-surface states with increasing oxide thickness in the case of MIS cells made on N type semiconductor. Thus if this fall is to be avoided the rate of decrease of the density-of-surface states with increasing oxide-thickness should be kept as small as possible. Similarly, the mechanism that controls the constancy of the short circuit current with oxide thickness is the split of imref of the minority carriers from the metal Fermi level, and this should be kept **below** a critical value by obtaining larger barrier heights, to keep the current constant.

The other mechanism to increase the open-circuit voltage is to interpose a thin oppositely doped semiconducting layer between the metal and the base semiconductor. This mechanism is of very general nature and its uses are not limited to photovoltaic devices only. If proper design is done, this technique provides a method for increasing the effective barrier height which is advantageous in most devices where Schottky barriers are employed. Some examples of such devices are Schottky gate, field effect devices, Schottky clamped transistors, etc. Hence, the methods developed for the design of increase of the barrier height in solar cells can also be used in the design of several other devices. For this purpose, the graph given in the text, showing the increase in the barrier height with the width

of the interfacial semiconducting layer and with the dopings as parameters can be utilized. Furthermore an analogous method can also be used by interposing a thin similarly doped semiconductor layer between the metal and the base semiconductor to obtain an effective decrease of barrier height. This aspect is of interest in designing the injecting and ohmic contacts. In the case of solar cells, injecting contacts are not of interest, but a consideration for the understanding of the behaviour of ohmic contacts based on the above principle has been given. Lastly the effects of both a thin insulating layer and an oppositely doped semiconducting interfacial layer in increasing the barrier height have been amalgamated. The advantageous effect of this has been to reduce the sensitivity of the open circuit voltage on oxide thickness while keeping the value high.

In all the cells mentioned so far a very thin metal layer is required on the illuminated side so that the light can go through. The disadvantages of a thin metallic layer from the point of view of long-duration-operation of a solar cell under atmospheric conditions are obvious. It has been shown that a way of obviating this disadvantage is to use lateral cells. The analysis of these cells has required a two dimensional calculation. The results have shown that the efficiency of these cells are dependent on the choice of the areas of both the exposed region of the

semiconductor and the metallic collecting region. A design
graph for this purpose has been plotted in the text.

From the summary of the work presented in the
present thesis, we come to the following conclusions:

(a) Schottky barrier solar cells are not promising
because of their low open circuit voltage.

(b) The potential of tunneling MIS solar cells has
not been completely realized so far because these are
complex devices, in as much as their performance depends
on cumulative behaviour of several parameters which are
simultaneously operative. There have been developments in
this area, but as would appear, the role of all the para-
meters are not yet well understood. For example, the
important role played by the variation of the density of
surface states with oxide thickness has only been pointed
out in this thesis. This makes it incumbent that different
methods of oxide growth which give different variation of
the -density-of-surface states on oxide thickness be
experimentally investigated and the suitable one chosen.

(c) Solar cells based on metal (thin)-insulator-(thin)-P
-N semiconductor and analogous structures seem to be
promising, but so far very little attention, both theore-
tically and experimentally, has been paid to these. The
most advantageous features of these cells is that they keep
the open circuit voltage high, but decrease the sensitivity

of the open circuit voltage on the oxide thickness as
compared to MIS cells. Thus, these cells would be tolerant
to less critical manufacturing processes than MIS solar
cells.

(d) The manufacture of the lateral cells provide an
advantage in as much as the choice of the metal for
collecting junction only depends on the electrical and
mechanical   properties and not on the optical properties
as in the case for all other cells considered above. Thus
in the case of lateral cells using MIS contacts. the barrier
height and the effective ideality factor would remain to be
the   ones   in dark which is advantageous in most of the
cases.

To conclude, it must be mentioned that none of the
cells mentioned above can have an ideal maximum efficiency
larger than the ideal maximum efficiency available in
P-N junction solar cells. However, as mentioned in the
beginning of this thesis the processing of P-N junction
cells is expensive and there is a search on to locate viable
alternative structures. We have presented some discussions
in this direction in this thesis.

REFERENCES

CHAPTER 1

1. B.Bhaumik and R. Sharan, Applied Phys.Lett., Vol.29, p.257, 1976.

2. B. Bhaumik and R. Sharan,"Two Dimensional Analysis of Lateral Schottky Barrrier Solar Cells" IEEE Trans. ED, submitted in April 1977, revised in Nov. 1977.

3. B. Bhaumik and R. Sharan, "Potential-Profile of Doped-Interface Schottky Barrier Diodes", IEEE Trans. ED, submitted in Nov. 1977, revised manuscript to be submitted.

4. Basabi Bhaumik and R. Sharan, "Effect of Minority Carrier Diffusion Length. On Efficiency of Schottky Barrier Solar Cell", National Solar Energy Convention 1976, held in Jadavpur University,Calcutta, p.111.

5. B. Bhaumik and R. Sharan, "Effect of Oxide Thickness on Short Circuit Current and Open Circuit Voltage of MIS Solar Cells", submitted to J. Appl. Phys.

6. C. Hu and J. Edelberg, Solid State Electronics, Vol.20, p. 119, 1977.

7. J.J. Loferski and L.Y. Chen, Technical Report NGR-40-002-093/2 to the National Aeronautics and Space Administration, June 1975.

8. H.J. Hovel, "Solar Cells", Semiconductors and Semimetals, Vol.11, Eds. R.K. Willardson and A.C.Beer,Academic Press, New York, 1975.

9. N.F. Mott, Proc.Roy.Soc.London, Vol.A 171, p.281, 1939.

10. K. Lehovec, Phy.Rev., Vol.74, p. 463, 1948.

11. D.L. Pulfrey and R.F. McQuat, Appl.Phys.Lett., Vol.24, p. 167, 1974.

12. F.A. Padovani, Semiconductor and Semimetals, Vol.7, Part A, edited by Willardson and Beer, Academic Press, 1971.

13. A.N. Saxena, Surface Science, Vol.3, p.151, 1969.

14(a). J.D. Levine, J.Appl.Phys., Vol.42, p.3991,1971.

(b) C.R. Crowell, Solid State Electronics, Vol.29,p.171, 1977.

15. S.M. Vernon and W.A. Anderson, Appl. Phys. Lett., Vol.26, p. 707, 1975.

16. V.A. Johnson, R.N.Smith and H.J.Yearin, J., Appl. Phys., Vol.21, p.283, 1950.

17. G.S. Visweswaran, Ph.D. Thesis (to be submitted at I.I.T.Kanpur).

18. K. Takahashi, Int.J.Electronics, Vol.26, p.253, 1969.

19. H.C. Card, J. Appl.Phys., Vol.47, p. 6964, 1976.

20. W.B.Berry, Appl.Phys.Lett., Vol.25, p.196, 1974.

21. A.R. Moore, Appl.Phys.Lett., Vol.27, p.26, 1975.

22. P.K.Dubey and V.V.Paranjape, J. Appl.Phys., Vol.48, p.324, 1977.

23. R.F. McQuat and D.L.Pulfrey, 11th IEEE Photovoltaic Specialist Conference, p. 371, New York, 1975.

24. M.P. Thekackara, "Solar Energy, Vol.14, p.109, 1973.

25. W.C.Dash and R.Newman, Phys.Rev., Vol.15, p.1151,1955.

26. J.J. Wysochi and P. Rappaport, J. Appl.Phys., Vol.31, p. 571, 1960.

27. S.M.Sze, Physics of Semiconductor Devices', John Wiley, New York, 1969, p.24.

28. J.S. Escher and D.Redfield, Appl.Phys. Lett., Vol.25, p.702, 1974.

29. F.J. Blatt., Physics of Electronic Conduction. Solids, McGraw-Hill, New York, 1968, p.348.

30. G.G.MacFarlane, T.P.McLean, J.E.Quarrington and V. Roberts, Phys.Rev., Vol.11, p.1249, 1958.

31. T.P. McLean, Progress for Semiconductors, Vol.5, edited by A.F. Gibson, Heywad, London, 1960, p.94.

32. R.Hackam and P.Harrop, IEEE Trans.ED, 49, 1231,1972.

CHAPTER 2

1. D.R. Lillington and W.G.Townsend, Appl.Phys.Lett., Vol.28, p. 97, 1976.

2. W.A. Anderson, A.E.Delahoy and R.A.Milano, JAP, Vol.45, p.3913, 1974.

3. E.J. Charlson and J.C. Lien, JAP. Vol.46, p. 3981, 1975.

4. J.P. Ponpon and P.Siffert, JAP., Vol.47, p. 3248, 1976.

5. R.J. Stirn and Y.C.M.Yeh, Appl.Phys.Lett., Vol.27, p.95, 1975.

6. M.A. Green, F.D.King and J. Shewchun, Solid St. Electron, Vol.17, p. 551, 1974.

7. S.J. Fonash, JAP, vol.46, p.1286, 1975.

8. L.C. Olsen and R.Bohara, Proc.11th IEE Photovoltaic, Specialists Conf. p. 381, 1975.

9. D.L.Pulfrey, IEEE Trans.   Vol.ED-23, 587, 1976.

10. L.C.Olsen,Proc. 12th IEEE photovoltaic Specialist Conf., 1976.

11. H.C. Card and E.S.Yang, Appl.Phys. Let., Vol.29, p.52, 1976.

12. P.T.Landsberg and C.Klimpke, R. Soc., Lond., Vol.A.354, p.101, 1977.

13. J. Buxo, G. Sarrabayrouse, and D. Esteve, Phys.Stat.Sol. Vol.42, p.173 1977 .

14. H.C. Card, Solid St. Electronics, Vol.20, p.971,1977.

15. L.C. Olsen, Solid St. Electronics, Vol.20, p.741, 1977.

16. A. Cowley and S.M.Sze, J.Appl.Phys., Vol.36, p.3212,1965.

17. S.M.Sze, Physics of Semiconductor Devices, Wiley Inter-science, New York, 1969.

18. E.H. Rhoderick, J. Phys. D: Appl.Phys., Vol. 3, p.1153, 1970.

19. H.C. Card and E.H. Rhoderick, J.Phys.D.: Appl.Phys., Vol.4, p. 1589, 1971.

20. W. Schokley and W.T.Read, Phys.Rev., Vol.87, p.835, 1952.

21. R.N. Hall, Phys.Rev., Vol.87, p.387, 1952.

22. W.A. Anderson, J.K.Kim and A.E.Delahoy, IEEE Trans. Vol.ED-24, p.453, 1977.

23. A.S. Grove, Physics and Technology of Semiconductor Devices, John Wiley & Sons, New York, 1967.

CHAPTER 3

1. Y.P. Pai, H.C.Lin, M.Peckerar and R.L. Kocher, IEEE
    Int.Electron Dev. Mtg., Tech.Digest, p.470, 1976
    (unpublished).

2. P.L. Hower, et.al.,"The GaAs Field Effect Transistors",
    Semiconductors and Semimetals, Vol.VIIA, p.147,
    Ed. R.K.Willardson and A.C.Beer, Academic Press,
    New York, 1971.

3. H.J. Hovel, Solar Cells, ibid, vol.11, 1975.

4. B. Bhaumik, and R. Sharan, Appl.Phy.Lett., Vol.29,
    p. 257,1976.

5. C.N. Krishnan and R.Sharan, IEEE Trans., Vol.ED-24,
    p.1264, 1977.

6. J.M. Shannon. Appl. Phys. Lett., Vol.24, p.88,
    1974.

7. J.M. Shannon, Appl.Phys.Lett., vol.25, p.75, 1974.

8. J.M. Shannon, Solid State Electronics, Vol.19, p.531,
    1976.

9. Van-der Ziel, Solid State Electronics, vol.20, p. 269,
    1977.

10. J. Basterfield etal, Solid State Electronics, vol.18,
    p. 290, 1975.

11. R.A. Smith, Semiconductors, Cambridge University Press,
    p. 80, 1964.

12. M.J.Hampshire, Solid State Electronics, Vol.18,p.580,
    1975.

13. R.S.Bennett and K.A.Thoma, Electronics Letters,vol.12,
    p.505, 1976.

14. J.E. Ludman and J.Silverman, Infrared Physics, Vol.17,
    p.177, 1977.

15. V.L.Rideout, Solid State Electronics, vol.18,p.541,1975.

16. D.M.White and D.M.Brookbanks,Appl.Phys.Lett.,vol.30,p.348,
    1977.

17. J.J. Coleman, Appl.Phys.Lett.,vol.31,p.283,1977.

18. H.C.Card,E.S.Yang and P.Panayotatos,Appl.Phys.Lett.,
    vol.30,p.643,1977.

CHAPTER 4

1. M.A. Green, Appl.Phys.Lett., vol.27, p.287, 1975.

2. J.J.Loferski, E.E. Crisman, W.Avmitage and L.Y.Chen,
    Proc. IEEE Photovoltaic Specialists Conf.p58,1973 .

3. C.Hu and J.Edelberg, Solid State Electronics, vol.20,
    pp. 119 ,   1977.

4. K. KTakahashi, Int.J.Electronics, vol.26,   p.253
    1969.

5. P.M.Morse and H.Feshbach, Methods of Theoretical Physics,
    vol.I, New York: McGraw-Hill 1953, p.719.

6. M.P. Thekachara, Solar Energy 14,   p. 109 ,   1973.

7. S.M.Sze, 'Physics of Semiconductor Devices', New York:
    Wiley, 1969, p. 643.

8. P.T.Landsberg and C.Klimpke, Proc.Roy.Soc.London, Vol.A354,
    p.101,   1977.

9. B. Bhaumik and R. Sharan, App.Phys.Lett., Vol.29,   p.257,
    1976.

APPENDIX A

LIST OF SYMBOLS

A^{**} Effective Richardson constant (Amp cm^{-2} $^{\circ}$K^{-2})

a   Area of the cell (cm^2).

b   Width of the depletion layer (cm).

D_n, D_p Diffusion constants of electron and hole, respectively (cm^{-2}/sec^{-1}).

D_s Density of surface states (states/cm^2/eV)

E_G Band gap (eV).

kT   Thermal energy (ev).

L_n, L_p Diffusion lengths of electron and holes respectively (cm).

n   Ideality factor.

n_j, n_p Excess minority carrier (electron) concentration (cm^{-3}).

N_C Effective density of states in conduction band (cm^{-3}).

N_V Effective density of states in valance band (cm^{-3}).

N_A Acceptor impurity density (cm^{-3}).

N_D Donor impurity density (cm^{-3}).

P_{in} Input radiation power density (W/cm^2).

$Q(\lambda)$ Photon flux density (cm^{-2}/sec^{-1}) per unit wavelength (λ).

q   Charge of the electron (coulomb).

S,s   Surface recombination velocity (cm/sec.)

T	Absolute temperature ($^\circ$K).
$V_{mp}(I_{mp})$	Voltage (current) for maximum power output (V(amp)) .
qV_n	Energy difference between conduction band and Fermi level (eV).
qV_p	Energy difference between Fermi level and Valance band (eV).
V_{OC}	Open circuit voltage (V)
V_S	Potential drop across the semiconductor (V)
V_i	Potential drop across the insulator (V)
W	Width of the cell (cm)
ε_o	Free space permitivity (Farad/cm)
ε_i	Relative permitivity of the insulator
ε_s	Relative permitivity of the semiconductor
ρ	Fixed charge in the oxide (Coulimb/cm^{-3}).
δ	Oxide thickness (cm).
$\alpha(\lambda)$	Absorption coefficient (cm^{-1}).
ϕ_M	Workfunction of metal (eV)
ϕ_B	Barrier height (V).
χ	Electron affinity (eV)
Δ	Potential drops across the oxide in thermal equilibrium (V).
ϕ_o	Energy level at surface (V).

APPENDIX B

CHARGE RELATIONS IN SCHOTTKY (MIS) SOLAR CELL

In Chapter 2, while discussing the characteristics of Schottky (MIS) solar cell the expressions for the barrier height and for various charges were required. These are given here following an analysis of Landsberg and Klimpke (Proc. R. Soc. Lond., A 354, 101-118, 1977). The symbols used here are defined in Appendix A.

B.1 Charges Per Unit Area

Surface state charge: Let us first consider the surface state charge, Q_i in thermal equilibrium. This is given as

$$Q_i = q \left[\int_0^{\emptyset_0} D_s(1-f_{to})dE_{to} - \int_{\emptyset_0}^{E_G} D_s f_{to} dE_{to} \right] \quad (B.1)$$

where D_s is the density of surface states, E_{to} is the energy of a recombination level at the surface and f_{to} is the corresponding Fermi-Dirac distribution function. If the density of surface states D_s is constant then Q_i becomes

$$Q_i = qD_s kT \left[\ln \left\{ \frac{1+\exp(q\emptyset_B/kT)}{1+\exp (q\emptyset_B-E_G)/kT} \right\} - \frac{E_G}{kT} \right] + qD_s\emptyset_0$$

$$(B.2)$$

Under illumination or when a bias is applied the MIS diode would be in non-equilibrium condition. In the case of low injection, the departure from equilibrium is not large and the system is said to be in quasi-equalibrium. A

quasiequlibrium distribution is completely specified by three quasi fermi levels associated with electrons, holes and the recombination level. Even for moderate departure from equilibrium the simplicity of quasi-equalibrium is lost and one has to consider recombination kinetics. The analysis of one-recombination- center model without trapping and for low-injection has been carried out in detail by Schockley and Read (Phys.Rev. 87, 835, 1952) and by Hall (Phys.Rev.87, 387, 1952) and is called the SRH theory.

They have obtained the expression for the probability of occupation of the recombination level as

$$f_t = \frac{G(o)n(o) + H(o)\, p_1(o)}{G(o)\,[\,n(o)+n_1(o)\,]\, +\, H(o)\,[\,p(o)+p_1(o)\,]} \qquad (\text{ B.3})$$

Here we have used the notation of Landsberg etal (Op.Cit.) n(o) and p(o) are, respectively, the electron concentration in the conduction band at the interface x=0 and the hole concentration in the valence band at the interface x = 0; $n_1(o)$ and $p_1(o)$ are the electron and hole concentrations respectively, when the Fermi level is at the trap energy in thermodynamic equilibrium. G(o) and H(o) are given by

$$G(o) = T_1^S + T_1 n(o) + T_2\, p(o)$$
$$H(o) = T_2^S + T_3\, n(o) + T_4 p(o) \qquad (.\ \text{B.4})$$

where reaction constants T_1^S, T_2^S, T_1, T_2, T_3 and T_4 are defined in Fig. B.1 and their values are given in Table.
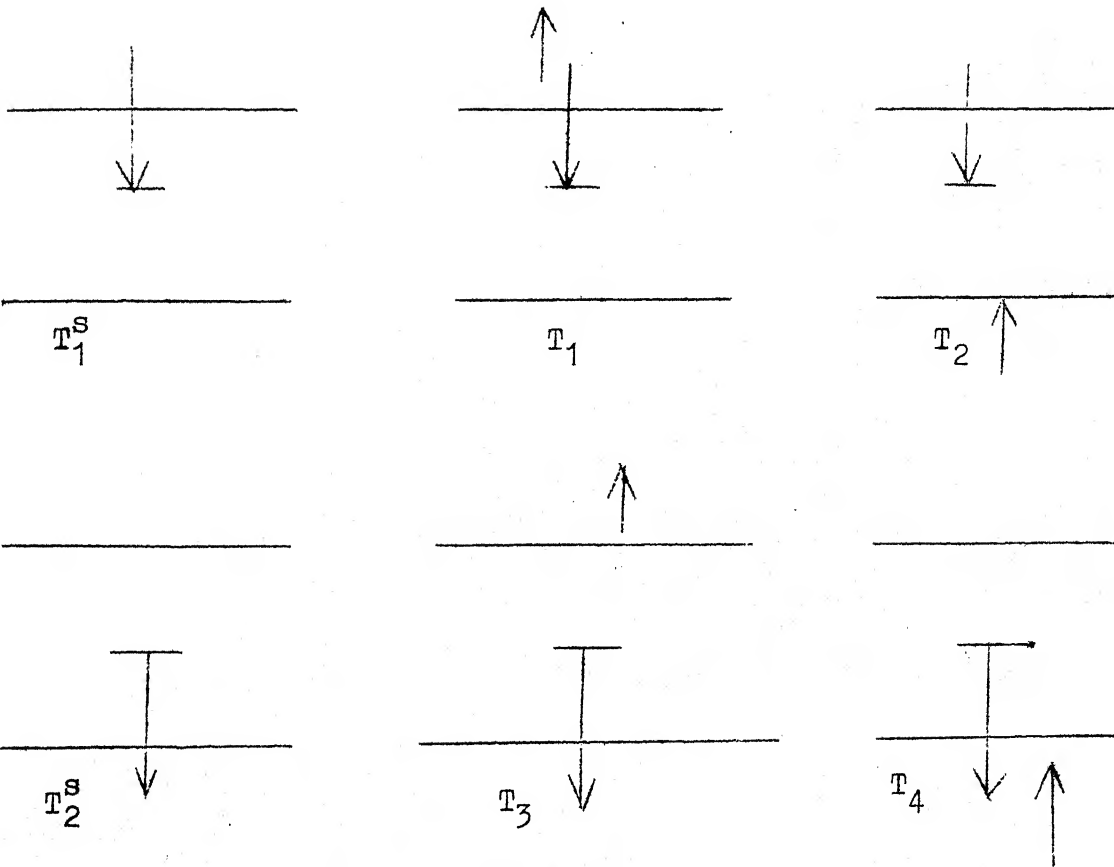
Fig.B.1

Definition of reaction constants occurring in eqn.(B.4).

The surface state charge under illumination Q_i^* is given by

$$Q_i^* = q \int_0^{E_g} D_s f_t dE_t \qquad (\text{B.5})$$

In case, the tunneling from interface states to the metal are ignored, f_t in eqn. (B.5) can be obtained from eqn.(B.3). The resulting form of Q_i^* is:

$$Q_i^* = \frac{qD_s kT}{2}[\ln\left[\frac{H(o)p_o(o)\exp(-2q\phi_B/kT)+\exp(-q\phi_B/kT)}{H(o)p_o(o)\exp(2(E_g-q\phi_B)/kT)+\exp(q(E_g-q\phi_B/kT)}\cdot\frac{(G(o)\,n(o)+H(o)p(o))+G(o)n_o(o)}{(G(o)n(o)+H(o)p(o))+G(o)n_o(o)}\right]$$

$$-\frac{(G(o)n(o)-H(o)p(o))}{(A-B)G(o)n_o(o)}\ln\{\frac{(\exp(q\phi_B/kT)-A)(\exp((q\phi_B-E_g)/kT)-B)}{(\exp(q\phi_B/kT)-B)(\exp((q\phi_B-E_g)/kT)-A)}\}]$$

$$+ qD_s\phi_o \qquad (\text{B.6})$$

With

$$\left.\begin{matrix} A \\ B \end{matrix}\right\} = - \frac{(G(o)n(o)+H(o)p(o))}{2G(o)n_0(o)} \pm [\{\frac{G(o)n(o)+H(o)p(o)}{2G(o)n_0(o)}\}^2$$

$$- \frac{H(o)p_0(o)}{G(o)n_0(o)}]^{\frac{1}{2}} \qquad (\ .B.7)$$

Although the general expression for calculations Q_i^* is given by eqn. (B.6), the lack of availability of experimental values of the reaction parameters and their variation with oxide thickness in both the cases of an 'illuminated' and 'biased' MIS diode, makes it difficult to obtain meaningful quantitative values. Here for the special cases of $G(o) = H(o)$ expression for Q_i^* has been developed. The advantage of the approximation $G(o) = H(o)$ is that the unknown recombination parameters cancel out. If we further make an approximation $[\frac{n(o)+p(o)}{2n_0(o)}]^2 \gg [p_0(o)/n_0(o)]$, eqn. (A.B.6) reduces to:

$$Q_i^* = \frac{qD_s kT}{2}\{[\ln[\frac{\exp(q\phi_B^*/kT) + (p(o)+n(o))/n_0(o)}{\exp((q\phi_B^*-E_g)/kT) + (p(o)+n(o))/n_0(o)}] - \frac{E_g}{kT}]$$

$$[1 + \frac{n(o)-p(o)}{n(o)+p(o)}]\} + qD_s\phi_0 \qquad (\ B.8)$$

It is interesting to note that if $p(o) \gg n(o)$, then eqn.(B.8) simplifies to:

$$Q_i^* = qD_s\phi_0$$

Let us now consider the interface charge Q_i^f in the case that the diode is forward biased, but there is no

illumination. The expression for Q_i^f is the same as that of Q_i^* in eqn. (B.6) excepting that ϕ_B^* should be replaced by ϕ_B^f and n(o), p(o) should be accordingly calculated. Also note that the reaction constants would be different in the two cases.

Space charge in depletion region: The space charge is the depletion layer Q_{SC}^* is

$$Q_{SC}^* = qN_Dw = [2 \epsilon_s q N_D(V_b-V_s)]^{\frac{1}{2}} \qquad (B.10)$$

by the depletion approximation with $w = [(2_s/2N_D)(V_b-V_s)]^{\frac{1}{2}}$. In equilibrium $V_s = 0$ and Q_{SC} is given by

$$Q_{SC} = [2 \epsilon_s qN_D V_b]^{\frac{1}{2}} \qquad (B.11)$$

.B.2: Potential drops and Barrier Height

The potential drop V_b-V_s across the depletion layer is given under illumination by

$$\Delta - V_i = \int_{-\delta}^{0} E_i(x) \, dx = \frac{\rho\delta 2}{2 \epsilon_i} + (Q_i+Q_{SC}) \frac{\delta}{\epsilon_i} \qquad (B.12)$$

Thus,

$$(\epsilon_i/\delta)(\Delta - V_i) = \frac{1}{2} \delta\rho + Q_i + Q_{SC} \qquad (B.13)$$

becomes in equilibrium,

$$(\epsilon_i/ \delta) \Delta = \frac{1}{2} \delta\rho_0 + Q_{i0} + Q_{SC0} \qquad (B.14)$$

Subtracting,

$$-(\epsilon_i/\delta)V_i = \tfrac{1}{2} \; (\rho - \rho_0) + (Q_i - Q_{i0}) + (Q_{SC} - Q_{SCO}) \quad (\text{B.15})$$

Now£ from $\emptyset_B = \emptyset_M - \chi - \Delta$, (B.11), (B.2) and (B.13i), the equilibrium barrier height is given by the solution of

$$\emptyset_B = \emptyset_M - \chi - \frac{\delta^2 \rho_0}{2\,\epsilon_i} + \frac{D_s\,\delta\,q}{\epsilon_i}$$

$$[E_G - kT \; \ln \{ \frac{1+\exp(q\emptyset_B/kT)}{1+\exp(\frac{q\emptyset_B - E_G}{kT})} \} \,] \; - \frac{\delta q^2}{\epsilon_i} D_s \emptyset_0$$

$$- \frac{\delta}{\epsilon_i} \{ \; 2\epsilon_s\, q\, N_D(\emptyset_B - V_n) \}^{\tfrac{1}{2}} \qquad\qquad (\text{B.12})$$

The values of the parameter used in eqn. (B.12) are given in Table B.1. Also note the values of tunnel exponent used are given in Table B.2.

Table   B.1: Data Adopted for MIS Solar Cell*.

Parameter	Numerical value	Dimensions
E_G	1.12	eV
	4.01	eV
T	300	K
ρ_o	$3 \times 10^{17} q$	$\sigma\,cm^{-3}$
$T_1^s = T_2^s$	1.12×10^{-8}	$cm^3 s^{-1}$
$T_1 = T_2 = T_3 = T_4$	3.66×10^{-25}	$cm^6 s^{-1}$
$A^{**} \simeq A_p^{**} \simeq A_n^{**}$	120	$A\,cm^{-2}K^{-2}$
ε_i	$11.8\,\varepsilon_o$	F/cm
ε_s	$3.9\,\varepsilon_o$	F/cm
D_p	12.5	$cm^{-2}\,sec^{-1}$
L_p	100	μm
N_D	10^{15}	cm^{-3}
n_i	1.6×10^{10}	cm^{-3}

* Taken from Landsberg and Klimpke (Op.Cit.).

Table B.2: Tunnel Exponent $\chi^{\frac{1}{2}} \delta$

$\delta(A^\circ)$	5	10	15	20	25
$\chi^{\frac{1}{2}} \delta$	0	2	4	8	14

APPENDIX C

SOLUTION OF TWO DIMENSIONAL CONTINUITY EQUATION

C.1 Solution in Dark

Let the carrier concentration in the collecting region be $n_C(x,y)$ where

$$n_C(x,y) = XY \tag{C.1}$$

Let the separation constant be $\lambda = \pm \beta^2$. Then one obtains:

$$\frac{1}{X} \frac{d^2 X}{dx^2} = \pm \beta^2 \tag{C.2}$$

$$\frac{1}{Y} \frac{d^2 Y}{dy^2} - \frac{1}{L_h^2} = \pm \beta^2 \tag{C.3}$$

It can be easily checked that for $\lambda = \beta^2$ there is no solution for eqn. (C.2). For $\lambda = -\beta^2$, we have

$$X = \tau \cos \beta x + \tau' \sin \beta x \tag{C.4}$$

$$Y = C \exp\{\sqrt{P}\, x\} + D \exp\{-\sqrt{P}\, x\} \tag{C.5}$$

where

$$P = \frac{1}{L_h^2} + \beta^2 \tag{C.6}$$

Use of B.C.'s $X = 0$, at $x = 0$ and W shows that the solution of eqn. (C.4) is

$$X = \sum_{q=1}^{\infty} \tau'_q \sin \beta_q x \tag{C.7}$$

Use of the B.C.'s $dn_C/dy = 0$ at $y = -\frac{L}{2}(m+1)$ shows that

$$Y = K \frac{\cosh[\sqrt{P}\{ y + \frac{L}{2}(m+1) \}]}{\cosh[\sqrt{P} \frac{L}{2}(m-1)]}$$

where $K = D \exp(\sqrt{P} \frac{L}{2}(m+1))\cosh\{\sqrt{P} \frac{L}{2}(m-1)\}$

It has been checked that the complete solution in the collecting region, i.e. $n_C(x,y)$ is obtained as the product of (C.7) and (C.8) and is given as eqn. (4.3) of the main text.

C.2 Solution in the Lighted Region

Let the carrier concentration in the lighted region be $n_L(x,y)$ and expressed as

$$n_L(x,y) = X_1(x) \, Y_1(y) \tag{C.9}$$

In this case let the separation constant be $\lambda = \pm \chi^2$. It can be shown that for $\lambda = \chi^2$ there is no solution. In the case $\lambda = -\chi^2$ one obtains

$$X_1(x) = A \cos \chi \, x + B \sin \chi x \tag{C.10}$$

$$Y_1(y) = E \exp (\sqrt{Q} \, y) + F \exp(-\sqrt{Q} \, y) \tag{C.11}$$

Use of B.C. $X_1 = 0$ at $x = W$, gives from eqn. (C.10)

$$A = -B \tan \chi W \tag{C.12}$$

Use of $D_1 \frac{dX_1}{dx} = SX_1$ at $x = 0$ gives for $B \neq 0$

$$\chi \cot \chi W = -S/D_h \tag{C.13}$$

The use of B.C.; $\dfrac{d\dot{Y}_1}{dy} = 0$ at $y = 0$ gives

$$E = -F \tag{C.14}$$

Note that eqn. (C.13) has multiple solutions. Use of this fact and eqn. (C.12) and (C.14) in (C.10) and (C.11) gives the third term of the solution of $n_L(x,y)$ as given in eqn.(4.4) of the main text.

The terms $g_1(x)$ and $g_2(x)$ of eqn. (4.4) are obtained as follows. When $\lambda = 1/L_h^2$, one has the solution $g_1(x)$ of eqn. (4.4). The term $g_2(x)$ is the particular integral due to inhomogenuity of the continuity equation. We have guessed the particular integral to be of the form:

$$g_2(x) = \frac{Q(\lambda)\,\alpha(\lambda)}{Dh(\alpha^2 - L_h^{-2})} \left\{ A_3 \exp\left[(-x+b)/L_h\right] - \exp(-\alpha(\lambda)x) \right\} \tag{C.15}$$

Using the boundary conditions, $g_2(x) = 0$ at $x = W$, in eqn.(C.15) we obtain the $g_2(x)$ of eqn.(4.4) of the main text.

APPENDIX   D

ALTERNATIVE ANALYSES OF LATER CELLS

D.1 Analysis of Lateral Cell by Fourier Series Expansion:

In a recent paper [Solid St.Electronics, 20,119,1977],
Hu and Edelburg have analysed the lateral cell structure of
using the technique of Fourier series expansion instead of
"boundary matching" as has been done by us in the previous
sections. We summarize, in the following, the relevant
portion of the analysis of the Hu et al so that a comparison
with the "boundary matching"can be done.

The differential equation in the two cases is the same,
as given by eqn. (3.1). However, the boundary conditions that
have been utilized are different, in as much as, in Hu's
analysis, the B.C. number (iii) in Table 3.1 is not needed.
Also note that we have analysed the structure based on
a P-type semiconductor, whereas Hu etal have done it for N-type
semiconductor. Their solution is written for holes which are
the minority carriers.

The solution is expressed as sum of particular
solution p_p and the homogeneous solution p_h. The solution
p_p is given by

$$p_p = \tau \alpha Q \cdot \sum_{m=0}^{\infty} \frac{e^{-\alpha d} u_m + C_m(1-e^{-\alpha d})\cos \lambda_m y}{1 - L^2 \alpha^2 + L^2 \lambda_m^2} W_m \qquad (D.1)$$

where L is the diffusion length in centimeters, $\lambda_m = m\pi/(L+B)$,

$u_o = 1$ and $u_m = 0$ for $m \neq 0$,

$$C_o = \frac{b-a}{b}; \qquad \underset{m \neq o}{C_m} = -(\frac{2}{L+B}) \frac{\sin(B \lambda_m)}{\lambda_m}$$

$$W_m = e^{-\alpha x} - \cosh \beta_m x + (\frac{\cosh \beta_m W - e^{-\alpha W}}{\sin \beta_m W}) \sinh \beta_m x$$

where $\beta_m = (\frac{1}{L^2} + \lambda_m^2)^{\frac{1}{2}}$

and d is the thickness of metal stripes.

The related homogeneous solution is obtained by the technique of eigenfunction expansion,

$$p_h = \sum_{m=o}^{\infty} A_m \sinh\{\beta_m(W-x)\} \cos\lambda_m y /\sin \beta_m W \qquad (D.2)$$

where the A_m's are the Fourier series coefficients of the excess hole concentration along the boundary $x = 0$ and A_m's are given by the following expression.

$$A_m = C_m \{ A_o R_o + \frac{Q_o}{S} [e^{-\alpha d} + C_o (1 - e^{-\alpha d})] \}$$

$$+ (1-u_m)(C_o + \tfrac{1}{2} C_m) [A_m R_m + (1-e^{-\alpha d}) \frac{Q_m C_m}{S}]$$

$$+ (\tfrac{1}{2} - \tfrac{1}{4} u_m) \sum_{\substack{j=1 \\ j \neq m}}^{\infty} (C_{m+j} + C_{m-j}) [A_j R_j + (1-e^{-\alpha d}) \frac{Q_j C_j}{S}]$$

$$(D.4)$$

where $R_m = -(D/S) \beta_m \coth \beta_m W$

$$Q_m = \frac{QL^2}{1-L^2\alpha^2 + L^2 \lambda_m^2} [\beta_m (\frac{\cosh \beta_m W - e^{-\alpha W}}{\sinh \beta_m W}) - \alpha] \qquad (D.4)$$

Note that eqns.(A.5) and (A.7) in Hu etal's paper have
algebraic errors which have been pointed out by us
and the corrected form is given in eqn. (D.3) and eqn.(D.4).
The infinite set of equations (D.3) is modelled as a system
of m simultaneous equations to be solved for the m lowest
order Fourier series coefficients A_m. At least m = 70
coefficients were needed by Hu etal for reasonable accuracy.
Once the solution for the minority carriers are obtained,
the calculation of efficiency etc. in the two methods is
similar hence would not be discussed again. Thus so far,
the comparison of the two methods is concerned it is to be
only done from the point of view of ease of numerical
computation in obtaining the minority carrier profile. Our
experience shows that solving for several simultaneous
equations would definitely be more horrendous than the
computations needed in the "boundary matching" methods.
Before concluding this section we would also like to
point out that though the surface recombination velocity
at the exposed part of the semiconductor has been incorporated
in the analysis of Hu etal, its physical significance has
not been explored at all nor have been the design aspects
emphasized, keeping an appreciation of the operative physical
mechanisms in view.

D.2 Numerical Analysis of Lateral Cell

The disadvantages of a dead layer on the top surface of a P-N junction solar cell were noticed by many workers but perhaps the first method of obviate this, was proposed by Loferski etal [Technical Report NGR-40-002-093/2 to the National Aeronautics and Space Administration, June 1975]. His suggestion was to use a grating structure where "unlike a standard diffused cell which has its front surface covered completely by a thin diffused skin region, a grating type cell would have part of its front surface covered by a grating of finely spaced fine grid lines which form a potential barrier with the base substrate. The grating structure junction could be a diffused P-N junction, an alloyed P-N junction or a Schottky barrier junction". Thus we see that Loferski's grating structure is the one which we have called the lateral cell. He has set up the two dimensional continuity equation which is the same as our eqn.(3.1) and has solved it numerically by using finite difference technique. For the solution of the simultaneous equations he has used the successive overrelaxation method. As is well known, the disadvantage of a numerical method as compared to an analytical solution is that each problem has to be solved on its own and general design guidelines cannot be obtained. Hence we feel that the analytical method given in Section 3.1 would be more convenient than the numerical method given by Loferski.

D.3 Lateral Schottky barrier Solar Cell - Simplified Model.

The analysis of lateral SBSC given in the previous section requires computation of the matching coefficients B_p's and C_q's which, though rigorous, is time consuming. In many cases, it would be desirable to develop an approximate analysis which is computationally simple. Such an analysis of the lateral SBSC is provided in this section. The simplification is brought out by the fact that in this case no iteration is required while solving for B_p's and C_q's.

The method consists of solving the continuity equation in the collecting region as done in the previous section and of modifying the continuity equation in the lighted region as follows:

$$D_n \frac{d^2 n_L}{dy^2} - \frac{n_L}{\tau_n} = -Q \alpha e^{-\alpha x} \qquad (D.5)$$

Here the diffusion component in the x-direction has been neglected. Hence the boundary conditions (i) and (ii) in the lighted region in Table 3.1 are not required. The solution of eqn. (3.16) is obtained as

$$n_L = 2A_1 \cosh\frac{y}{L_n} + \tau_n Q \alpha e^{-\alpha x} \qquad (D.6)$$

where A_1 is the coefficient to be determined later.

In the collecting region the solution of the two dimensional continuity equation is given by eqn.(4.3) as in Section 4.1.

Using the condition that $y = -L$, $n_C = n_L = f(x)$ and $\partial n_C / \partial y = \partial n_L / \partial y$, the coefficient C_q's, and A_1 can be expressed as

$$C_n = \frac{2\tau_n\, Q\alpha\{\beta_n(1-(-1)^n\, e^{-\alpha W})\}}{W(\alpha^2+\beta_n^2)\{1+P_n L_n \tanh(\frac{P_n(m-1)L}{2})\coth\frac{L}{L_n}\}} \tag{D.7}$$

and

$$A_1 = -\frac{L_n}{2\sinh(L/L_n)}\sum_{q=1}^{\infty} C_q \sin(\beta_q x)\, P_q \tanh(P_q \frac{m-1}{2}L) \tag{D.8}$$

Once the coefficients C_q's are known the expression of short circuit current is given by

$$I_{SC}(\lambda) = \frac{4q\, Q\alpha\, L_n^2}{W}\sum_{q=1}^{\infty}\frac{\beta_q^2\{1-(-1)^n\, e^{-W}\}\tanh\{\frac{P_q B}{2}\}}{P_q(\alpha^2+\beta_q^2)\{1+L_n P_q \tanh(\frac{P_q B}{2})\tanh\frac{L}{L_n}\}} \tag{D.9}$$

Note that the symbol q has been used to denote charge of the electron as well as an index in the summation. The particular use is clear from the context.

The plot of I_{SC} for AMO sunlight versus the width of the metal stripe for several values of L is shown in Fig. D.1. In the calculation of eqn.(D.9), fourteen terms in the summation have been taken. The following points regarding the plot of Fig. D.1 should be noted.

(1) It is worthwhileto compare the results of the approximate model as given in Fig. D.1, with those of two dimensional calculation given in Fig.4.3. One notes that the basic trend of the results in the two cases is the same. However, the numerical values are different and the amount of variation is given later. Here we only want to point to a general trend that is always present. This is that the value of I_{SC} found from the approximate calculation is always less than that from the two dimensional calculation. The reason is the use of one dimensional continuity equation in the lighted region. In this case the effective length that the carriers have to traverse before collection is increased, thereby increasing the chances of recombination thus lowering the short circuit current.

(2) The amount of difference between the graph of Fig.4.3 and Fig. D.1 depends upon the values of L and B being considered. One finds that for L $>$ 50 µm for the whole range of B, the difference between the two calculations is less than 20%. In case one is only interested in getting an approximate idea but with lots less numerical effort it is obvious that the approximate method leading to Fig.4.3 would be more convenient than the two-dimensional analysis. For example, one such use can be envisaged when one is interested in studying the temperature variation of the short circuit current as mentioned in Chapter 1.

Such calculation of variation of I_{SC} with temperature using the expression for the absorption coefficient given in eqn.(1.21) for silicon, is given in Fig. D.2.
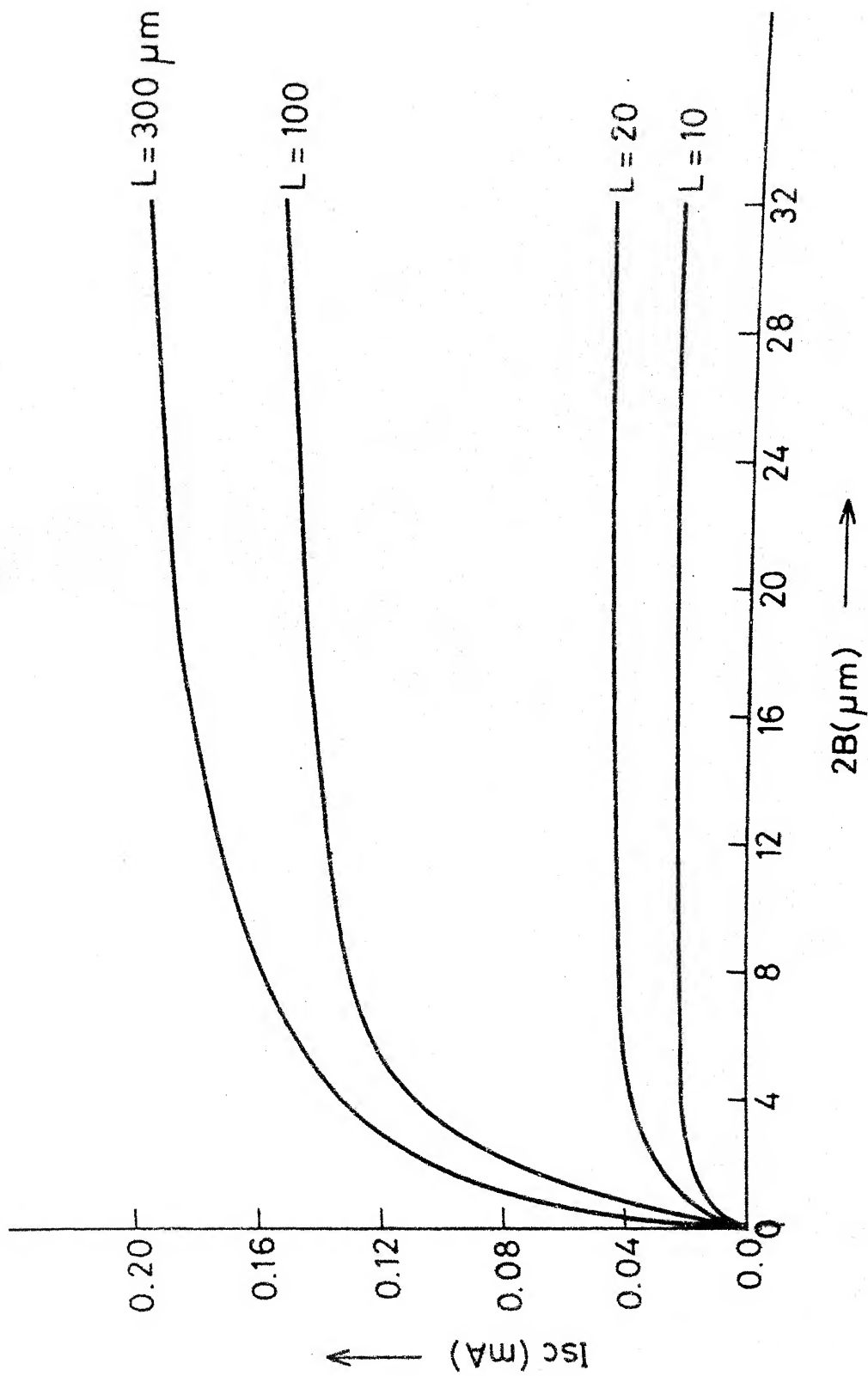
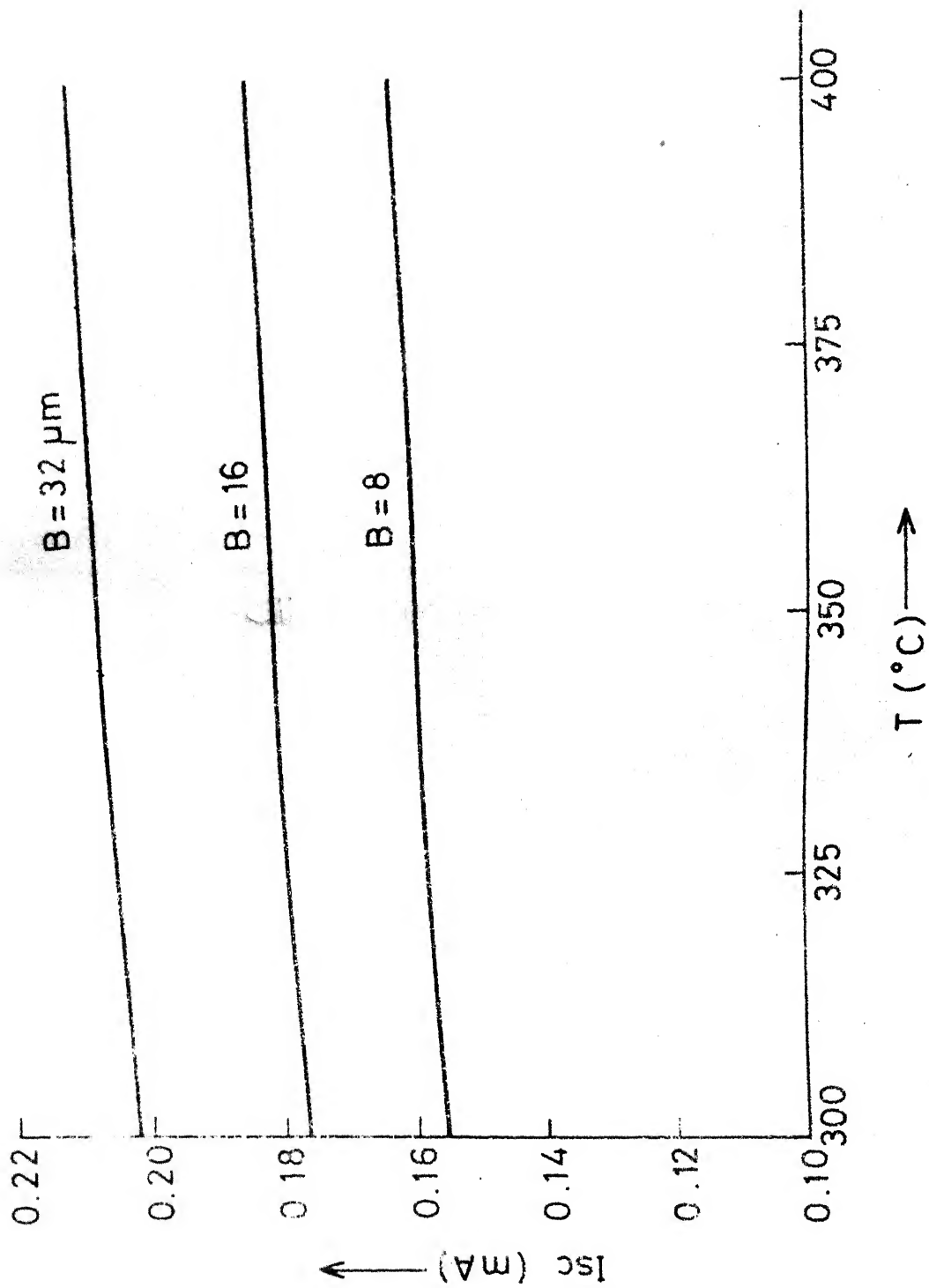Fig. D.1 Plot of the short circuit current Isc versus the width of metal finger for several values of L.

Fig. D.2 Temperature variation of short circuit current with L=300 μm and B as a parameter.

A 60736

Date Slip

This book is to be returned on the date last stamped.

....	....
....	....
....	....
....	....
....	....
....	....
....	....
....	....
....	....
....	....
....	....

CD 6.72.9

EE-1578-D-BHA-STU.